Microchips for Isothermal Amplification of RNA

- Development of microsystems for analysis of bacteria, virii and cells

Thesis submitted for the degree of Doctor scientiarum

by

Anja Gulliksen

Department of Molecular Biosciences

Faculty of Mathematics and Natural Sciences

University of Oslo

2007

Table of contents

Acknowledgement

First of all I would like to express my deepest gratitude to my supervisors, Professor Reidun Sirevåg, Dr. Eivind Hovig, Dr. Frank Karlsen and Dr. Henrik Rogne for their professional guidance, help, support, positive feedback and enthusiasm during this work. Their careful efforts have been of great importance, in particular during the writing processes for the contribution of good ideas, and productive and critical discussions. Dr. Henrik Rogne has been deeply missed after he lost his fight against cancer the 1st of April 2006.

Thanks to NorChip AS for being the initiator of the project, and for providing research facilities and consumables, and for introducing me to the exciting field of µTAS. I would also like to thank all colleagues working at NorChip AS for their support, technical assistance and for warm atmosphere, whenever I show up at Klokkarstua. My Ph D. fellow and closest colleague, Lars Solli, deserves special thanks for fruitful discussions, conference companionship, and valuable support through the ups and downs during the project. Appreciations also go to Dr. Ivan Silva for proofreading of the whole theory part of this thesis. I would also like to thank NorChip AS for giving me the opportunity to continue working in the exhilarating world of µTAS.

I would like to express my gratitude to the entire departments of Microsystems and Nanotechnology, and Optical measurement systems at SINTEF for valuable technical support

Summary

The goal of the present work was to develop a microchip for amplification and detection of mRNA by employing nucleic acid sequence-based amplification (NASBA) technology. The technology platform should in principle be adaptable for any clinical analysis using mRNA or ssDNA as a target. To demonstrate the microchip functionality, identification of human papillomavirus (HPV) type 16, the etiological agent for cervical cancer has been used.

The work shows for the first time successful real-time amplification and detection employing NASBA in microsystem formats using custom-made instruments. The first silicon-glass chips contained reaction chambers of 10 nl and 50 nl, which decreased the NASBA reaction volume by a factor of 2000 and 400, respectively. Further, experiments employing cyclic olefin copolymer (COC) microchips for simultaneous amplification and detection, automatically distributed the sample into 10 parallel reaction channels with detection volumes of 80 nl. In order to detect the simultaneous amplification in the reaction channels, a second custom-made optical detection system with increased sensitivity, heat regulation and an automatic non-contact pumping mechanism, was made. Dilution series of both artificial HPV 16 oligonucleotides and SiHa cell lines showed that the detection limits for the microchips were comparable to those obtained for experiments performed in conventional routine-based laboratory-systems. For experiments related to the development of a self-contained microchip for NASBA, the detection volume was increased to 500 nl due to the advantage of an increased fluorescence signal.

For the NASBA reaction, biocompatible surfaces are critical. It was not possible to amplify any target in microchips with native silicon or COC surfaces. Adsorption measurements indicated clearly that fluorescently labelled mouse IgG bound non-specifically to the hydrophobic native COC surfaces, while PEG coated COC surfaces showed adequate protein resistance. Of the coatings tested for the COC microchips, surfaces modified with PEG showed the best biocompatibility. Successful amplification was obtained with silicon microchips when the surfaces were modified with either SigmaCote™ or SiO_2.

In order to integrate the NASBA reagents on chip, a thorough evaluation of the reagents to be spotted and dried was performed. Because of the limited number of microchips

available, it was necessary to map the most critical parameters on macroscale prior to transfer to the microscale. The DMSO and sorbitol enclosed in the standard NASBA reaction mixture were difficult to dry, and therefore it was necessary to add these compounds to the oligonucleotides or the sample of extracted nucleic acids before the sample was applied on the amplification chip. The standard NASBA reagents consist of the two main solutions, mastermix and enzymes, in addition to the sample. Both the mastermix and the enzymes were stable only when spotted and dried separately. Protectants, such as PEG and trehalose were essential for recovery of enzymatic activity after drying on macroscale. The times for diffusion of modified molecular beacons in dried mastermix and of fluorescently labelled mouse IgG in the dried enzyme solution were ~60 seconds and ~10 minutes, respectively. So far, only dried enzymes with 0.05% PEG protectant have been successfully amplified on chip. Successful amplification using a rehydrated mastermix on microchip still remains.

Optimal design and fabrication methods of the microchips were found to be crucial for chip performance. Rough surfaces do not only create background noise for the optical measurements, but it also contributes to generation of bubbles and problems related to manipulation of the sample within the channel network. The silicon microchips were manufactured with optically smooth surfaces. However, low surface roughness was not easily obtained for the COC microchips. Of the fabrication methods evaluated, it was the injection moulded chips which showed the smoothest surfaces, closely followed by the hot embossed chips. Milled and laser ablated chips produced the roughest surfaces.

A novel non-contact pumping mechanism based on on-chip flexible COC membranes, combined with actuation pins in the surrounding instrument, was tested and evaluated. The mechanism enabled metering, isolation and movement of nanoliter sized sample plugs in parallel reaction channels. The COC chips with integrated pumps were able to simultaneously move parallel sample plugs along the reaction channels in four different positions. Each reaction channel contained a set of 4 actuation chambers in order to obtain metering, isolation and movement of the sample plug into the detection area. The pump accuracy depended on the evaporation of sample and the deformation of the COC membranes.

The results presented in this work are promising with regard to the development of a complete integrated and self-contained mRNA amplification microchip for multi-parallel target testing of clinical samples.

List of Abbreviations

Abbreviation   Explanation

Abbreviation	Explanation
µTAS	micro total analysis system
AMV-RT	avian myeloblastosis virus reverse transcriptase
bp	base par
BSA	bovine serum albumin
cDNA	complementary DNA
CLSM	confocal laser scanning microscopy
CNC	computer numerical control
COC	cyclic olefin copolymer
dabcyl	4-(4'-dimethylaminophenylazo) benzoic acid
DMSO	dimethyl sulfoxide
DNA	deoxyribonucleic acid
dNTP	deoxyribonucleoside triphosphate
DRIE	deep reactive ion etching
dsDNA	double-stranded DNA
ECL	electrochemiluminescence
ELISA	enzyme-linked immunosorbent assay
ELGA	enzyme-linked gel assay
FAM	6-carboxy-fluorescein
FITC	fluorescein isothiocyanate
FRET	fluorescence resonance energy transfer
HPV	human papillomavirus
LCR	ligase chain reaction
LED	light emitting diode
LOC	lab-on-a-chip
LOD	limit of detection
mRNA	messenger RNA
NASBA	nucleic sequence-based amplification
PCR	polymerase chain reaction
PEG	polyethylene glycol
PEO	polyethylene oxide
PMT	photomultiplier tube
POC	point-of-care
POE	polyoxyethylene
PVP	polyvinylpyrrolidone
RNA	ribonucleic acid
RNAi	RNA interference
RNase	ribonuclease
RNase H	ribonuclease H
rNTP	ribonucleoside triphosphates

rRNA	ribosomal RNA
RT-PCR	reverse transcriptase polymerase chain reaction
siRNA	small interfering RNA
ssDNA	single-stranded DNA
T_g	the glass transition temperature
tRNA	transfer RNA
TTP	time-to-positivity

List of Publications

Papers included in the thesis

I. Anja Gulliksen, Lars Solli, Frank Karlsen, Henrik Rogne, Eivind Hovig, Trine Nordstrøm and Reidun Sirevåg, **Real-time Nucleic Acid Sequence-Based Amplification in Nanoliter Volumes**, *Analytical Chemistry*, 2004, 76, 9 – 14

II. Anja Gulliksen, Lars Solli, Klaus Stefan Drese, Olaf Sörensen, Frank Karlsen, Henrik Rogne, Eivind Hovig and Reidun Sirevåg, **Parallel Nanoliter Detection of Cancer Markers using Polymer Microchips**, *Lab on a Chip*, 2005, 5, 416 – 420

III. Lars A. Solli, Anja Gulliksen, Olaf Sörensen, Frank Karlsen, Lars R. Sætran, Liv Furuberg, Henrik Rogne and Klaus S. Drese, **A novel non-contact pump mechanism for parallel movement of nanoliter sized liquid plugs using flexible diaphragms**, *manuscript*

IV. Anja Gulliksen, Michal Mielnik, Bente F. Hoaas, Eivind Hovig, Frank Karlsen, Henrik Rogne and Reidun Sirevåg, **Aspects towards the development of an isothermal amplification microchip**, *manuscript*

Introduction

Since the mid-1980s, researchers have repeatedly demonstrated the practical use of nucleic acid based assays for clinical laboratory work. Since then, nucleic acid based technologies have advanced rapidly, resulting in improved sensitivity, specificity, speed and ease of use. Potential applications for nucleic acid technologies are broad, including detection of pathogens in clinical medicine, genetic screening and diagnosis, monitoring therapy and persistence of infection during drug treatment. In addition, it has also been applied to veterinary medicine, food safety, and forensic analysis.

The identification of unique DNA or RNA sequences or differentially regulated specific genes in an individual, may indicate the presence of genetic diseases or conditions, such as precancerous states or predisposition to cancer itself, tissue compatibility, or bacterial and/or viral infections. Since messenger RNAs (mRNA) are directly involved in all biological activities in eukaryotic cells, bacteria and virii, mRNA can give valuable and important clinical diagnostic information. For this reason, mRNA, rather than DNA, is often preferred as a clinical diagnostic marker.

However, in many cases, target nucleic acids may be present only in very small quantities, making it difficult or impossible to detect by direct analysis. In such cases, nucleic acid amplification is often employed in order to increase the number of copies of the target to a detectable level. For detecting mRNA, two of the most commonly used amplification techniques are reverse transcriptase polymerase chain reaction (RT-PCR) and nucleic acid sequence-based amplification (NASBA).[1, 2]

A few years back, nucleic acid assay based analyses were mainly utilized as research tools, rather than for routine diagnostic surveillance. However, in recent years nucleic acid assays have become more commonly used for diagnostics.[2, 3, 4] Today almost all clinical samples of tissue, blood etc., taken from patients at the local doctor's office, are sent to remote laboratories for analysis. This is expensive and time consuming, increases patient anxiety, and it delays the start of possible treatment. Ideally, such analyses ought to be performed at the local doctor's office by using fully automatic and accurate micro total analysis systems (μTAS), a technology whose development was initiated in the early 1990's. The concept of

µTAS builds on performing all the necessary steps that are required for a chemical analysis, such as, sample preparation, chemical reactions, analyte separation, analyte purification, analyte detection, and data analysis, in an integrated and automated fashion on a miniaturized device.[5, 6, 7] The chemical analyses are preferably performed on inexpensive disposable microchips in order to cut down on costs of production and to avoid contamination issues. Another term widely used is lab-on-a-chip (LOC), which indicates generally the scaling down of single or multiple lab processes to a chip format. The goal is to achieve increased efficiency through smaller scales, and to undertake analysis that cannot be done conveniently by other means. Typical channel diameters are, usually, between, ten to several hundred micrometers, see Figure 1. Microfluidics deals with the behavior, precise control and manipulation of small volumes of fluids. The field of microfluidics has made it possible to facilitate with high accuracy, the handling of sample and reagents of extremely small volumes (smaller then a few picoliters).[8]
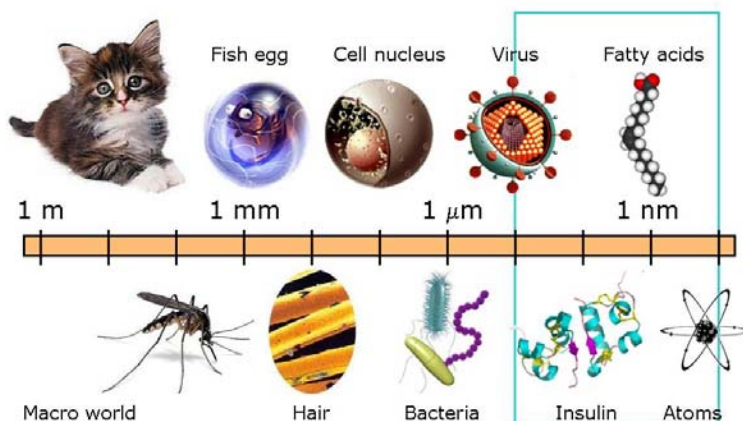
Figure 1 A perspective of the certain objects found in every day life related to size. The order of magnitude defined for nanotechnology lies within the blue rectangle. (The image is adapted form the Norwegian Research Council.)

There are several obvious advantages related to the miniaturization of biological assays.[9, 10] In general, key advantages of these microfabricated systems are:

- Complete automation (sample in – answer out)
- Reduced sample and reagent consumption, resulting in less waste
- Higher analysis control and efficiency due to short mixing times

- Better process control, because of a faster response of the system
- Increased sensitivity and specificity
- Online and real-time monitoring
- High throughput due to reduced analysis times and parallel sample processing
- Reduce the risk for carry-over contamination because of disposable chips
- Reduced exposure to hazardous samples and procedures
- Cost-effective disposable chips because of mass production
- Lower power requirements enable portable systems which can be used in the field
- Lower cost of analysis due to reduced amounts of expensive reagents
- Automatization of molecular assays eliminate manual handling standardizing the protocol which avoid variability between laboratories and within a laboratory

Clinical molecular diagnostics is predicted to be one of the most promising applications for these miniaturized LOC systems, in particular with respect to point-of-care (POC) testing.[11, 12, 13, 14, 15, 16, 17]

Scope and outline of this thesis

The purpose of this work has been to develop a microchip for amplification of mRNA, which can be used for diagnosis. The NASBA technology was chosen as the amplification method because it was well documented for analysis of clinical samples.[18, 19, 20, 21] This method has the advantage of being isothermal, thus avoiding the need for thermocycling at high temperatures, which is necessary in the case of a RT-PCR approach.

A microchip for amplification and detection of RNA can function both as a single unit chip, but also as a part of a larger integrated diagnostic POC instrument. A complete automatic diagnostic instrument would need a sample preparation unit which can receive and treat fresh clinical samples to obtain a pure solution of nucleic acids, which in turn, can be transferred to an amplification chip.

The work to develop a diagnostic microchip for mRNA analysis was approached in the following manner:

1. Downscaling of the NASBA reaction to the nanoliter level using silicon-glass chips and a custom-made optical system for fluorescent detection.

2. Development of a cyclic olefin copolymer (COC) chip in order to distribute one sample into parallel reaction channels for simultaneous parallel amplification of mRNA. The limit of detection (LOD) of cell lines and synthetic oligonucleotides were examined on microchips and compared to that observed in conventional systems.

3. Integration of NASBA reagents on the microchips was performed by deposition and drying in specific areas, to obtain fully automatic diagnostic systems.

In the following chapters a detailed description of the various techniques used in this work is presented. Chapter 1 briefly summarizes the transcription-based amplification technology and discusses the differences between RNA and DNA, and the significance of concentration in a clinical setting. An introduction to the µTAS technology is found in Chapter 2. Then follows short overviews of microchips currently on the market, choice of material, fabrication technologies, surface modification, storage of reagents, actuation, and detection mechanisms. Chapter 3 gives a summary of the 4 appended papers. In Chapter 4, the results obtained in this work are discussed. Concluding remarks and future perspectives are found in Chapter 5.

1 Background

Cancer affects more people than any other disease. About one third of the world population is likely to get this diagnosis during their lifetime. Human papillomavirus (HPV) is considered the etiological agent for cervical cancer, which is the second most common female cancer form world wide and the third most common cancer regarding mortality.[22, 23, 24] The activity of this virus has the potential to start the production of harmful proteins, which might stimulate growth of cervical cells which will, eventually, lead to the loss of cell cycle control. Cervical cancer is currently diagnosed by cytological methods, which have poor reproducibility and limited sensitivity.[25] A molecular based diagnostic LOC system, placed at the local doctor's office, would quickly identify multiple high-risk HPV mRNA transcripts of all women with persistent transforming infection with higher accuracy and reproducibility in comparison with conventional cytology. This work has focused on making microchips for detection of HPV which is the core knowledge of NorChip AS. However, the microchips are general detection platforms and the target to be analysed on the chip can easily be changed.[26]

1.1   RNA versus DNA

DNA molecules contain the coding sequences for RNA and protein molecules, of which the latter are the molecules actually performing the work in a biological system. Figure 2 shows the sequence of events from the genomic DNA in the nucleus of a eukaryotic cell to the synthesis of proteins in the cytoplasma.

RNA has the same coding sequence as DNA, but in contrast to DNA, RNA is either directly or indirectly involved in the processes of the machinery of a cell. Different RNA (*e.g.* tRNA, rRNA, siRNA, RNAi) molecules form three-dimensional structures that are directly involved in the regulation or activation of the biological processes in the cell. In contrast to DNA, mRNA, therefore, provides important information about the various activities of eukaryotic cells, bacteria and virii. Since ribosomal RNA (rRNA) can persist for long periods in dead cells, attention has turned to the use of mRNA as a marker for viability. Messenger RNA usually has a short half-life (seconds) within viable cells, due to rapid degradation by

specific enzymes (RNases) which are themselves very stable even in environments outside the cell itself.[2, 27] However, mRNA degradation can be dependent on the susceptibility of the transcript, or regions thereof. Synthesis of mRNA in viable cells may depend on the physiological state of the cells, so the targeted mRNA transcripts of genes should be constitutively expressed in all physiological states. By choosing RNA instead of DNA a higher number of molecules will be available to serve as targets. Even in cells with low levels of expression, the number of RNA copies will exceed the number of DNA copies. An exception to this rule is cells with integrated virus which is not transcribed and can only be detected after DNA amplification or by direct hybridization.
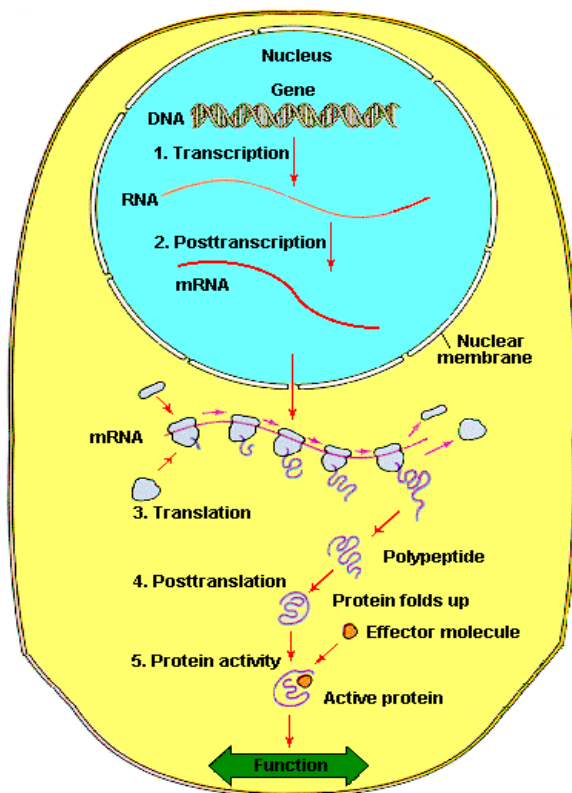
Figure 2 A schematic diagram of the fundamental processes from DNA to protein in a eukaryotic cell. DNA undergoes a transcription resulting in mRNA in the nucleus. The intermediated mRNA will again be translated to proteins by assembling amino acids resulting in polypeptide chains with the help of ribosomes and tRNA in the cells cytoplasma.

Proteins would give the most accurate clinical description of viability of the cells, but the use of a protein as target for routine diagnostics has the disadvantage of low sensitivity, reproducibility and specificity. In contrast, the main disadvantage using DNA as a target for routine diagnostics has been the lack of information about biological or clinical activity. During the last decades, microarray technology and varied amplification methods have shown that mRNA is a valid target for routine molecular diagnostics and for future POC testing.[11, 28]

Using mRNA as a target for routine diagnostics may provide information of clinical activity, regulation or processes, in addition to higher or equal sensitivity, reproducibility and specificity to DNA.

1.2   NASBA

NASBA is a transcription-based method which can amplify any RNA and single-stranded DNA (ssDNA) sequence isothermally (41°C), by the simultaneous use of the activities of the three enzymes; avian myeloblastosis virus reverse transcriptase (AMV-RT), ribonuclease H (RNase H) and T7 RNA polymerase.[29] A schematic diagram of the NASBA reaction is shown in Figure 3. Target sensitivity and specificity are dependent on the efficiency of the hybridization kinetics of the two primers, the molecular beacon probes, the three-dimensional polymer structures surrounding the target, and the quality of the target.[30, 31] However as a rule, more than $10^9 - 10^{14}$ antisense RNA molecules can be generated in about 1.5 hours.[29, 32, 33]

NASBA is highly specific for RNA and that only in the absence of target RNA or in case of an large excess (> 1000-fold) of DNA over RNA, can DNA be amplified in NASBA.[34, 35] The sensitivity of the assay decreases drastically when DNA is used as target as compared with the corresponding RNA. This indicates that even in the presence of identical amounts of RNA and DNA, the RNA will out-compete the DNA for the enzymes used in NASBA, due to the higher affinity for RNA. However, in general the reaction is not affected by double-stranded DNA (dsDNA) contamination.

Today, one of the most commonly used methods for mRNA detection is RT-PCR. This method makes first use of reverse transcriptase to produce RNA:DNA hybrids, which then is followed by a PCR amplification. The main product of this reaction is dsDNA. Using PCR, the number of molecules doubles for each step, and thus it requires approximately 20 cycles to amplify one million-fold.[29] With NASBA, however, 10 – 100 copies of RNA are generated in each transcription step, so fewer amplification steps are required to achieve a similar amplification rate. Consequently, both the total incubation time and the overall error frequencies are reduced with NASBA. Errors that are inherent in some enzymatic reactions (for example, reverse transcriptase) are cumulative, and therefore one would expect that fewer cycles reduce such errors. Consistently, samples with as few as ten molecules of input produce

positive results, and samples with even fewer input molecules (as determined statistically) are detectable. Thus, intron-flanking primers or DNase treatment is not required when mRNA or retroviral RNA is to be analyzed with NASBA, which in contrast is necessary for *e.g.* RT-PCR. DNase treatment, by itself, is not completely effective for all purposes, and the use of intron-flanking primers to distinguish between mRNA- and DNA-derived amplicons[36] is not suitable for prokaryotes.[37] In contrast to RT-PCR, NASBA is isothermal and does not require thermocycling. Microchips along with detection instruments can therefore be made less complex than for RT-PCR.

Figure 3 (a) Schematic diagram of the principle of NASBA. Due to the activity of AMV-RT, primer 1 (with a 5'-terminal T7 promoter sequence) is extended, resulting in a RNA:cDNA hybrid. Simultaneously, RNase H degrades parts of the RNA of the hybrid, which in turn makes possible annealing of the target specific primer 2 to the newly formed cDNA. Primer 2 is extended by AMV-RT, resulting in a double-stranded DNA (dsDNA) molecule with a functional T7 promoter. The T7 RNA polymerase recognizes and binds to the T7 promoter sequence and generate RNA transcripts complementary to the original RNA sequence.[38, 39, 40] The newly formed antisense RNA molecules are templates for the synthesis of dsDNA molecules, which again can be transcribed. At this step, the amplification process starts with primer 2, because the newly generated RNA template is antisense to the original target. (b) The amplification reaction is possible to monitor in real-time, due to the fluorescent light produced by the molecular beacon probes when they hybridize to the amplified antisense RNA.

1.3   Limit of detection

Reduction of the volumes in microsystems will decrease the absolute number of molecules available for detection. Hence, the microfluidic systems' ability to manipulate small volumes of fluid is one of the strengths, but also a weakness, because low numbers of molecules are more difficult to detect.[41] However, small volumes are not always suitable for diagnostic applications, due to the limited number of target molecules in the sample fluid. In Figure 4, a plot of sample volume versus analyte concentration (copy number) is shown, which indicates the minimum volume required for statistically significant detection of analyte.[42]
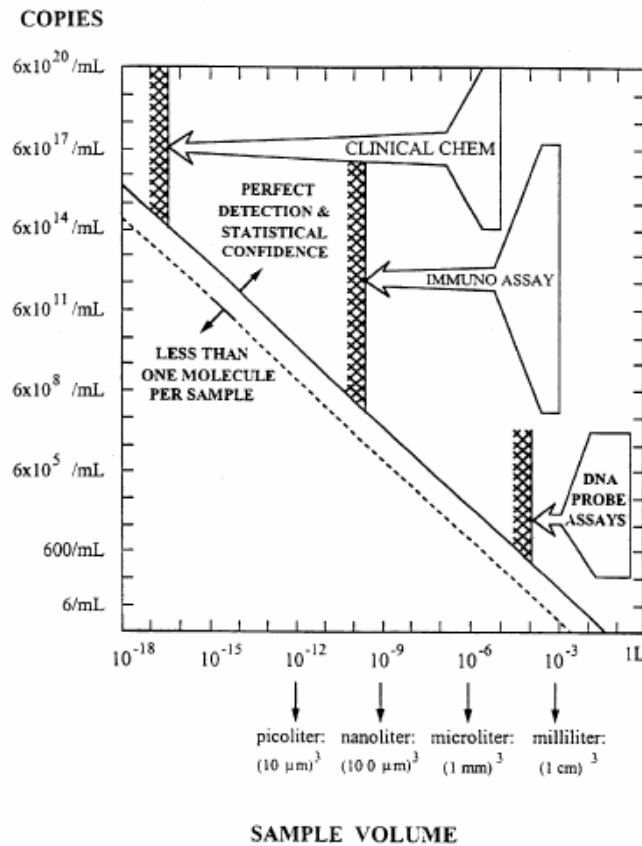
Figure 4 The minimum volume required for statistically significant detection of analyte. The plot shows sample volume versus analyte concentration (copy number).[42]

In the case of infectious diseases, bacteria may be present at less than 10 copies per milliliter of blood. For drinking water and food, only a few bacteria per liter or gram of food is sufficient to cause disease.[42] Therefore, the very nature of microfluidics devices makes sample

concentration a necessary task prior to detection in almost any LOC application to enhance the detection limit. Figure 5 and Table 1 illustrate the relation between fluid volumes, number of molecules within the fluid volume and the physical dimensions.
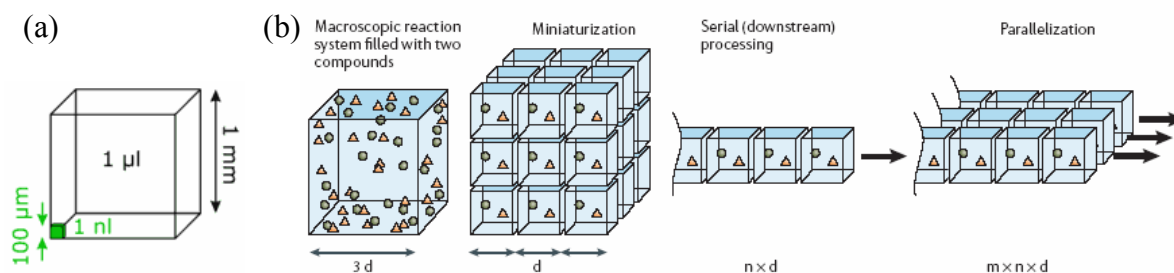
Figure 5 (a) Illustration of the relation between volumes and dimensions. (b) Miniaturization of a macroscopic reaction system.[43] d, length of edge; n and m, numbers of reaction systems serial and parallel, respectively.

Table 1 Volumes with correlating dimensions and number of molecules within the volume.

Volume	1 μl (10⁻⁶ l)	1 nl (10⁻⁹ l)	1 pl (10⁻¹² l)	1 fl (10⁻¹⁵ l)
Cube dimension	1 mm	100 μm	10 μm	1 μm
Number of molecules (1 μM solution)	6×10^{11}	6×10^{8}	6×10^{5}	600

The sensitivity of miniaturized chemical analysis systems usually depends on the obtainable detection limit which is mainly determined by capabilities of the detector of the system. Therefore, adequate, high-sensitivity detection techniques are indispensable in this field. In addition, it is important to have in mind that the detection limit of an assay generally is restricted by the background signal, *i.e.* the signal for zero analyte concentration.[44] The two key factors for choosing a detection method for microfluidic devices are sensitivity of the method and its ability to be scaled down.[45]

UV-visible absorbance detection is the most commonly used approach for detection in flow-based chemical analysis, whilst fluorescence detection is more commonly used in conjunction with microdevices.[45] Fluorescence differs in principle from absorbance, in that excitation and fluorescence occur at different wavelengths. In the case of fluorescence, one is no longer dependent on the ratio of the two signals at a single wavelength, but is instead looking for a signal of light at other wavelengths. In order to minimize signal-to-noise ratio the

excitation source and the detector are often placed in an angle, since spectral filtering not always is enough. The small dimensions of microfluidic channels limit the path length available for absorbance measurements, severely diminishing the sensitivity of absorbance measurement on-chip. For fluorescent measurements, the fluorescent signal of a single molecule is independent of the dimensions of the detection volume and remains constant.[46] However, the background signal that is generated by impurities in the sample, stray light, and scattering scales linearly with the size of the detection volume.[47] Optical detection requires an optical geometry consisting of a light source, lenses, filters, diffractive elements and detectors, making the instrument bulky. Consequently, efforts have been made to miniaturize this equipment and integrate micro-optical elements into microfluidic devices associated with optical detection.[45, 48]

Other labelled and label-free optical methods such as chemiluminescence, electroluminescence, absorbance, refractive index detection, radioactivity-based, Raman spectroscopy, surface plasmon resonance and thermooptics, as well as electrochemical methods of amperometry, conductimetry and potentiometry are also being studied within the field of microsystems.[48, 49, 50] Electrochemical detection has the potential to be very compact and fully integrated detection method within microsystems, because the analyte is detected by small and compact electrodes, and detection is dependent on electrode surface area rather than on available detection volume.[51] The limits of detection (in concentration terms) do not degrade as rapidly for electrochemical detection as they would for optical techniques. Electrochemical detection is generally attractive for this reason, however, they are far inferior in comparison to fluorescence in terms of sensitivity.[45] Additionally, mass spectrometric detection method schemes have been tested on-chip.[48] Detection technologies for miniaturization are being pursued by either downscaling existing methods or trying new approaches.[49]

When employing fluorescent molecular beacons in NASBA, rapid, specific and sensitive real-time RNA amplification are accomplished.[30] Other detection technologies would require post-NASBA detection and would increase the complexity of the microchip and instrument. In order to develop the simplest microsystem for the easiest operation, fluorescent detection was chosen.

2 Microchips

2.1 Status of microchips

Future LOC devices may revolutionize the way doctors diagnose disease and monitor treatment. Portable devices for rapid automated analysis of body fluids or tissue samples from sample preparation to data readout could be performed within minutes or even seconds. The electrophoresis chip, LabChip® from Caliper/Agilent is considered the first LOC product on the market (Figure 6a). A portable blood analyzer system, i-STAT, from Abbott Point of care is also available (Figure 6b).[52, 53] Cepheid has also launched the GeneXpert® which consists of a automated sample preparation cartridge and a thermocycler for PCR/RT-PCR with optical fluorescent detection in ~ 35 minutes (Figure 6c).[10, 54, 55] The microfluidics-based cartridge consists of multiple chambers that are designed to hold the biological sample in lysis buffer; purification and elution buffers; PCR/RT-PCR reagents, and to retain all sample-processing waste. Wet reagents[10] or lyophilized PCR reagents in bead form[55] are loaded manually into the cartridge reservoirs before the assay is performed, and all subsequent fluid movement within the cartridge is controlled by the software. The plastic cartridge has a large detection volume (80 µl) and can detect up to four different fluorescent colours.[10] Other companies engaged in the field to explore the potential of microfluidics include *e.g.*: Affymetrix, Agilent Technologies, Alderon Biosciences, Caliper Life sciences, Cepheid, eBiochip Systems, GenProbe, Idaho Technology, Nanogen, Nanosphere, Roche Molecular Diagnostics, HandyLab, Micronics, Gyros, Micronit, Motorola, Texas Instruments, Samsung and Philips.[56] Over the past years several companies have also been established to provide fabrication facilities and off-the-self solutions of microfluidic components.[57, 58, 59]

So far, many assays have been applied on chip, such as sample preparation, genotyping, sequencing, purification, separation, hybridization and amplification of nucleic acids, drug screening, and single cell manipulation. Several other diagnostic systems are being developed as well. Currently, one of the most common research areas of microfluidic devices is in connection with nucleic acid analysis.[11, 48, 60] Northrup *et al.*, in 1993, were the first to report on PCR on a microchip.[61] Since then, the implementation of PCR on chip has been accomplished using several different approaches. A thorough description of amplifying DNA

using different PCR approaches on chip can be found in the in the numerous reviews available.[62, 63, 64, 65, 66]

Figure 6 LOC on the market. (a) The electrophoresis chips, LabChip® from Caliper/Agilent.[52] (b) i-STAT blood analyzer from Abbot Point of care.[52] (c) Self-contained cartridges of the GeneXpert® system from Cepheid.

However, only a few groups have described simultaneous amplification and detection of mRNA by RT-PCR on chip.[67, 68, 69,70, 71, 72, 73] In the first studies of amplification of mRNA on chip, the material was removed from the chips for analysis after the reaction had taken place. The reaction volumes were also quite large, in the microliter range.[69, 70, 71] Recently, Marcus *et al.*,[72] on the other hand, have demonstrated a microfluidic chip assay with 72 parallel RT-PCR reactions with 450 pl reaction chambers and endpoint detection. The system was able to detect less then 50 β-actin transcripts from a total RNA template.

Only few reports describing the use of NASBA on microchips have been published. In addition to the work presented in this thesis, only Xtrana Inc. (Broomfield, CO) has presented data and a prototype of a fully automatic microchip-based system performing NASBA on chip.[74] The microfluidic card demonstrates sample preparation, nucleic acid extraction and amplification on solid phase material and lateral flow strip detection. The drawbacks of the Xtrana approach are relatively large reaction volumes (10µl) in addition to only one single target detection and no real-time detection, resulting in time-consuming analyses.

Researchers from Cornell University (Ithaca, NY) and Innovative Biotechnologies International, Inc., (Grand Island, NY) have used macroscale NASBA-amplified RNA sequences to generate material to be used as samples in connection with the development of a microfluidic biosensor for rapid identification of pathogenic organisms and viruses. In these experiments, the microchips do not perform any amplification on the chip. The biosensors have been based on fluorescence detection and bead-based sandwich hybridization and lateral-

flow assays.[75, 76, 77, 78, 79, 80] The methods require incubation with capture probes and magnetic beads extending the time with approximately 15-20 minutes.[77, 79]

2.2   Challenges of microchips

As for many other applied research fields, the expectations with regard to rapid commercial implementation of µTAS and LOC systems have been enormous, however, the expectations have not been fulfilled. Since the µTAS technology is relatively new, many challenges are still ahead and more research is necessary before microfluidics platforms can be used to adapt or replace existing macroscale assays. In general, it takes 10 – 15 years between the first scientific breakthrough until large scale commercial implementation.[58] In order for µTAS to become successful, the technology will require both a broad range of different types of components and subsystems, which need to be integrated into complete and functional systems.[81]

Miniaturization is more than simply scaling down well-known systems as the relative importance of forces and processes changes with scale. As the dimensions decrease, the ratio of surface area to system volume increases, and accordingly the relative importance of the surface forces. A fundamental rule for downscaling is that volume-dependent effects (length^3) often are of minor importance compared with surface-dependent effects (length^2). This gives rise to various effects, characteristic for the microscale flows. Microsystems feature laminar flow, where the viscous forces dominate inertial forces. Hence, turbulence is often unattainable so mixing only occurs through transport of molecules by diffusion. In addition to the familiar pressure-driven flows, fluid motion can be generated by taking advantages of capillary effects, electrical fields and magnetic fields. Microfluidic flows can be precisely controlled and manipulated to an extent not possible in the macroscopic world. At microscale, the temperature and the surface or interfacial tension of the liquids, the chemical properties of surface materials and the geometrical features of the channel walls have a large impact on microfluidic flow.

Some applications such as capillary electrophoresis greatly benefit from an increased surface area-to-volume ratio, while other applications do not. Phenomena such as adsorption become increasingly difficult to deal with in *e.g.* biological assays. Many analytical techniques

in molecular biology are highly sensitive to minor changes in the chemistry of the reaction and, therefore, pose a significant challenge in process scale-down to the microchip format. This is particularly the case in a multi-component reaction, where the concentrations of several components need to be maintained within a fairly small range. The behaviour of many biochemical bench-top reactions has been found to be quite different in the presence of inorganic reaction vessel materials and higher surface area-to-volume ratios encountered in microstructures than in macroscopic reaction systems. While the walls are usually assumed to play only a minor role in the latter, they play a significant role as a reaction component at smaller size scale. However, adsorption can in some degree be controlled by surface modification.

Evaporation usually poses a significant problem for microfluidic devices, although, evaporation can also be exploited for liquid pumping and sample concentration.[82, 83] In most cases, severe problems arise because of liquid loss. This effect is increased at elevated temperatures. The liquid loss can cause change in reagent concentration, complete disappearance of the reagents/sample or operational malfunctioning. By applying pressure on the system, ensuring tight sealing to avoid leakage and minimize diffusion lengths (dead volumes), less liquid will evaporate.

The main cause for gas bubbles in miniaturized chips is that air might be encapsulated while filling the device with liquid.[84] Encapsulated air bubbles usually alter the performance of the device and have to be avoided to get reproducible data. The filling can be disturbed by pinning of the liquid meniscus by surface roughness or impurities which can contribute to incomplete filling and result in trapped air. Since different fabrication methods produce different surface properties, it is important to consider the fabrication method with regard to surface roughness and chemical composition.

μTAS is a multidisciplinary field requiring knowledge of physics, surface chemistry, biology, instrumentation, fluid mechanics, fabrication technology and computer science. It is a challenge to get researchers to communicate and understand the significance of all disciplines in order to build useful and functional μTAS devices. Many future cases of μTAS will be results from the assembly of a microfabricated chips with conventional, possibly miniaturized, components such as pumps, valves, mixers, light sources, deterctors and electronics. The more elements that are miniaturized and integrated into microfluidic devices, the easier it will be to

develop portable instruments for POC technology.[45, 85, 86] However, complete integration of all elements on chip makes it complex, expensive and more prone to error if robust components are not being deployed. The concept of functional integration in μTAS, and all the accompanying advantages, must therefore be balanced against complexity, cost and feasibility. Another problem to solve is the interconnections and packaging of a final product.[43] For μTAS, this requires fluidic, mechanic, optical, and electronic interconnections. Complex engineering is necessary for efficient delivery of fluids into microfluidic systems, which rely on the creation of high fidelity of macro-to-micro interfaces. Furthermore, μTAS must be packaged so they can be handled safely without damaging the delicate microstructures on the chip.

Yet another obstacle which needs to be dealt with is on-chip reagents storage.[15,81] Long-term stability of reagents is required to ensure robust self-contained POC diagnostic systems. In order to be able to use the μTAS not only at the local doctors' office or at home, but also in the field, the reagents should withstand high storage temperatures as freezers or refrigerators not always are available.[15]

One important problem is that limited technology exist concerning sample preparation on chip.[81, 87] The samples might be dilute or complex (blood, saliva, faeces etc.) which in both cases would require special treatment before analysis. In order to isolate the target, large quantities of sample might be required which causes problems when the devices are small. Thus, the microsystems can easily be clogged due to the amount of large particles within the samples.

A significant challenge arising directly from the adoption of small volume systems is to efficiently detect analyte molecules. Detection is undoubtedly one of the primary issues determining the practicality and application of microfluidic systems.[49] Much attention has been paid on the development of miniaturized and sensitive detection methods. In order to obtain optimal detection conditions, stray light, scattering and autofluorescence etc. needs to be eliminated.

2.3 Fabrication of microchips

2.3.1 Silicon and glass versus polymers

Silicon is a well characterized material. It is unique, as it makes the combination of mechanical and electrical function in single devices possible. This permits the integration of thermal cycling devices (a good heat-dissipating substrate) or detection and control circuitry. However, the use of silicon poses some problems, due to optical opacity, cost, difficulty in component integration, and surface characteristics that are not well suited for biological applications. The use of glass instead of silicon in µTAS application is due to the unique properties of glass, *e.g.* resistance too many harsh chemicals, optically transparency, and its dielectric properties. Other advantages of glass are its hardness, high thermal stability, and relative biocompatibility.[88] It is possible to produce pure silicon chips, glass chips or chip hybrids consisting of both silicon and glass. Silicon- and glass-based microfluidic devices are well suited for chemical applications that require strong solvents, high temperatures, or chemically stable surfaces.[89]

Micromachining of silicon and glass involves the use of wet and dry etching, photolithography, and a variety of other techniques, all of which require the use of cleanroom facilities and equipment. This makes the production cost of these devices quite high, which limits their usage as disposable devices.

Recently, the use of polymers rather than silicon and glass chips has been exploited. Polymer-based microchips have emerged as inexpensive and disposable alternatives. The current trend for biomedical applications strongly points towards use of polymer-based substrates.[8] Many common plastics have been used for fabrication of microfluidic chips with excellent device-to-device reproducibility.[48, 90, 91] Polymers have numerous desirable advantages and characteristics as substrates for microfluidic devices. For example the raw materials and fabrication methods are relatively inexpensive. Methods exist which makes fabrication of polymer microchips quite fast and versatile and applicable to both prototyping and high-throughput production.[62, 63, 82, 88, 92, 93, 94, 95]

A key feature for many polymeric materials is superior biocompatibility (low non-specific binding) when compared to silicon and glassy materials.[92] Most polymers exhibit low surface charge which can be advantageous for several applications.[90] It is possible to obtain

flexibility and variation of the coating of the polymer with regard to chemical resistance against acids and alkalis that is superior to silicon substrates which can easily be etched away. The surface properties of polymers can be readily modified to meet the fluidic and/or biocompatibility requirements of a biochemical analysis system. Most detection methods within the biotechnological field involve optical measurements. The transparency of polymers is therefore a major beneficial feature compared to the non-transparent silicon. However, autofluorescence of certain polymeric materials in different regions of the spectrum might pose problems for optical detection techniques.[96] Polymer chips are disposable therefore cross-contamination can be avoided.

The disadvantage of most polymers is poor chemical resistance to non-aqueous solvents, and their surface chemistry can be difficult to control. Many polymers are hydrophobic and therefore the surfaces have to be treated specifically to avoid adsorption and to obtain capillary filling. Fabrication methods, as well as the polymer itself, along with various surface treatments, can influence the surface charge density and charge location.[90] Some plastics contain a number of additives that have an effect on their processing and shelf life. Such additives include fillers, plasticizers, stabilizers, antioxidants and UV stabilizers, which if leaked into the microfluidic network can inhibit certain biochemical assays.[90] Polymeric materials usually have low dielectric breakdown voltages, and the thermal conductivity of most polymers is much lower then for silicon and glass.

Sealing of the microsystems is critical and leaky channels are a frequent problem. Commonly used bonding procedures for silicon and glass chips are; anodic bonding, thermal fusion bonding and adhesion bonding.[88] Dependent on the method, the wafers can be bonded with or without using any adhesives. When joining the two wafers the surfaces must be ultra clean and flat. Precautions are therefore taken to ensure that there is no surface contamination or particles that could prelude a good bond. The bonding procedures often require high voltages (200 V – 1000 V) and temperatures (180°C – 1000°C).[51, 97] As for silicon and glass chips, polymer chips have to be sealed to enclose a complete microsystem. Several methods are available for this purpose. Many polymers are thermally bonded at temperatures above their glass transition temperatures (T_g), the temperature at which the polymer begins to soften. However, elevated temperatures cause destruction of the microstructure elements. Another bonding method uses solvent to wet the bonding surfaces. In solvent welding the surfaces of

18

both polymer parts are slightly wetted and, thus, loosened using specially tailored solvent mixtures. A drawback of this technology is that all surfaces – also the microcapillary structures are entirely exposed to the solvents used. Adhesive bonding uses an intermediate layer to "glue" the substrates. A number of epoxies, UV-curable epoxies and photoresists can be used for adhesive bonding. Also in this case it is difficult to prevent the glue from flowing into the channels by capillary action. Polymer tapes with a pressure sensitive adhesive layer can be used as well. Laser welding is a localized thermal bonding process, in as much as the interface between polymer chip and lid is briefly melted and then cooled again. This technique requires that the polymer chip absorb the laser energy and that the lid is transparent.

Choice of material depends on the application (*e.g.* biocompatibility and optical smoothness). Plastics are appropriate for the channel structures, glass for optical windows, and silicon for high-level electronic functionality.[98] In addition to the more traditional materials, biomaterial and artificial materials, such as calcium alginate, gelatine, biodegradable thermoplastics, photocurable "liquid" Teflon, silicon elastomers, thermoset polyester, and acrylic copolymer have been tested as well.[99]

In the present work, both silicon-glass chips and cyclic olefin copolymer (COC) chips have been tested. As the goal is to produce disposable microchips, most of the tests are performed on polymer. COC has excellent optical properties, which are advantageous for fluorescence-based biochemical analysis due to low autofluorescence and other bio-optical applications. Their light transmittance extends through the visible spectrum into the near UV. They withstand all common sterilization regimes, including gamma radiation, steam and ethylene oxide. They are highly pure and have excellent water-vapour barrier properties and low moisture absorption.[100] In addition, COC has properties well suited for production such as good material flow, low shrinkage and high glass-transition temperatures. COCs are good electrical insulators, with relatively constant electrical properties over a wide range of temperatures and frequencies. Most metallic films exhibit excellent adhesion to the COC material and it is resistant to aqueous acids and bases, as well as most polar organic chemicals such as acetone, methanol, dimethyl sulphoxide (DMSO), and iso-propyl alcohol.[95] However, COC are disturbed by aliphatic and aromatic hydrocarbons, and should not be exposed to solvents such as hexane and toluene, and certain oils and fats.[100]

The COC surfaces are inert and native COC exhibits a contact angle of ~92˚ with water.[95] However, plasma treatment can be used to modify the surfaces of COC substrate to obtain better biocompatibility characteristics. The desirable combination of mechanical, optical, and chemical properties makes COC currently one of the best commercial candidate materials for the mass production of microfluidic chips, in spite of the fact that it is quite expensive compared to the other polymers.[91]

2.3.2   Microfabrication methods

Micromachining technologies have traditionally been silicon-based, due both to the role of this semiconductor in IC technology and its excellent mechanical properties. Today the manufacturing of microfluidic chips has grown into a field of it own, with constant improvement of chip material and fabrication techniques.[99] Microfabrication makes it possible to reproduce the same carefully designed μTAS several times with the same specifications. As a general rule, the choice of fabrication method is determined by several factors, such as available technologies and equipment, cost, speed, fabrication capabilities (*e.g.* desired feature size and profile), and the preferred material substrate. In the present work, five methods were used. Silicon microchips were fabricated using the deep reactive ion etching (DRIE) process developed at Bosch, while the COC polymer microchips were manufactured by milling, laser ablation, injection moulding, and hot embossing. Table 2 gives an overview of some typical characteristics over the microfabrication methods used in this work with regard to the silicon chips and the COC polymer chips.

The DRIE process produce nearly vertical sidewall features. Depending on the process parameters, only slight scalloping of the sidewall will be generated due to the alteration between etching and passivation. When high-aspect ratio (depth:width > 1) and optical smooth surfaces are desired, DRIE is the method of choice.[51] However, the manufacturing of silicon microstructures for applications in μTAS by the DRIE process is an expensive and not very flexible process, quite large volumes are required for each microchip and thus not suited for rapid prototyping of test-devices. The technique is, however, well adapted for large-volume production of commercial products.

Milling cuts polymer material mechanically and computer numerical control (CNC) controls the position and movement of the cutting tool. This makes the milling process flexible

and it is easy to change the design quickly. With CNC milling it is not possible to achieve very small feature sizes, structures with sizes down to 100 μm are typical.88 Low surface roughness in the nanometer range can be obtained under optimized conditions.101 Normally, surface roughnesses of 2 – 10 μm are obtained, Table 2.

Laser ablation involves the use of a high-powered pulsed laser to remove material from a sheet of thermoplastic. In addition to pulse energy, the depth of the ablated channel is also dependent upon the pulse rate and the absorption characteristics of the substrate. Depending on the laser setup, channels can obtain a Gauss distribution. In other cases the channel bottom can be flat, however, overlapping ablation tracks may result in grooves. Laser ablated areas may also result in melted surfaces with large surface roughness. Generally, laser ablated channels have greater surface roughness than imprinted, hot embossed or injection moulded channels. The degree of roughness is highly dependent on the absorption of the polymer at the exciment wavelength. The smallest feature size attainable strongly depends on the quality of the optical system and the laser wavelength. Laser ablation is therefore advantageous for prototyping purposes due to being a direct technique, not requiring any die.[48, 96]

Laser ablation has the capability to modify the surface of channel walls concurrent with microchannel formation. Many reactive species are formed both at the polymer surface and in the gas phase during the laser ablation process. The incorporation or reaction of these ablation products at the nascent channel walls can result in surface chemical functionality that is significantly different from that in the bulk of the polymer.

Both injection moulding and hot embossing requires a die. The die can be made with CNC metal micromachining, electroplating or silicon micromachining. The production of dies is quite time-consuming, and therefore, dies do not offer a convenient method for changing of designs.[89] Considerable effort is put into the design of molded parts and their die, to ensure that the parts will not be trapped in the die, and that the die can be completely filled during the process. The quality of the replication depends on the quality of the fabricated dies.[48] The die can be used many times depending on its mechanical strength which is dependent on the material used. Both injection moulding and hot embossing can reproduce structures with features as small as a few nanometers.[88] Limitations of injection moulding for microfluidics include resolution and material choices. Injection moulded microchips can be ready in only 1-3 minutes and, thus, suited for large-volume productions.[102] However, making only a few

test chips with this process is quite expensive. On the other hand, hot embossing is fairly straight forward, as well as inexpensive, offering low cost devices, provided there is access to the necessary hydraulic press equipment and a patterned die. An overall cycling time of the hot embossing process is in the order of 5-7 minutes.[102] A wide variety of polymers have been successfully hot embossed. The microchips produced from hot embossing are usually one-layer planar structures.[48]

Table 2 Overview of various microfabrication methods with some of their characteristics. All values are for fabrication of COC chips (provided by IMM, Mainz, Germany).

Method	Material	Feature size	Roughness	Aspect ratio	Rapid prototyping	High-throughput	Large volumes
Deep reactive ion etching[1]	Silicon, glass	~5 μm	< 10 nm	20-30	-	+	+
Injection moulding[2]	Thermoplastics	100-200 μm	0.3 μm with polished die	1-2 for 100-200 μm channels[3], 5 and more for larger channels[3]	-	+	+
Hot embossing[2]	Thermoplastics, elastomeres	~100 μm	0.3 μm with polished die	1-2 for 100-200 μm channels[3], 5 and more for larger channels[3]	+	-	-
Milling	Metal, glass, thermoplastics	~100 μm	typically 5-10 μm, with liquid cooling ~2 μm	for 100 μm mills: 1.5, for 200 μm mills: 2; for 300 μm mills and larger 5 and more	+	-	-
Laser ablation	All solids and liquids	10-20 μm	0.5-0.8 μm for small channels, > 5 μm for larger channels due to pulse rate	1.5-2 for small channels, more for larger channels	+	+	+

[1] – Silicon as the material

[2] – Requires mould made by milling, electroplating or micromachining

[3] – For milled moulds

2.3.3   Surface modification

Early work on silicon-glass and later polymer PCR microchips revealed the surface biocompatibility issue.[9, 103, 104, 105, 106, 107, 108, 109] For most microfluidic systems with biological applications, the surfaces are modified toward minimizing non-specific interactions, especially for proteins and cells. Proteins tend to adhere onto hydrophobic surfaces. Native silicon and most of the commodity polymers available are hydrophobic.[91] For a surface to be effective at protein rejection, the surface coating must be heavily hydrated, hydrophilic or neutral, densely packed, and conformational mobile. Neutral surfaces minimize electrostatic interactions, while highly hydrophilic surfaces minimize hydrophobic interactions. Hence, neutral and hydrophilic polymers have minimal or weak interactions with most globular proteins.

The surfaces of the microchips are important for microchip functionality and uniform surface treatment of complex shapes and geometries are therefore essential for microfluidic systems and for the biomedical applications therein. Surface modifications can be divided into two broad categories: 1) chemically or physically altering the atoms or molecules in the existing surface (*e.g.*, plasma activation and laser ablation), or 2) coating the existing surface with a material having a different composition.[110] A major challenge in surface modification is precise control over functional groups. Many surface modifications schemes produce a spectrum of functional groups such as hydroxyl, ether, carbonyl, carboxyl, and carbonate, in contrast to the intended functional group. However, charge density and charge location can be controlled in some degree by several parameters including (1) choice of polymer material, (2) fabrication protocol and (3) various surface treatments. Stability of surface chemistries and structures can change over time in response to the external environment. The driving force for these surface changes is the minimization of the interfacial energy.[110] As a result of unspecific adsorption, the surfaces capture compounds from solution passing through the channels, changing their concentration in solution. Any molecules deposited on the wall of the channel will also change the character of the surface. Analyte adsorption is a parameter that is highly dependent on several material characteristics including hydrophobicity and surface charge.[90] A specific concern for material used in optical devices is that the surface modification does not induce cloudiness or haze into the material.

Coatings used to modify the surfaces are mainly categorized as static or dynamic.[62, 111, 112] The static coatings can be covalently bonded to the surface, or physically

24

adsorbed relying on either hydrophobic interaction or hydrogen bonding or combinations thereof. Static coatings are applied in the fabrication of the chip before starting the microfluidic assay. For most silicon microchips a thin layer of silicon dioxide (SiO_2), which will function as a static coating, is deposited on the surfaces. Several publications have shown that SiO_2 layers are sufficient for enhancement of *e.g.* PCR.[9, 103, 104, 113] Silanization (*e.g.* with SigmaCote™) is another widely used process to prevent adsorption in silicon/glass microchips.[103, 113, 114] Of interest is that though silanization has been successfully applied to microfluidic devices, criticisms regarding the reproducibility of such coatings have been argued.[113]

Proteins such as bovine serum albumin (BSA) adsorb physically on to a large range of materials and can be used in microfluidic chips to make biocompatible surfaces.[115, 116] BSA is often used as a blocking agent to prevent non-specific binding within common biological assays such as for immunoassays (*e.g.* enzymed-linked immunosorbent assay, ELISA). Another approach of surface passivations is by using polymers such as polyethylene glycol (PEG),[113, 117] polyacrylamide, parlyene[69, 118] *etc.* PEG coated surfaces are one of the most successful ways to resist protein adhesion and biological attack. PEG is also known as polyethylene oxide (PEO), polyoxyethylene (POE) and polyoxirane.[119] PEO is the same polymer as PEG, but PEO typically signifies a larger molecular weight. PEG refers to molecular weights of less than 25 000 g/mol. PEG molecules can exhibit many forms. They can be linear or highly branched polymers, be covalently bound or physically adsorbed. PEG appears to be the most mobile, the most dynamic and the least interactive of all neutral and hydrophilic water-soluble polymers readily available.[120] The ability of PEG coated surfaces to prevent proteins and other biomolecules to adsorb at the surfaces are probably due to its unique solution properties and molecular conformation in aqueous solution.[121] It has an inert character which exposes uncharged hydrophilic groups and show very high surface mobility.[120] PEG will exhibit non-polar conformations near hydrophobic surfaces, leading to a more densely coated material, and will exhibit polar conformations far from the hydrophobic surface.[122] Thus, PEG surfaces usually consist of long PEG chains that protrude out from the insoluble surface into an aqueous solvent. Proteins and other biomolecules are prevented from approaching a PEG-coated surface because of an enhanced steric stabilization force. There are two main contributors to this repulsive force: an excluded volume component and a mixing

interaction component. The former is an elastic response from the loss of conformation entropy. When a protein gets close to a PEG-covered surface, the available volume for each polymer is reduced, and consequently, a repulsive force is developing owing to loss of conformational freedom of the PEG chains. The second is the osmotic interaction between the protein and the PEG-covered surface. In this case, the number of available conformations of PEG segments is reduced owing to either compression or interpenetration of the protein chains generating an osmotic repulsive force.[119, 121]

Dynamic coatings are introduced with the sample in the microsystem.[62, 64] Presumable, these substances will spontaneously migrate and adsorb to the inner surface of the microchip and prevent binding by components of the sample or reagent mixture. The most frequently used dynamic coating include proteins such as BSA[115, 123, 124, 125, 126] polymer solutions (PEG, polyvinylpyrrolidone (PVP))[107, 108, 109, 113, 126] and the non-ionic surfactant Tween 20. BSA is often included into reaction solutions to stabilize polymerase enzymes in addition to reduce undesired adsorption of the polymerase onto the inner surfaces of the reaction chamber. Excess enzyme often serves the same function as BSA, providing additional protein which stabilizes the enzyme and balances any negative effects arising as a result of enzyme interaction with solid surfaces and/or air-liquid interface. BSA may prove to be insufficient if the volume of the reaction chamber is in the low-microliter to nanoliter scale.[113] Dynamic passivation using polymers and proteins are attractive because they are inexpensive, and the coating procedure adds no additional steps into either microchip fabrication or the overall assay procedure.

It is important to note that these two passivation methods are not mutually exclusive. Hybrid coatings combining dynamic and static coatings are often used.[62, 64] For instance, combinations of silanization-BSA,[127] SiO_2-BSA,[105] SiO_2-PEG/PVP[109] as well as BSA-BSA[115] have been demonstrated. Covalent bonded coatings exhibit longer lifetimes than the physically absorbed dynamic coatings. However, dynamic coatings are usually easier to prepare.

In the present work, BSA has been used as dynamic coating in all chips. In addition, SigmaCote™, SiO_2 and PEG have been used for surface coatings.

2.4 Reagents on microchips

2.4.1 Inhibition and contamination

The main disadvantage of all amplification assays is the susceptibility to contamination of samples. The accuracy of nucleic acid based assays depends on the awareness of risk factors and the proper use of procedures for prevention of contamination. Reaction inhibition can be total or partial, and can become visible as complete reaction failure or as reduced sensitivity of detection. Inhibition of nucleic acid amplification reactions is typically caused by inhibitors interfering with the cell lysis necessary for extraction of nucleic acids, by nucleic acid degradation or capture and inhibition of enzyme activity. Inhibitory factors include organic and inorganic chemicals, detergents, antibiotics, buffers, enzymes, polysaccharides, fats and proteins.[128] However, their modes of action are not yet fully understood. Sources of contamination are diverse including water, reagents, disposables, equipment, sample carry over, amplicons, and environment.[128, 129]

False negative results may be obtained if clinical samples contain substances which inhibit the amplifications enzymes. It is, therefore, of extreme importance to try to reduce the amount of inhibition in these assays trough proper sample preparation. The quality of the assay depends on how the sample is taken, and how the sample material is handled and processed before analysis takes place. It is of importance that the targets of interest are not destroyed before performing the analyses. In most cases, the sample preparation step is the most difficult part of the procedure and the end result will strongly depend on the quality of this step. Therefore, it is crucial to inactivate enzymes like RNases and DNases in the cell sample during sample preparation as these enzymes will degrade the sample and subsequently inhibit the amplification.[130, 131] Equipment used in reagent preparation or production of microchips should be treated aseptically in order to minimize the chance for contamination and inhibition due to these enzymes or other compounds influencing the amplification. Cross-contamination caused by as few as only one contaminating amplicon or organism in the reaction mixture can produce false positive results. Suboptimal reaction conditions can influence the result obtained. By including both positive and negative controls, the integrity of the results of the assay will be maintained.

Miniaturization of the reaction volumes changes the environment in contact with the reagents, causing phenomena (*e.g.* adsorption) which are not a problem in the conventional microtitre plates. Accordingly, adsorption of crucial reagents from the reaction mixture must be prevented.

2.4.2   Adsorption of proteins

As mentioned earlier, protein adsorption is a major problem in microchips. When proteins in solution are in contact with another phase with which it is immiscible, protein molecules tend to accumulate at the interfaces between the two phases.[132] Protein adsorption is triggered by chemical and physical phenomena related to the surface materials and the surrounding medium in contact with them. The reduction in interfacial free energy is the main driving force for adsorption. Biocompatible materials reduce protein adsorption by minimizing the interfacial free energy between the surface and the solution.

Globular proteins are more or less spherical, with molecular dimensions in the range of a few to a few tenths of a nanometer. Proteins consist of amino acids which exhibit a wide variety of side chains which can be acidic, basic and have large variation in polarity. The protein itself has loops, tails, helices, and sheets that can make their way through coating layers and interact with the substrate below, Figure 7.[120]

(a)   (b)
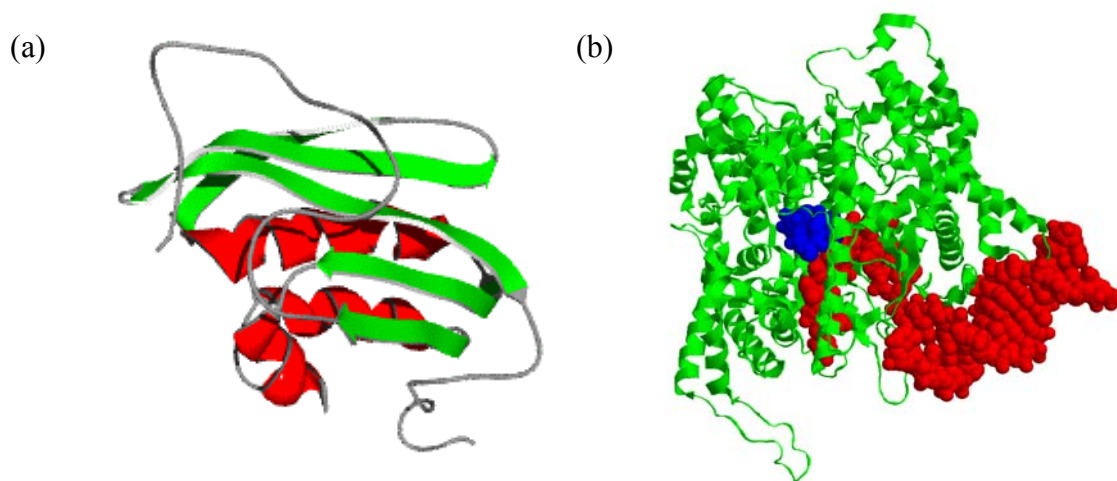
Figure 7 Proteins contains loops, tails, helices and sheets. (a) HIV RNase H. The green arrows represents sheets, red is helices and the grey is loops and tails.[133] (b) T7 RNA polymerase. The T7 RNA polymerase (green molecule is bound to a dsDNA (red) and producing mRNA (blue).[134]

The hydrophobic effect is considered to be the major driving force for the folding of globular proteins. It results in the burial of the hydrophobic residues in the core of the protein, shielding these groups from contact with water. Charged groups are predominantly found on the surface of the protein in contact with water. However, the smaller the protein molecules are, the larger the deviation from sphericity it will be. Small protein molecules are more often asymmetrical and tend to have a relatively more hydrophobic surface than larger and more spherical molecules.[132] In general, hydrophobic areas on globular proteins are small and limited in area.[121] The groups on the surface of a protein are the ones most likely to interact with a solid surface, although interior groups might be exposed through conformational changes. Proteins adsorb to most interfaces due to a large repertoire of intermolecular interaction between proteins and surfaces.[120] The major interactions that drive the interfacial activity and adsorption of proteins are the water structure-driven hydrophobic effect, electrostatic interactions, and strong hydrogen-bonding interaction characterized by cooperative, multiple hydrogen bonds.[120] It has been reported that hydrophobic surfaces adsorb more protein than hydrophilic ones, and that dehydration of hydrophobic surfaces promotes protein adsorption from aqueous solution.[135] It is assumed that protein adsorption is related to the number and size of the hydrophobic patches on the protein's exterior and that the surface adsorption of proteins increases with hydrophobicity and size. Transferring a protein molecule from an aqueous solution to an interface involves a change in the environment, and this process may induce structural rearrangements.

Electrostatic repulsion between surface and protein does not always prevent adsorption. Charge antagonism can effectively be annihilated by co-adsorption of low-molecular-weight ions from solution. The complex surfaces of proteins in combination with the fact that many real surfaces are heterogeneous, complicates the prediction of how a protein will interact with a surface.

Protein adsorption takes place at a timescale of seconds to a few minutes.[120, 136] Changes in conformation can occur immediately upon adsorption, but time-dependent conformational changes also occur. Orientation of proteins on the surface can vary. Protein adsorption is often apparently irreversible or only partially reversible by dilution, although there are examples of reversible adsorption. The desorption process depends upon the incubation time of the protein with the substrate: the longer the incubation time, the slower the

desorption.[137] The desorption can be affected by changing the pH, increasing the ionic strength or by introduction of a complex agent.[138] Although the protein may be irreversibly adsorbed with respect to dilution, it still can be exchanged by protein molecules in solution, or by low molecular-weight compounds. The amount of a protein that a given surface will adsorb depends on the solution it contacts, especially the protein content of that solution, the amount of other proteins present, the history of the surface with respect to protein contact, as well as conditions such as flow.[139] The protein-surface interaction appears to contain a large number of time-dependant or dynamic phenomena in addition to normal kinetic constrains caused by the diffusion of protein molecules to the solid surface.[140]

2.4.3   Protectants and reagent stability

In this work, NASBA reagents from the PreTect™ HPV-proofer kit (NorChip AS) were used. The kit contains all reagents needed to perform an amplification reaction. It consists of lyophilized reagent spheres, lyophilized enzyme spheres with their respective diluents in addition to a stock solution of KCl. Lyophilization is considered one of the best methods for stabilization of certain reagents for long-term storage. The lyophilized spheres need to be dissolved before reaction. In order to make a self-contained microchip, which ensure long-term stability of the NASBA reagents, the dissolved reagents needed to be spotted and dried in the reaction chambers on the microchip. However, it is not possible to dry all the reagents in the NASBA mixture. Thus, these reagents have to be introduced into the reaction mixture through the sample. To stabilize the enzymes during the drying step on the microchip is considered the most critical step in the process.

The NASBA amplification technology depends on the simultaneous activity of three different enzymes: AMV-RT, RNase H and T7 RNA polymerase.[29] Shortly, AMV-RT is a RNA-dependent DNA polymerase that catalyzes the polymerization of DNA using template DNA, RNA or RNA:DNA hybrids. The molecular weight of the avian enzyme is 160 kDa and the enzyme consists of two polypeptide chains.[141] The enzyme requires a primer (DNA primers are more efficient than RNA primers) as well as Mg^{2+} or Mn^{2+} for polymerization of DNA, and it possesses an intrinsic RNase H activity. AMV-RT is optimal at 42°C, however, it is stable at higher temperatures (37 – 58°C) as well. The optimum pH for the avian enzyme is

8.3. The length of the cDNA synthesized by AMV-RT is greatly reduced when reactions are carried out at a pH that differs from the optimum by as little as 0.2 units.

RNase H is a non-specific endoribonuclease which hydrolyses the phosphodiester bonds of the RNA moiety in DNA:RNA hybrids. A minimum of 4 base pairs (bp) in a RNA:DNA hybrid is required for activity. The enzyme does not hydrolyze single- or double-stranded DNA. RNase H is a monomer of 17.6 kDa[141] which contains two domains, one of which has a Mg^{2+}-binding site enmeshed in β-strands. The enzyme is inactivated after 20 minutes at 65°C.

T7 RNA polymerase is a DNA-dependent RNA polymerase that recognizes and initiates synthesis of RNA on double-stranded DNA templates that carry the appropriate T7 specific promoter. The RNA polymerase has extremely high specificity for its 25 bp cognate promoter sequence. The T7 RNA polymerase has a molecular weight of 107 kDa[141] and the optimal activity is in the pH range of 7.7 – 8.3. Full activity requires Mg^{2+}, a DNA template, T7 promoter and all rNTP. The T7 RNA polymerase gives rise to 100 – 1000 specific RNA molecules.[39, 40] The RNA produced when using the T7 RNA polymerase is biologically active as mRNA.

Macromolecules, especially proteins and polypeptide-containing compounds commonly exist in their native state as a complex, three-dimensional folded structure, the tertiary structure. Often, the activity of the enzymes is critically dependent on the tertiary structure and is severely reduced or even eliminated if the structure is denatured. Enzymes are usually unstable in aqueous systems at room temperature and needs to be stored frozen. As mentioned previously, lyophilization is also considered to be one of the best methods for stabilization of fragile enzymes for long-term storage. During lyophilization water is removed from a frozen sample by sublimation and desorption. However, the lyophilizing process of *e.g.* enzymes is not trivial. The enzyme structures are easily distorted during the freezing and drying processes. Cryoprotectants can protect the enzyme from denaturation during the freezing process, while lyoprotectants can prevent protein inactivation during drying. By mixing stabilizing protectants with the enzymes of NASBA before spotting and drying, improved long-term storage stability is possible.[142]

Cryoprotectants protect molecules against stress such as shearing, caused by the formation of crystals during the freezing process. Cryoprotectants protect largely by

preventing large ice-crystals from forming. Commonly used cryoprotectants are DMSO, sorbitol and glycerol. However, it has not been possible to employ these compounds in this work, since they tend to form a hard crust instead of a powder during drying. The NASBA reagents include both DMSO and sorbitol; however, these compounds have to be added in the reaction mixture together with the sample.

PEG is another cryoprotectant widely used. It stabilizes enzymes during freezing, due to preferential exclusion of PEG from the enzyme's surface because of steric hindrance.[143] Increasing the concentration of the protectant will increase the stability of the enzyme during freezing. However, PEG is an extremely strong protein precipitant and should not be added in too high concentrations.

Lyoprotectants stabilize and support enzymes during the drying process. In general, drying results in a decrease of both α-helix and random structures and an increase in β-sheet structures.[142] Lyophilization in the absence of stabilizers has been observed to induce significant conformational changes on enzymes.[144] The most common lyoprotectants are sugars (*e.g.* trehalose, sucrose, lactose) and polyols (*e.g.* mannitol). While trehalose seems to be the most commonly used lyoprotectant, other compounds like sucrose, mannitol, and lactose are also effective. The amount of trehalose necessary to preserve activity is proportional to the concentration of enzyme.[145] It is possible to preserve sensitive macromolecules by drying at ambient temperature and at atmospheric pressure in the presence of trehalose. The unique properties of trehalose in preserving the structure and function of proteins such as enzymes and antibodies, and other macromolecules in the dry state, is due to hydrogen bonding of trehalose molecules via their hydroxyl groups, to appropriate groups on the macromolecule. Trehalose substitutes the structural (bound) water molecules so that there is no collapse of macromolecular structure upon drying.[146]

Polymers such as PVP and BSA have been reported to protect multimeric enzymes against inactivation by inhibiting dissociation during freezing and drying.[147] The polymers can stabilize the quaternary structure by inhibiting dissociation in the frozen solution, during the initial phase of the sublimation step of lyophilization.

In the present work, PEG, trehalose, PVP as well as BSA have been tested with regard to inhibition of the NASBA reaction and preservation of enzymes during the drying process.

2.4.4   Storage of reagents on microchips

For fully automatic µTAS devices without protocols, it is required that all reagents necessary for complete analysis can be stored on the microchips for a prolonged period of time. At present, the reagents are typically introduced in the reaction chamber via interconnections from *e.g.* large syringes, pumps or by larger local reservoirs on chip.[115, 148] However, a couple of new storage microfluidic cartridges preloaded with wet reagents have been reported.[55, 149, 150, 151] By drying and storing the reagents directly in the reaction chambers of the microchips, one can reduce handling time and contamination risk. So far, only a few examples of microfluidic systems have been described with dried proteins incorporated in a microchip.[152, 153] Storage of reagents on microchips require several process steps; dissolution of lyophilized reagents, spotting, drying, sealing and storage.

The easiest way to introduce reagents on chip is by applying the reagents as liquids. As precise dispensing of liquids in the range below one microliter has become increasingly important in the chemical, biological and pharmacological industries, several devices are available. The driving force for the development of technology for spotting of small volumes has come through the expansion of the microarray field.[154, 155, 156] More recently, new methods and devices for reagent dispensing have been developed to meet the increasing interest in miniaturization of biological and chemical assays. These testing platforms demand precise metering of the smallest amounts of reagents on planar substrates or in cavities. Today very sophisticated spotting systems can create regular arrays or arbitrary spotting patterns of many thousands of different substances on an area of a few square inches, depending on the instrument used. Commercially available dispensing robots typically can dispense volumes of 50 nl or more per droplet or dispense cycle. Microfluidic devices, on the other hand, may be able to support fluid volumes even within the smaller picoliter range.[157, 158, 159, 160, 161, 162]

Two main spotting techniques are presently available; contact spotting and non-contact spotting. The contact spotters are based on pins, rings or tips. The printing head characteristics determine the probe spot quality and reproducibility.[163] In addition to the properties of the spotted liquid, the hydrophilic or hydrophobic properties of the substrate determine the size and the shape of the spot. The drawbacks of pen-like devices for patterning surfaces are the lack of control after deposition of the material, problematic drying and mechanical wear.[44] Contact spotters are useful in dispensing volumes from typically slightly under a nanoliter to

several nanoliters.[164] Additionally, the physical contact between the metallic (or composite material) spotter tips and the surface can denature delicate proteins and are therefore in many cases not recommended for the spotting of proteins.[165] Such spotters can also damage the surface via physical scratching. Nanoliter spots have a tendency to evaporate quickly. To minimize such effects, glycerol might be added to protein solutions during the spotting step. However, while this solution minimizes the evaporation effects, it dramatically increases the viscosity of the sample solution leading to surface tension effects that might make delivery difficult.[165] Capillary and adhesive forces at the tip can result in large errors when moving into the nanoliter range and provide a risk of cross-contamination.

The non-contact spotters are based on solenoid, piezo, ink-jet, microfluidic devices and laser principles. Non-contact spotters give a high level of reproducibility since the droplets spotted always have the same size, and it is therefore easier to dispense reagent solutions of different composition.[164] Some of these spotters are also capable of making very small droplet sizes, even in the picoliter range.[157, 164] Aqueous reagent solutions can easily be positioned at substrates with hydrophobic areas due to the surface tension obtained on the hydrophobic surface.[163] The spotted aqueous droplets will only marginally spread out. Non-polar solutions, on the other hand, will wet hydrophobic surfaces quite well. However, such surfaces are not preferred in all cases as proteins tend to adsorb to hydrophobic surfaces and become inactive. The spreading on hydrophilic surfaces will also depend on the wetting properties of the spotted reagents. Non-contact spotters are generally recommended for the spotting of proteins on surfaces.[161] Such spotters have low mechanical load on the liquid to be spotted and as a result, the kinetic energy of the delivered liquid is low.

Several methods exist for drying biological material. Air drying and freeze-drying are two commonly used methods. Air drying is the simplest form of drying at ambient pressure. However, it usually requires elevated temperature or long periods of time, and the effects of surface tensions and the long timescale over which drying occurs, tends to result in severe irreversible denaturation of sensitive biological reagents. Freeze-drying is the method of choice for preserving biological and pharmaceutical products.[142, 154] The water content is reduced to values that will no longer support biological activity or chemical reactions. Furthermore, the porous structure of the 'cake' achieved by freeze-drying allows for extremely rapid reconstitution of the sample. Other drying methods may produce an impermeable 'skin'

in the top layers of the dried reagents. This film may trap excessive residual moisture, which can lead to instability and decay. Although, freeze-drying is considered the gentlest drying method for preservation of biological material, it was not suitable for the present work due to the spotting procedure. Instead air drying was employed.

Water evaporates rather quickly, even at standard room temperature and humidity. The evaporation is critical when the spotted droplets of reagents are in the nanoliter range. Evaporation itself is a complex process. The dynamics of the drying processes for single-component systems are mostly determined by the internal cohesive energy of the droplets, irrespective of the substrate surface and droplet size. In most applications, the droplets also have different kinds of dissolved molecules, which may contribute to the drying dynamics.[166, 167] Two processes are included in drop evaporation: diffusion of liquid molecules into the air (diffusion part) and flow of the liquid molecules from inside the drop to the free outer shell liquid layer within the liquid-vapour interface (evaporation part). The diffusion part remains steady during drying and is not sensitive to the variation of temperature. The evaporation part, however, is an active factor and determines the differences in drop evaporation behaviours.[167]

In the absence of water molecules, the side chains of the amino acids interact with each other and 'lock up' the conformation. This deprives the enzyme molecule of the flexibility that is necessary for its catalytic activity. The enzyme activity depends on the ionization state of the active-site residues. Upon rehydration, an enzyme which is in a native conformation in the dried state exchanges the water substitute (protectants) for water and remains in the native state. Enzymes that are unfolded in the dehydrated state and do not refold properly upon rehydration, looses activity. Unfolded enzymes often have a tendency to aggregate.[168] Water 'deposition' follows a definite sequence of events. First it gets deposited on charged and polar amino acids, and then around the hydrophobic clusters.

2.5   Microfluidics and actuation

Microfluidics is the study of transport processes of fluids in microchannels. Typical channel diameters are of around ten to several hundred micrometers, which facilitate handling and analysis of volumes significantly smaller than a nanoliter. Microfluidic chips are the primary

element of most LOC devices and μTAS. The chips may consist of valves, mixers, pumps, filters and heat exchangers *etc.* The components allow metering, dilution, flow switching, particle separation, incubation of reagents, and sample dispensing or injection. Due to these components functionalities, both continuous-flow and droplet-based (plug-based) microfluidics are possible.[169] There is a wide range of methods to generate fluid flow in microfluidic devices, including the use of electricity (electroosmosis, electrophoresis, dielectrophoresis, electrowetting), mechanics (syringe or vacuum pumps, thermopneumatic pumps, membrane actuated pumps, centrifugal force, ferrofluidic plugs), magnetism (magnetohydrodynamic pumps), capillary effects or fluid motion due to evaporation and osmosis *etc.*[85,89, 170]

The fundamental physics of fluidic systems change dramatically as the volume decreases. On the microscale level, other forces than those experienced in every day life become dominant. On small scales, inertia is insignificant, while viscosity becomes very important. Thus, microfluidic devices exhibit almost exclusively laminar flow, and depend solely on diffusion as transport mechanism of molecules. Another characteristic feature of microfluidics is the dominance of surface effects due to the large surface area-to-volume ratio on the micrometer scale. Gravity can almost always be neglected on microscale. For such reasons, downscaling existing large devices and expecting them to function well at the microscale is often counterproductive.

2.5.1   Diffusion

In a liquid or gas, all molecules move by Brownian motion in all directions, as long as no external forces are applied. Each molecule moves in certain directions for a certain time, until it hits another molecule, after which it changes direction. Because the molecules are indistinguishable from one another, no net flow is observable. Diffusion is a transport phenomenon being the spontaneous spreading of matter (molecules), heat or momentum. A solution in equilibrium will seek uniform distribution of its molecules; generating concentration gradients through the solvent. The net movement of molecules will be from the area of high concentration to the area of low concentration. The statistical movement of a single molecule in a fluid in two dimensions can be described as in, Equation 1.[88]

$$x = \sqrt{2Dt}$$

1

where x is the average distance moved after an elapsed time t between molecule collisions, and D is the diffusion constant which depends on the size and shape for a given molecule. The diffusion coefficient for a solid spherical particle is given by Equation 2:[171]

$$D = \frac{kT}{3\mu\pi d}$$

2

where k is the Boltzmann constant, T is the absolute temperature, μ is the dynamic viscosity and d is particle diameter. A large diffusion constant means fast movement. In general, the larger a molecule is, the smaller is its diffusion constant. The dimension of a microchannel has a large influence on the diffusion and mixing of liquids in a channel. Table 3 shows characteristic diffusivities of typical species used in microsystems.

*Table 3 Typical diffusivities for various species in water at room temperature.[172]*

	Characteristic diffusivities				
Species	**Typical size**	**Diffusion constant, D [μm^2/s]**	**Time of diffusion 10 μm [s]**	**Time of diffusion 100 μm [s]**	**Time of diffusion 1 mm [s]**
Solute ion	0.1 nm	2×10^3	~0.025 sec	~2.5 sec	~4 min
Small protein	5 nm	40	~1.25 sec	~2 min	~4 hours
Virus	100 nm	2	~25 sec	~42 min	~3 days
Bacterium	1 μm	0.2	~4 min	~7 hours	~4 weeks
Mammalian/human cell	10 μm	0.02	~42 min	~3 days	~41 weeks

Mixing is one of the challenges in microfluidic devices due to the absence of inertial effects (turbulence) on microscale flows. All strategies to improve mixing have examined the possibilities to either reduce the diffusion distances or to agitate the flow. Strategies to improve mixing include splitting streams into smaller streams and folding and relaminating the streams again and again, thereby again minimizing the diffusion distances by increased interfacial contact. Another strategy for mixing is through chaotic advection. Here unique channel designs, including bas-relief structures on channel floors and 3-dimentional serpentine microchannels may be used to induce chaotic advection.[173] Thus, chaotic flows may occur

under certain rare conditions, when geometries change rapidly and do not allow the flow to reach a steady state before the next change in geometry. A third method is the employment of active mixers, which use external energy to induce temporary fluctuations. In contrast to the turbulent flows in macroscale, chaotic flows on microscale are quickly damped.

2.5.2   Surface tension and contact angle

Surface tension (γ) or interfacial energy is energy per area of an interface between two phases, whether they are solids, fluids or gases. Surface tension is caused by the attraction between the molecules of the fluid interface due to various intermolecular forces. The molecules prefer to be in the interior where the highest number of bonds is possible. In the bulk of the liquid, each molecule is pulled equally in all directions by neighbouring liquid molecules, resulting in a net force of zero (Figure 8a). At the surface of the liquid however, the molecules are surrounded by fewer neighbours, and the liquid tends to minimize the number of "broken" bonds by minimizing the surface area. All molecules at the surface are therefore subject to an inward force of molecular attraction which can be balanced only by the resistance of the liquid to compression. The lack of chemical bonds results in a higher energy for the surface molecules. Therefore, the liquid surface will tend to minimize its surface area, often resulting in curved surfaces.
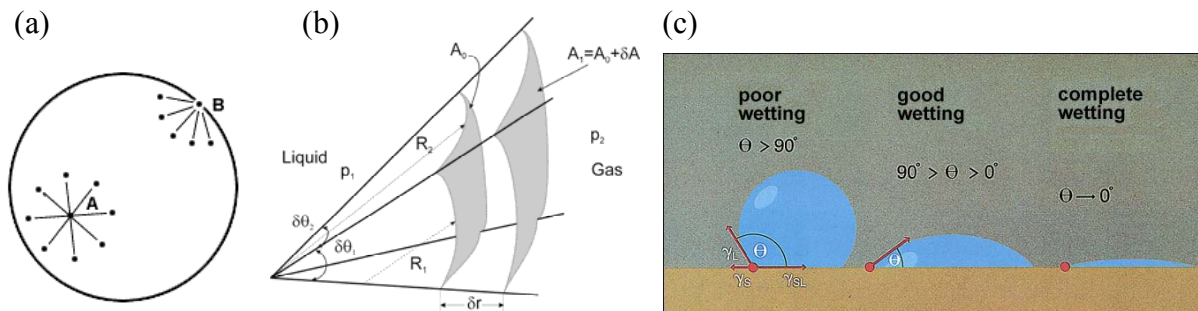
Figure 8 (a) Schematic drawing to illustrate the surface tension caused by intermolecular forces acting between molecules at the liquid/gas interface and in the liquid bulk. A – The bulk molecules are pulled equally in all directions by the neighboring liquid molecules. B – The surface molecules are subjected to an inward force of molecular attraction to compensate for the lack of chemical bonds in the direction of the gas phase.[174] (b) Differential expansion of a small section of a liquid/gas interface with locally constant curvatures. (c) The contact angle (θ) is defined as the angle between the solid-liquid and the liquid-gas interface at the contact line. The wettability of a liquid on a surface can be described by the contact angle.[174]

The pressure difference built up across the interface is balanced by the intermolecular forces. An expression for the pressure difference can be derived[138] by considering the energy required to expand a curved surface, A, (Figure 8b). This pressure difference, Δp, is known as the Young-Laplace equation (Equation 3):

$$\Delta p = \gamma \left(\frac{1}{R_1} + \frac{1}{R_2} \right)$$ *3*

where R_1 and R_2 are the radius of the curvature. Δp is defined positive and is thus the pressure of the concave side minus the pressure of the convex side.[138]

Wetting is the contact between a liquid and a surface, when the two are brought into contact. Chemical affinities between a surface and a liquid at the molecular level determine the wettability of a surface and the resulting shapes of liquid drops. When a liquid has a high surface tension (strong internal bonds), it will form a droplet, whereas a liquid with low surface tension will spread out over a larger area (bonding to the surface). On the other hand, if a surface has a high surface energy, a drop will spread out, or wet, the surface. If the surface has low surface energy, a droplet will form. This phenomenon is a result of the minimization of interfacial energy. If the surface is high in energy, it will tend to be covered with a liquid because the interface then formed will lower its energy.

The contact angle (θ) is defined as the angle (measured inside the liquid) that is formed on the junction of the three phases, at the solid-liquid-gas junction, as depicted in Figure 8c. It can be expressed as in Equation 4 and is known as Young's equation.[138]

$$\gamma_L \cos \theta = \gamma_{SG} - \gamma_{SL}$$ *4*

where γ_L is the liquid-gas interfacial energy, γ_{SG} is the solid-gas interfacial energy and γ_{SL} is the solid-liquid interfacial energy. The contact angle is a result of the static equilibrium of the minimum interfacial energies of all phases. A contact angle of 90° or larger generally characterizes a surface as not-wettable, and one less than 90° means that the surface is wettable. In the context of water, a wettable surface may also be termed hydrophilic and a non-wettable surface hydrophobic. For a hydrophobic surface, the hydrophobic effect is

dominant. The hydrophobic effect is the property that causes electrically neutral and non-polar molecules to self-associate in the presence of aqueous solution. Matter seeks to be in a low energy state, and bonding reduces chemical energy. Water is electrically polarized, and is able to form hydrogen bonds internally. However, water molecules are incapable of forming hydrogen bonds to non-polar molecules (*e.g.* alkanes, hydrocarbons, fluorocarbons and inert atoms), therefore water repels the hydrophobic molecules in favour of bonding with itself. Contact angles can often be changed by chemically modifying surfaces or by addition of certain solute molecules into the medium that adsorb on the surface. The contact angle is independent of the surface geometry. However, the contact angle is not always stable and static. Contact angle hysteresis is a common phenomenon and arises when a three-phase boundary becomes trapped in transit, lacking sufficient energy to surmount the energy barrier to a lower energy state. In this case, it is generally observed that the contact angle on a liquid advancing is different from the receding on a surface. Contact hysteresis is not fully understood, but is generally attributed to surface roughness, surface heterogeneity, liquid-surface interactions or due to a dynamic contact angle.[138]

2.5.3 Capillary forces

The two concepts, contact angle and surface tension, is the basis for understanding the capillary forces that act on liquids inside microchannels. The dynamics of surface tension-driven fluid follow from a balance of capillary and viscous forces.[172] The surface tension along with the dimensions and the geometrical angles of the microchannels determine how strong the capillary forces are, and can lead to pressure gradients in the liquid. The pressure difference of the meniscus causes flow transport, so it is similar in many ways to pressure-driven flows.[8] Variations of the Young-Laplace equation (Equation 3) makes it possible to calculate the pressure differences across the menisci of liquid plugs in microchannels. The equations depend on the cross sectional shapes (*e.g.* circular or rectangular) of the microchannels. In Figure 9a, the liquid-gas interface in a circular microchannel is illustrated. The curvature of the interface, R, can in this case be expressed as $R= r/\cos\theta$, where r is the radius of the microchannel. In a similar manner can the curvature for a rectangular shaped cross section be expressed as $R=(1/h+1/w)/\cos\theta$, where h and w is the height and width of the channel, respectively. Figure 9b presents a liquid plug in a microchannel, where the two

menisci of the plug are equal in size and the plug rests in equilibrium. The pressure difference across the two menisci in Figure 9b is zero. A liquid plug that is not in equilibrium is shown in Figure 9c. The pressure difference across the two menisci in this case is non-zero. The pressure is higher on the right side meniscus than the left, resulting in a force that will pull the plug towards the right. In Table 4, some variations of the Young-Laplace equation (Equation 3) for channels with rectangular and circular cross sections are given. The cross section of the microchannels used in the present work was rectangular.
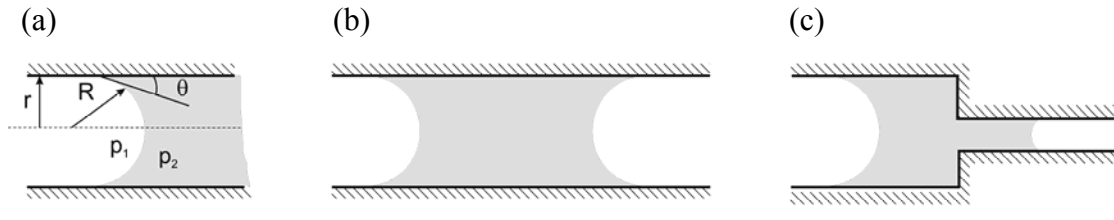
Figure 9 Liquid-gas interfaces in microchannels. The liquid is coloured grey. The cross section of the microchannels might be either circular or rectangular. The radius, r, of a circular cross section is shown in (a). The height, h, and width, w, of a microchannel with a rectangular cross section are not shown. The width is perpendicular to the text plane. (a) The driving force a liquid plug. (b) Liquid plug in equilibrium. (c) The liquid plug is not in equilibrium.

Table 4 A variation of the Young-Laplace equation (Equation 3) for channels with different cross sectional shapes.

Case	Circular	Rectangular
One meniscus	$\Delta p = \dfrac{2\gamma \cos\theta}{r}$	$\Delta p = 2\gamma \cos\theta \left(\dfrac{1}{w} + \dfrac{1}{h} \right)$
Two meniscus	$\Delta p = 2\gamma \cos\theta \left(\dfrac{1}{r_1} - \dfrac{1}{r_2} \right)$	$\Delta p = 2\gamma \cos\theta \left[\left(\dfrac{1}{w_1} + \dfrac{1}{h_1} \right) - \left(\dfrac{1}{w_2} + \dfrac{1}{h_2} \right) \right]$

The capillary pressure along a flow path can be altered by changing either the channel geometry or surface properties. Aqueous liquid held between hydrophobic walls forms convex surfaces which result in elevated pressure inside the liquid plug.[170] Non-wetting areas arrest capillary intrusion. In aqueous liquid plugs surrounded by hydrophilic walls, a concave surface is created and the pressure inside the plug is lowered. Each wettable ($\theta < 90°$) wall of the microchannel contributes to generate a negative pressure front of the liquid and to draw aqueous liquid into the channel.[44]

Capillary flow can be disturbed by pinning of the liquid meniscus which often is caused by contact angle hysteresis. This uncontrolled effect prevents the exact prediction of the movement of the liquid front. In the case of pinning, the pressure drop in the meniscus is significantly affected.

In microsystems involving liquid plugs enclosed by gas, the effects of pressure changes due to heating of the system and evaporation of the liquid must be taken into account. The plugs can be displaced due to increased vapour pressure if parts of the channel system are closed. If the gas phase is not in equilibrium with the liquid phase, the liquid will evaporate until the gas phase is saturated with molecules from the liquid, which can result in shrinkage of the plug volume. These effects depend largely on the size of the dead volume.

2.6   Detection technology

The amplified single-stranded RNA transcripts of the NASBA reaction are ideal for use in a hybridization-based detection system with sequence-specific probes. The first two detection methods described in relation to NASBA were electrochemiluminiscense (ECL) and enzyme linked gel assay (ELGA), which both are endpoint analyses.[27, 34, 175] Today, the most widely used probes are fluorescent molecular beacons which hybridize to the amplicons during amplification, enabling real-time detection.[30, 31, 34, 176, 177, 178, 179] This cuts down the total analysis time, in addition to providing information about the kinetics of the reaction. In contrast to ECL and ELGA, no extra detection step is required when employing molecular beacons and the tubes can remain closed and carry-over contamination is therefore prevented.

Molecular beacons are short ssDNA molecules composed of a hairpin-shaped oligonucleotide that contains both a fluorophore and a quencher group, as depicted in Figure 10.[31, 180] The loop part of the molecule contains the sequence complementary to the sequence of the target nucleic acid, whereas the stem is unrelated to the target and has a double-stranded structure. One arm of the stem (5' end terminal) is labelled with a fluorescent dye, *e.g.* 6-carboxy-fluorescein (FAM), and the other arm (3' end terminal) with a non-fluorescent quencher *e.g.* 4-(4'-dimethylaminophenylazo) benzoic acid (dabcyl). The fluorescent dye serves as an energy donor and the non-fluorescent quencher plays the role of an acceptor. The stem holds these two moieties in close proximity of each other, causing the

fluorescence of the fluorophore to be quenched by energy transfer. When the hairpin structure is "closed", the probe is unable to fluorescence. When the probe encounters a target molecule, the molecular beacon undergoes a conformational reorganization that forces the stem to open, because the loop hybridizes to the target molecule. This hybrid is longer than the stem, and therefore more energetically favourable. Furthermore, the fluorophore and the quencher are separated from each other, leading to the restoration of fluorescence.
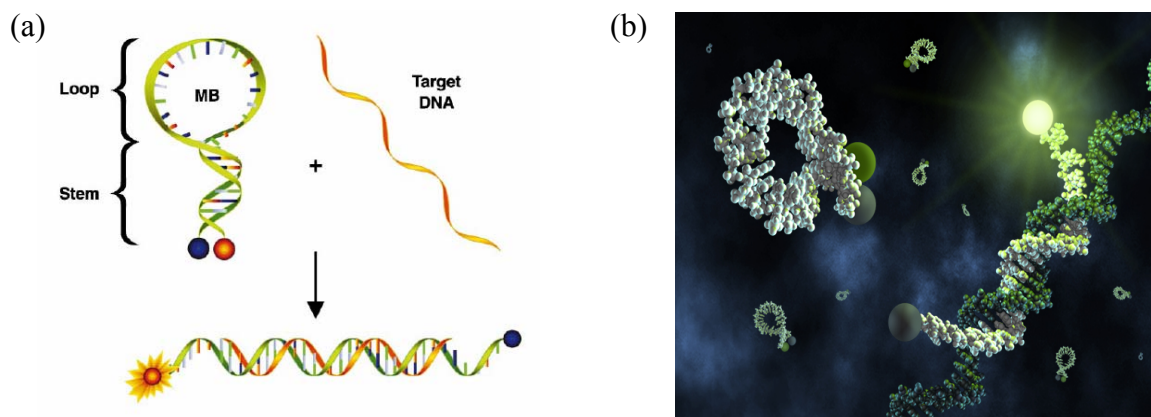
Figure 10 Conformational structure of molecular beacon probes. (a) Prior to hybridization the fluorescence is minimal due to the stem-loop structure of the molecular beacon), maintaining the fluorophore (red/yellow) and the quencher (blue) in close proximity leading to quenching.[178] When introducing the target to the molecular beacon, it undergoes a spontaneous conformational change forcing the stem apart. Consequently, the fluorophore and quencher separates and result in the restoration of the fluorescence. (b) Computer art of unhybridized stem-loop molecular beacons and a fluorescent hybrid. (bioMérieux, Marcy l'Etoile, France)

Two forms of energy transfer may take place in molecular beacons: direct energy transfer and fluorescence resonance energy transfer (FRET).[181] Direct energy transfer depends on *contact* between the fluorophore (donor) and quencher (acceptor). The collision between the fluorophore and the quencher changes the energy level of the excited fluorophore, resulting in quenching. The quenching moiety dissipates the received energy as heat.

The mechanism of FRET involves a donor fluorophore in an excited electronic state, which may transfer its excitation energy to a nearby acceptor chromophore (quencher) in a non-radiative fashion through long-range dipole-dipole interactions.[163] The theory supporting energy transfer is based on the concept of treating an excited fluorophore as an oscillating dipole that can undergo an energy exchange with a second dipole having a similar resonance frequency. The principle of FRET is described in Figure 11.
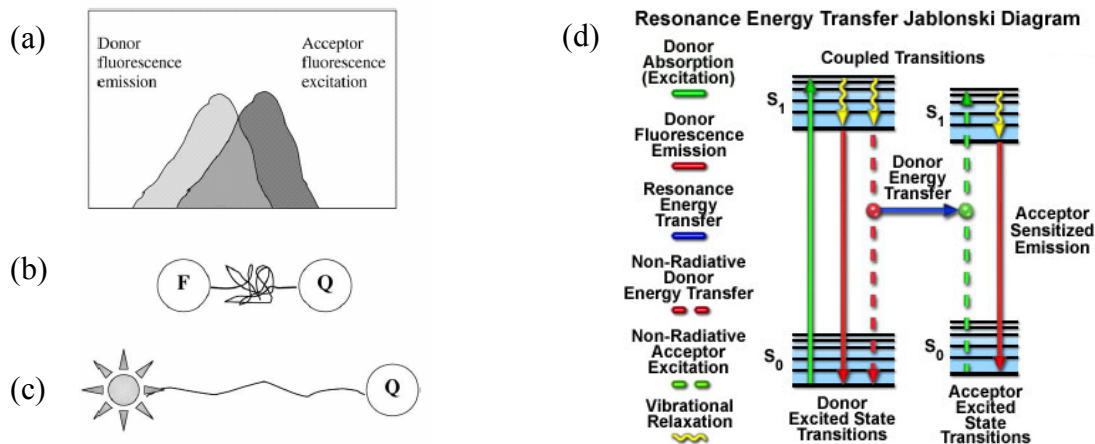
Figure 11 The FRET concept. (a) The overlapping spectra of the donor emission and the acceptor excitation, (b) with donor (F) and quencher (Q) in proximity, no fluorescent signal is generated, but (c) when separated, the donor is able to emit fluorescence uninhibited.[163] (d) The coupled transitions involved between the donor emission and acceptor absorbance in FRET. Absorption and emission transitions are represented by straight vertical arrows (green and red, respectively), while vibrational relaxation is indicated by wavy yellow arrows. The coupled transitions are drawn with dashed lines that suggest their correct placement in the Jablonski diagram should they have arisen from photon-mediated electronic transitions. In the presence of a suitable acceptor, the donor fluorophore can transfer excited state energy directly to the acceptor without emitting a photon (illustrated by a blue arrow). The resulting sensitized fluorescence emission has characteristics similar to the emission spectrum of the acceptor.

Molecular beacons in solution with their targets can exist in three states (Figure 12a): bound to target (phase 1), free of target in the form of a hairpin (phase 2), and free of target in the form of a random coil (phase 3).[182] Poor signal-to-background ratios may be caused by the presence of uncoupled fluorophores in the preparation, or by the presence of oligonucleotides that have a fluorophore, but not a quencher. It is therefore of importance to use pure molecular beacons. The fluorescence of a solution at a given temperature is the sum of the fluorescence of the molecular beacons in each of the three states. Figure 12b shows the thermal denaturation of a typical molecular beacon. At lower temperatures, the molecular beacons are in a closed hairpin state and do not fluoresce. However, when the temperature increases, the helical order of the stem gives way to a random-coil configuration, separating the fluorophore and the quencher, restoring fluorescence. When the molecular beacon is bound to the target, the molecular beacons fluoresce brightly at low temperatures, but as the temperature is slowly raised fluorescence decreases significantly, before it increases as the temperature increases.

The fluorescence curve obtained when using molecular beacon probes is dependent on two factors: the NASBA-driven time-dependent increase in RNA levels and the binding of the molecular beacon to this RNA. Time-to-positivity (TTP) is defined as the time in minutes when the fluorescence signal is above the background or no template signal.[179, 183]

(a)

(b)
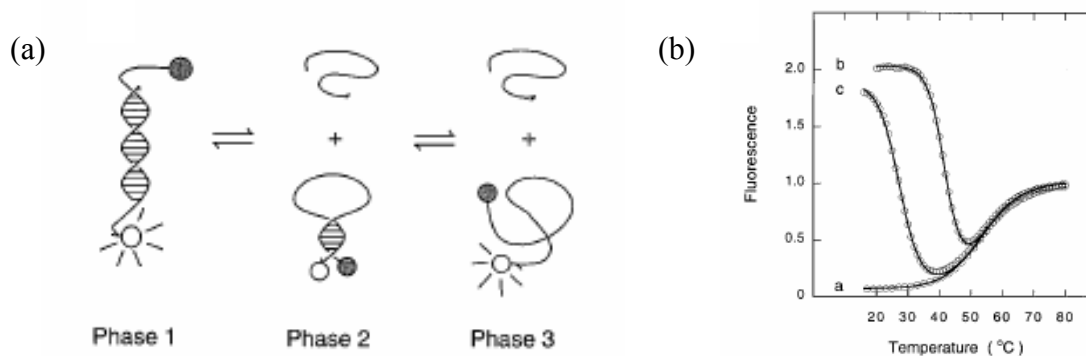
Figure 12 (a) Schematic representation of the three molecular beacon phases: bound to target (phase 1), free of target in the form of a hairpin (phase 2), and free of target in the form of a random coil (phase 3). (b) Thermal denaturation profile of solutions containing molecular beacons: trace a, in the absence of targets; trace b, in the presence of excess of perfectly complementary targets; and trace c, in the presence of an excess of mismatched targets.[182]

2.6.1   Fluorescence detection in microchips

The most commonly used detection method adapted to the microsystem technology is fluorescence detection. The advantages of fluorescence detection is superior sensitivity, high specificity enabling real-time measurements, and multiplexing capabilities.[163] Microsystem technology enables structures on the micrometer and nanometer scales, using these features it has been possible to achieve the requirements for the analysis and manipulation of samples on a single molecule scale.[46, 47, 184, 185] Despite the excellent sensitivity of fluorescent detection, it has some disadvantages. As most samples are not fluorescent, it is often necessary to fluorescently label the samples. The guided excitation light can also generate heat, which will increase the temperature of the region of measurement and could effect the analytical assay.[101] The ultimate sensitivity of optical detection is to a large degree dependent on the noise and drift over time caused by thermal expansion and vibration within the system.[186] Unless the microsystem contains an internal self-calibration of the fluorescent signal feature, it will be

difficult to obtain quantitative data.[187] Dye molecules tend to leach and photobleach as a function of time, and therefore it is hard to control their concentration. High intensity illumination accelerates photobleaching. By adding antifade reagents, photobleaching may be reduced.[188] Additionally, quenching of the fluorophores that result in non-emissive transition to the ground state is also possible. Interaction between the fluorophore and the many substances in the measured solution may also interfere with the measurment.[187]

Background noise is often the important limitation to ultrasensitivity. The background signals may originate from the sample constituents, or from unbound or non-specifically bound probe (reagent background), and scattering due to; reflection, refraction, luminescence from the optics, solutions or chip substrates. Optical noise is generated every time light is reflected or refracted from an optical interface. The surface roughness of the microfluidic chips is a critical parameter for optimal quality of the measurement. When the surface roughness is large, the excitation and emission lights in the measurements are scattered and the optical pathway is disturbed, and this may reduce the sensitivity of the system and generate crosstalk in a multichannel system. Light is also lost through reflection caused by changes in the refractive index at the surface between two materials. Considerations of assembling devices with direct contacting of refractive-index matching materials and components will minimize losses and generation of stray light at the various interfaces. Therefore, selecting the appropriate chip material is of importance. It must be transparent to light, specifically in the excitation and emission wavelengths. The material should exhibit no or minimal autofluorescence, which otherwise leads to a high background signal. Autofluorescence is generally higher for polymer materials compared to glass.[90] The autofluorescence of polymers can often be related to the intrinsic bulk polymer, additives, impurities or degradation products. The differences in magnitude of the initial fluorescence for similar polymers can also be explained by differences in the polymer production processes between vendors, and the post-production age and handling of material.[96] Stored polymers that have been exposed to light over a period of time can loose a significant fraction of its fluorescence compared to newly fabricated polymers. Thus, there is a huge potential for device-to-device variation among polymer chips.[96]

Another problem regarding the materials used in microfluidic chips is that they are transparent in the visible region and have higher refractive indices than that of air or the

surrounding environment. Therefore, the fluorescence emission and scattered excitation light can propagate through the chip as wave guides. This is especially the case for *e.g.* POC systems which will require multi-channel microfluidic chips.[189] The propagated light can interfere with the detection of the fluorophores in the adjacent channels and chambers and/or cause photobleaching of the adjacent fluorescent samples. This crosstalk complicates the on-chip detection of fluorescently-labelled reporters primarily through an unpredictable fluctuation in the intensity of fluorescence.[189]

2.7   Functional µTAS

The driving force behind the development of microfabricated devices is the commercialization of microfluidic technology with its enormous potential of large-scale applications. A market analysis from 2005 stated that application of microfluidics in the life sciences had a global market of around 500 million euros, which could rise to about 1.4 billion euros by 2008.[190] Research has been concentrated on those areas that have the highest potential for short term commercial success. The most interesting applications of microfluidics chips and µTAS devices are those that would demand large volumes of microchips to low prices, such as public health monitoring, environmental monitoring, and for use in the medical systems of developing countries.[15, 81]

In the past decade, biology has quickly advanced from a state of mostly manual labour to early stages of automation. However, very few academic laboratories or companies use microfluidic devices for routine analyses, the macroscopic robots are still the choice for most when it comes to automatization.[191] One reason for this could be lack of interaction between technology developers within µTAS and the technology users. So far, integrated microfluidic systems lag behind the possibilities offered by robots and conventional fluid-handling tools when it comes to sophistication and parallelism. Most likely, it is only when the integrated microfluidic chips surpasses robotic capabilities and cost that widespread adoption of the microfluidic chips will be used in academic and industrial settings. Developing microfluidic devices that rival current robotic systems will require technology platforms that are capable of manipulating much smaller volumes while performing more complex tasks with higher degree of parallelization and integration.

Simulation tools are now used to make researchers able to rapidly determine how changes of design will affect chip performance, thereby reducing the number of prototyping iterations. However, the transition from simple microfluidic components to highly integrated systems is difficult as microsystems contain a network of microfluidic components that are linked in a more or less complicated manner. Most individual microfluidic components are often of little use unless they can be integrated in a functional system. It is highly desirable to decrease the reliance on external equipment, in order to achieve a higher degree of portability and hence fully realize the advantages of μTAS technology. However, the integration of microfluidic components, electrical components and optical components makes the system more complex and more prone to error unless all parts of the system are made robust. For instance, the functionality of microfluidic valves and pumps has shown to be unreliable. If only one part of the system not succeeds, the whole analysis will fail.

There are still several challenges related to integration of microfluidic components. Sample preparation is less developed than both separation and detection on microscale. In order to reach the goal of total integration, further integration of sample collection and sample preparation will be necessary to improve the interface between the microfluidic device and the surrounding macro environment, and to minimize potential cross-contamination. In addition, sealing and packaging represents a critical step in the production of microsystems. The available technology for efficient pumping, valving and on-chip reagent storage is limited as well.[81] Examples of integrated microfluidic systems can be found elsewhere.[69, 116, 192, 193, 194]

3 Summary of papers

Paper I

This article describes the first step in a project designed to downscale the nucleic acid sequence-based amplification (NASBA) reaction. The results present in the paper shows that it was possible to accomplish NASBA of artificial oligonucleotides in detection volumes of 10 nl and 50 nl. Reaction chambers operating with 10 nl as well as 50 nl were obtained using silicon-glass microchips. This is a reduction of the conventional reaction volume by a factor of 2000 and 400, respectively. A custom-made instrument with heat regulation and fluorescent detection was developed as well. NASBA is a well established method for diagnostic analysis, and the results from this work show the possibility of developing a LOC concept for the NASBA technology.

Paper II

In this work further development towards performing NASBA in nanoliter volumes is presented. It is described how it is possible to test a sample which is distributed automatically by capillary forces into 12 parallel and identical reaction chambers. The detection volume is 80 nl. Furthermore, the chip material was changed from silicon and glass to COC. The results from the experiments show that the detection limits of the artificial samples as well as the cell line samples are the same for cancer markers in nanoliter volumes as for conventional reaction volumes of 20 µl. A custom-made instrument was manufactured to increase light intensity, reduce component cost, and to integrate automatic actuation and optical positioning. The results obtained clearly substantiates that it might be possible to develop a LOC concept for the NASBA technology.

Paper III

The making of a novel non-contact pumping mechanism which enabled metering, isolation and movement of nanoliter sized sample plugs in parallel reaction channels is presented in this

manuscript. The mechanism was based on flexible COC membranes integrated on the microchip, combined with pins for actuation in the surrounding custom-made instrument. The COC chips with integrated pumps were able to simultaneously move parallel sample plugs along the reaction channels in four different steps. As the integrated pumps were designed to be used for NASBA, all the tests were performed at temperatures of 39˚C, 41˚C and 65˚C. The experiments revealed that the accuracy of the pump was highly dependent on the evaporation of sample and deformation of the COC membranes. The novel concept of this non-contact pumping mechanism shows potential as actuation mechanism for LOC devices. The advantages of these non-contact pumps are less risk for cross-contamination, between the separate reaction channels on the chip as well as between chips since no parts of the instrument are in contact with the sample. In addition, the integrated pumps membranes are low-cost which is essential for the production of disposable chips.

Paper IV

This manuscript presents experiments done both on macroscale and microscale, approaching a microchip in which all reagents are integrated. The goal was to apply the nucleic acids sample at the inlet of the microchip so that the NASBA procedure would automatically be performed on chip. Various methods for fabrication of microchips were investigated with regards to surface roughness and background fluorescence. Coating of the surfaces was required for amplification, as the native hydrophobic COC surfaces adsorbed proteins. A confocal microscope was used to determine the time for the dried mastermix and enzymes to dissolve. Protectants (trehalose, PEG, BSA and PVP) were added to the enzyme solution in order to protect their three-dimensional structures during drying and storage. On macroscale, successful rehydration and amplification were obtained for both dried mastermix and dried enzymes using HPV 16 oligonucleotides as well as CaSki cell lines as sample. However, only the dried enzymes gave successfully amplification of HPV 16 oligonucleotides on the COC chips. No amplification was observed for the dried mastermix on chip, and therefore this needs to be investigated further. It is suggested that the sequence in which the reagents were added to the microchip was of importance. Thus, the results of this work give some guidelines towards the development of a self-contained NASBA chip with regards to design, fabrication, surface modification, and amplification performance.

4 Results and discussion

The microchips developed in this work are general technology platforms that can be adapted to perform any clinical analysis which requires amplification of RNA or ssDNA. The objective of the present work was to develop a microchip for amplification and detection of mRNA by employing the real-time NASBA technology. Detection of HPV type 16 was used as a model target employing artificial HPV 16 oligonucleotides, SiHa cell lines and CaSki cell lines to demonstrate the functionality of the microchips.

Microfluidic technology focuses on picoliter, nanoliter and microliter fluid volumes and has allowed detection of single molecules at volumes in the picoliter range.[185, 195, 196] The reduction of reaction volumes lower the cost of analysis as the consumption of expensive reagents is reduced. However, these small volumes are not always suitable for realistic POC diagnostic applications. In most cases, the clinical samples contain low concentrations of the analyte of interest. In order to make reliable and robust µTAS applications, the sample volume, as well as the reaction volume should be large enough so that stochastic sampling effects will not be an important factor. On the other hand, if the sample volume required for detection becomes too large, microsystem technology will not be the best solution, as this will defeat the advantages of the approach.

The present work shows for the first time successful real-time amplification and detection employing NASBA in a microsystem format using a custom-made instrument. The NASBA reaction has been downscaled to the nanoliter level on silicon-glass chips, as well as on COC chips. The silicon-glass chips described in **Paper I** contained reaction chambers of 10 nl and 50 nl, which was a reduction of the conventional NASBA reaction volume by a factor of 2000 and 400, respectively. The 50 nl reaction, however, showed the same progress as in the conventional polypropylene tubes, while the 10 nl amplification curve had a different progress towards earlier signal increase. Several factors such as concentration variations and more efficient heat transfer of the silicon chip in comparison to the polypropylene tubes can contribute to the results obtained for the 10 nl reaction chambers. It is not possible to directly compare the results obtained for the 10 nl and 50 nl reaction chambers, as neither the target nor the concentrations of the sample are the same. To our knowledge, 10 nl is the smallest

detection volume known for NASBA. However, in comparison, the minimum reported size of reaction volumes for PCR and RT-PCR are 39.5 pl[197] and 450 pl[72], respectively.

While the silicon microchip only recorded fluorescent amplification signals of one reaction chamber, the COC microchips distributed the sample into 10 parallel reaction channels, with detection volumes of 80 nl, for simultaneous amplification and detection (**Paper II**). Dividing the sample to increase the number of simultaneous amplifications reactions are beneficial for diagnosis, as many diseases require identification of multiple targets. A second custom-made optical detection system was produced, in order to automatically detect the 10 parallel amplification reactions on the microchip. The NASBA results of the HPV 16 oligonucleotides and the SiHa cell line showed that all parameters (TTP, average slope, number of positive reactions) display the same trend for the microsystems as for the conventional methods, except for the fluorescence level ratios of the amplification reactions. As this ratio is almost constant for the microchip experiments, it decreases with sample concentrations for the conventional experiments. The fluorescence level is determined by the concentration of the molecular beacons in the reaction mixture. If the amplification reaches full reactant consumption, the final fluorescence should theoretically be independent of sample concentration, but reached at different times. However, dilution series of both artificial HPV 16 oligonucleotides and SiHa cell lines showed that the detection limits for the microchips were comparable to those obtained for the conventional routine-based laboratory-systems.

Further experiments with a silicon microchip containing detection volumes from 100 nl to 600 nl showed that the detection volume of 500 nl were most advantageous for artificial HPV 16 oligonucleotides, due to the relative increase in fluorescence signal (**Paper IV**). The reaction volume of the microchips was adjusted from 10 nl, 50 nl and 80 nl to 500 nl as the focus changed from cost of reagents on chip to robustness and reliability of the diagnostic application. The dilution series of HPV 16 oligonucleotides and the SiHa cell lines (**Paper II**) revealed that the limit of detection (LOD) of the conventional system and the 80 nl detection volume of the microchip was the same, 10^{-6} µM and 20 cells/µl, respectively. A SiHa cell may contain only 2 copies of the DNA virus but the number of mRNA transcripts in each cell is not known.[198] It was possible to detect even lower concentrations in both systems, but the results were inconsistent, most likely due to sampling effects. However, the custom-made instrument

was able to detect fewer molecules than the conventional system. It might be possible to obtain consistent amplification at lower concentrations than within the 80 nl microchips if the detection volume is increased to 500 nl. However, this was not tested in the present work.

For a conventional system employing 20 µl reaction volumes, it has been reported that as few as 50 copies of *in vitro* RNA/reaction have been detected in the case of NASBA, using molecular beacon.[199] However, the LOD is dependent on the target and, the LOD can vary from assay to assay due to the characteristics of the primers, the molecular beacon, type of sample material, the concentrations of the reagents within the reaction mixture, surface chemistry, heat transfer, and the quality of the detection system. The LOD of an assay is therefore not only limited by molecular restrictions of the reaction itself, but also of the surrounding system. One of the most sensitive assays, the micro PCR assay, was demonstrated by Lagally *et al.*[200] when a single molecule of DNA template was amplified in a glass device with reaction chambers of 280 nl. Marcus *et al.*[72] reported successful RT-PCR on chip for 72 parallel 450 pl reaction volumes for as few as 34 mRNA copies. Parallelization and simultaneous detection is important for high-throughput, and Leamon *et al.*[197] demonstrated simultaneous PCR amplification of up to 300 000 parallel reactions with individual reaction volumes of 39.5 pl. Belgrader and coworkers[201] reported that PCR amplification of "real" samples containing a starting template concentration as low as 5 *Erwinia herbicola* cells was feasible on silicon microchips.

On the other hand, Cepheid has developed a microfluidic device, GeneXpert®, for PCR and RT-PCR which implies detection volumes of 80 µl.[10] Its four-channel optics system is capable of dye detection with a limit of < 2 nM for FAM and Texas Red.[202] In comparison, the detection limit of HPV 16 oligonuclotides (**Paper II**) was consistent at 1 pM (10^{-6} µM). However, the GeneXpert can perform RNA isolation of pre-sliced and lysed cancer tissue samples, reverse transcription, and quantitative PCR in ~35 minutes.[10, 54] As microfabricated devices provide very rapid thermal energy transfer cycling, compared to conventional thermocyclers, it results in reduced analysis time on chip. However, as NASBA is isothermal, it can not benefit of increased heat transfer efficiency in the same manner as RT-PCR and PCR. Kopp et al.[114] demonstrated that a continuous-flow PCR chip had heating and cooling times less then 100 ms, which resulted in total reaction times of 90 seconds to 18.7 minutes for 20-cycle PCR amplifications (176 bp). But for NASBA the TTP will in most cases reveal if

the samples are positive long before the reaction is finished, unless the concentration of target is very low.

In most of the experiments performed in the presented work, which were not related to detection limits, a high concentration (0.1 µM) of HPV 16 oligonucleotides was added to the reaction mixture to ensure amplification. This corresponds to a copy number in the range of 10^8 - 10^{11} per detection volume between 10 nl and 20 µl. For a high viral load sample (*e.g.* HIV), the number of RNA copies entering the amplification reaction is in the order of $10^5 – 10^6$.[32]

Two complementary mechanisms have been suggested for partial or complete inhibition of biological assays on microscale. Straight chemical inhibition[103, 106] or surface adsorption[105, 106] have been proposed, due to increased surface area-to-volume ratios in microchips. Of these, surface adsorption is regarded to be the most dominant for most assays. Bare silicon and silicon nitride have showed consistent inhibition of the PCR reaction, while silicon dioxide and polymer coatings have resulted in good amplifications.[103] The inhibition of the PCR reaction in glass-silicon chips is mainly caused by the adsorption of Taq polymerase to the walls of the chambers.[103, 105, 106, 203] Oda et al.[204] reported that DNA polymerase can also adsorb to metal. Protein adsorption is triggered by chemical and physical phenomena related to the surface materials and the surrounding medium. However, proteins tend to adsorb on to hydrophobic surfaces more than to hydrophilic surfaces. Both native silicon and COC surfaces are hydrophobic with regards to aqueous solutions. The net effect of polymerase adsorption can be counteracted by the addition of a titrated amount of competing protein BSA (dynamic passivation) or render the surface hydrophilic or neutral by static passivation. It is reported that the addition of BSA to counteract adsorption of Taq polymerase gives far better results than a simple five-fold increase of the Taq polymerase concentration.[106] Lou and coworkers[108, 109] have demonstrated that PEG and PVP are efficient for dynamic passivation of native and SiO_2-precoated silicon-glass chips in relation to PCR and ligase chain reaction (LCR) amplification. For many silicon-glass chips it was not enough to precoat the surface with SiO_2, as additional BSA was required to produce a positive reaction.[127] The NASBA reaction performed in conventional polypropylene tubes has been tested for biocompatibility of these reagents (**Paper IV**). However, this was tested in relation to stabilization of enzymes

during drying and has not yet been tested for dynamic surface passivation in microchannels. Panaro *et al.*[107] have described the surface effects and compatibility of PCR reactions on several common plastics, plastic tubing and disposable syringes. The results clearly show that some components of the material may inhibit the PCR reaction. The cause of the initial inhibition might be due to substances within the plastic that are released by the PCR reaction mixture or residual substances from the machining process.

Surfaces biocompatible with NASBA have been found to be a critical issue, in the same manner as for PCR. In microchips with native silicon surfaces (**Paper I**) and native COC surfaces (**Paper II**, **Paper IV**) it was not possible to amplify any target. Münchow *et al.*[117] showed that it was not possible to obtain PCR amplification in COC chips (Grade 5013) with reaction areas of native COC. However, PEG coated channels were reported to show good amplification. The NASBA reaction contains three different enzymes, in contrast to only one enzyme of PCR, and two enzymes of RT-PCR. As these enzymes consist of amino acids with a variety of side chains which can be either acidic, basic and have large variation in polarity, they respond differently towards a specific coating. In this work, it was not possible to label the three enzymes separately for adsorption measurements. Thus, the fluorescently labelled IgG mouse antibody was used as a model system. Adsorption measurements indicated clearly that fluorescently labelled mouse IgG bound unspecific to the hydrophobic native COC surfaces of the chip performing NASBA, while antibodies were rejected on the PEG coated COC surfaces (**Paper IV**). The amplification results obtained indicate that the NASBA enzymes adsorbed to native COC surfaces, as no amplification could be observed.

Successful amplification was obtained in silicon microchips modified with both SigmaCote™ and SiO_2 (**Paper I**, **Paper IV**). For silicon-glass chips, silanization compounds[103] and SiO_2 layers[9, 103, 104, 106] are the most commonly used coating types. For the COC chips, PEtOx-BP, PDMAA-BP and PEG were tested (**Paper IV**). Of the coatings tested for the COC microchips, it was the surfaces modified with PEG that showed the best biocompatibility with regards to NASBA. PEG is commonly considered the most effective polymer for protein resistant surfaces, because of its unique solution properties and its molecular conformation in aqueous solution.[121] However, the roughness of the surface to be coated can play a significant role for the coverage of coating on the surfaces. Surface

roughness can therefore contribute to a heterogeneous coating by leaving specific areas without coating. These uncoated areas are likely to adsorb reagents from the reaction solution.

In contrast to enzymes, DNA is not adsorbed to the walls in noticeable amounts.[106] However, depending on the pH, DNA can easily adsorb to glass and SiO_2. At pH 7.0, glass is negatively charged. When these surfaces are negatively charged, adsorption of divalent cations may occur. Due to the double layers thus formed, and because of the negative charge of DNA, it can be adsorbed on these surfaces.[205] Adsorption of oligonucleotides have not been tested in the present work, as this was regarded less important than protein adsorption.

In order to integrate the NASBA reagents on chip, a thorough evaluation of the reagents to be spotted and dried was needed. Because of the limited number of microchips available, it was necessary to map the most critical parameters on macroscale before transfer of knowledge to microscale (**Paper IV**). The DMSO and sorbitol enclosed in the standard final NASBA reaction mixture did not dry easily. Hence, it was found necessary to apply these compounds to the oligonucleotides or the sample of extracted nucleic acids before applied to the amplification chip. The standard NASBA reagents consist of the two main solutions, mastermix and enzymes in addition to the sample. The mastermix and enzymes were only stable, with subsequent successful amplification when spotted and dried separately. In a similar preliminary experiment for integration of PCR reagents on a chip, Weigl *et al.*[206] were able to dry and rehydrate the full PCR mixes in 96-well plates containing mastermix, and enzymes with varying concentration of trehalose. In this work, the protectants PEG and trehalose were also shown to be essential for recovery of enzyme activity in the NASBA reaction after drying on macroscale. The protectants were tested on both oligonucleotides and CaSki cell lines, as previous results (data not shown) have revealed that oligonucleotides are more easily amplified than both cell line samples and clinical samples. However, when testing PVP and BSA, as well as different combinations of the protectants, only amplification of the oligonucleotides could be observed.

The quality of the assay depends on how the sample material is collected and how the sample material is handled and processed before analysis takes place. The extracts of nucleic acid of the cell line contain a pool of genomic DNA, non-coding and coding RNA of various structures. Complex intramolecular structures in addition to a large spectrum of different kinds

of molecules complicate the process of hybridization of primers and binding of enzymes to the targets. It is important that everything except the nucleic acids is removed through the extraction. In the case of oligonucleotide samples, all the molecules are targets. However, it is important to purify the target, as impurities produced during synthetization may be inhibiting.

In order to prepare for the temperature control of the chip, it was also shown that the dried enzymes were stable at 65°C for up to 2 hours, while enzymes in solution were inactivated after only 3 minutes at 65°C (**Paper IV**). The mastermix and sample are normally heated to 65°C for 3 minutes prior to addition of enzymes. This procedure is performed to break down the secondary structures of the nucleic acids, and to ease the hybridization of primers to the target of interest. These experiments showed that the enzymes are more temperature stable when dry, than when in solution. This was expected, as drying of reagents are normally used for long-term storage.[142]

It was necessary to render both the mastermix and enzymes fluorescent prior to drying in order to evaluate the rehydration and diffusion rates of these reagents into the sample on chip (**Paper IV**). Molecular beacons without quenchers were dried with the mastermix to record the rehydration rate of the mastermix. These molecules were amongst the largest of the compounds in the mastermix and thus, have the slowest diffusion. The diffusion depends on temperature, viscosity, size and shape of the molecule. The modified molecular beacon is slightly smaller than the regular molecular beacon, although not much, and this difference would most likely not affect the diffusion rate significantly. However, these experiments were performed at room temperature, while on chip rehydration will occur at 65°C. Higher temperatures increase the diffusion coefficient, which again leads to faster diffusion times. The time for diffusion of the modified molecular beacons in the mastermix was ~60 seconds, which roughly corresponds to the calculated time needed to obtain a homogeneous suspension. Diffusion measurements of the molecular beacons without quencher in the mastermix implied that the dissolution process was diffusion-limited.

The fluorescently labelled mouse IgG (150 kDa) dried with the enzymes, modelled the diffusion rate of the largest NASBA enzyme (AMV-RT, 160 kDa). The IgG were assumed to be smaller and with a different shape compared to the globular AMV-RT enzyme. The rehydration/diffusion processes for the dried enzymes was significantly slower than for the dried mastermix. A homogeneous suspension was observed after approximately 10 minutes at

room temperature. The estimated time for diffusion for the IgG was ~3 minutes. However, the estimate is based on a model for spherical molecules. As the real shape and size was not known, parameters could contribute to the deviation between observation and estimate. During drying, films which are difficult to dissolve may be created on the surface of the reagents. It is not unlikely that this was the case, as similar experiments showed that the dried reagents were not dissolved at all. Hence, in this case, the measurements implicated that the rehydration process of the enzymes was slower than their diffusion into the bulk liquid. The experiment was performed at room temperature, but ought to have been performed at 41˚C as it will eventually be performed on the chip.

Only dried enzymes with 0.05% PEG protectant have been successfully amplified on chip (**Paper IV**). The TTP was ~15 minutes, showing that the rehydration rate of the enzymes is sufficient to obtain amplification. The fluorescent ratio is about 6 times, revealing that the activity of the dried enzymes was recovered upon rehydration. Puckett *et al.*[153] and Garcia *et al.*[152] have shown the ability to dry biological reagents, and later to reconstitute them, on a microfluidic platform without inhibition of the assay.

Successful amplification of the rehydrated mastermix on the microchips employing NASBA still remains. The reason for this is not clear, as the dried mastermix worked on macroscale. The order in which the reagents were applied to the chip could be one explanation. On chip, the rehydration of the mastermix was accomplished by applying a mixture of the enzymes, DMSO/sorbitol and oligo sample. The dried and highly concentrated mastermix deposited on the chip could influence the activity of the enzymes in the mixture entering the chip. For instance, the T7 RNA polymerase is extremely sensitive to salt concentrations. It is obvious that the order in which the reagents has to be applied must be investigated more thoroughly.

Paper IV indicates that the ratio of concentration between the mastermix and enzyme reagents is of importance. Optimization of the NASBA reagents on chip still remains to be tested. However, some work has been performed to optimize PCR on silicon-glass chips, as well as polymeric devices. [69, 105] As many of the reagents are the same for both reactions, it might be advantageous to test similar conditions for NASBA. Variations on the composition of reagents are possible, but the concentration of some components is critical. In general, the

enzyme concentrations for PCR were increased by a factor of 1.5-4 to produce yields equivalent to the tube-based assays.[69, 105] Increased amounts of BSA are often applied, due to its ability to provide a dynamic coating. In addition, BSA stabilizes labile enzymes, and it can even be required for enzyme activity. As NASBA requires BSA for enzyme activity, it is likely that increased concentrations of BSA are required for optimal results. Furthermore, a significant increase in enzyme concentration would require experimental titration of Mg^{2+} ions, as it is an essential co-factor in many enzymes, including RNase H and DNA polymerases. However, high concentrations of Mg^{2+} ions could have a net influence on the pH, thus triggering a cascade of experimental titrations for other reagents (*e.g.* KCl). The Mg^{2+} ion concentration required for optimal amplification may depend on the specific set of primers, and also for the template used, as it is bound by oligonucleotides and dNTPs. Salt-dependent electrostatic effects are major factors in determining the stability, structure, reactivity and binding behaviour of all nucleic acids. The cations stabilize the base pairs in the following order: $Ca^{2+} > Mg^{2+} >> K^+ > Na^+$, showing that both the charge and the ionic radius affect the stabilization of the duplex.[207] The optimal KCl concentration in the reaction mixture can vary for different targets and primer combinations. The salt concentration alters the secondary structure of the nucleic acids. An optimal salt concentration for the NASBA amplification is obtained when the secondary structure of the target is minimal, to allow good annealing with the primers. Hence, the KCl concentration will also affect the hybridization kinetics of the individual primers and thereby increase the specificity of the primer annealing. If the concentration of molecular beacon probes is too low, it will limit the detection of fluorescence. However, if it is too high, it would disturb and inhibit further RNA amplification.[30] Optimal concentration of DMSO is template dependent. For NASBA applications, the DMSO concentration should normally not exceed 16-17% in the final mixture, as it may inhibit the reaction. If the concentration is too low non-specific amplification may occur.[208] Addition of DMSO improves the specificity, efficiency and yield of the amplification reaction. DMSO and sorbitol have been reported to lower the melting temperature of nucleic acids duplexes.[209] Additionally, DMSO has been shown to accelerate strand renaturation and is believed to provide increased thermal stability for nucleic acids, thus preventing depurination. DMSO is an agent that disrupts mismatching of nucleotide pairs.

Design and fabrication methods of the microchips used were found to be crucial for chip performance. Rough surfaces do not only create background noise for the optical measurements, but also contribute to generation of bubbles and problems related to manipulation of the sample within the network of channels and chambers. The silicon microchips were manufactured with optically smooth surfaces, which are defined as having a surface roughness of less than 1/10 of the excitation wavelength (**Paper I**). However, low surface roughness was difficult to obtain for the COC microchips. Of the fabrication methods evaluated, it was the injection moulded chips which showed the smoothest surfaces closely followed by the hot embossed chips (**Paper IV**). Milling and laser ablation typically used for rapid prototyping, produced the roughest surfaces. For the milled microchips, it became clear that the rough surfaces also contributed to loss of liquid as the plugs were transported through the channels. Additionally, it was observed that cross-sectional constrictions in the channels resulted in loss of liquid when the liquid plugs were moved through these structures. A self-contained microchip for performing NASBA will include an increased number of geometrical constrictions. It is likely that some liquid will be lost during transport through the network, and therefore increasing the reaction volume to 500 nl will ensure that sufficient sample is left for detection.

Liquid loss was also experienced due to evaporation, which increased at elevated temperatures. In order to minimize the evaporation within the system, it was important to close the chips and to reduce the dead volume and the diffusion lengths. For the non-contact pump mechanism (**Paper III),** it was shown that the total sample volume was reduced after the sample plugs were moved from the first reaction site to the third reaction site. The volume lost was 3.3 nl after 2 minutes at 65˚C and 4.1 nl after 7 minutes at 41˚C. In addition, the evaporation increased the partial vapour pressures in the upstream closed side of the channel and thus expanded its volume. In some cases, this resulted in a movement of the sample plugs towards the second position. The inlet hole and the air venting at the waste chamber was not sealed during these experiments. If microreactors are open to the surrounding environment, the amplification volume will shrink. Thermal gradients might also induce bubble movement, and the evaporation itself could cause liquid pumping.[148] Consequently, reaction chambers should be closed. Physical valves can be used to keep in place the reagents and prevent migration and evaporation.[69, 116] Mineral oil has been commonly used to seal off reactions chambers to avoid

evaporation on microchips as well.[204, 210, 211] However, Panaro et al.[107] found that mineral oil can inhibit PCR either completely or partly. The reason for this could be that the compounds which are dissolved in oil will migrate into the oil and no longer be available for the reaction. For open PCR reactors, significant bubble formation has been observed.[212] The thermocycling of the PCR reaction reaches maximum temperatures of ~95°C, thus close to the boiling temperature of water. For NASBA, which is isothermal at 41°C, one would expect less bubble formation. However, bubble formation was a large problem for chips performing NASBA when the surface roughness of the reaction chambers was large, even though the chips were sealed (**Paper IV**). For the silicon and COC chips in **Paper I** and **Paper II**, bubble formation was not found to be a significant problem. For the chips with large surface roughness, bubbles were mostly trapped during filling and tended to stick to the channel surface and disturbed the reagent flow. In some cases, these bubbles expelled the reagents from the reaction chambers, thereby reducing the amplification efficiency. Bubbles trapped inside a microchamber may undergo expansion, contraction, and relocation inside the microfluidic network, depending on the temperature regulation of the microsystem.[213] A possible remedy to minimize or eliminate bubble formation is to design reaction chambers which avoid the trapping of air bubbles, and to pressurize the reaction chambers by closing them.[213]

The sealing between the chip itself and the top layer enclosing the channel system was of importance, due to the possibility of leakage, which in turn can enhance evaporation. The silicon-glass chips used in the experiments described in **Paper I**, were sealed by the use of anodic bonding. This technique makes strong sealing between the chip and the top layer, but requires high temperatures (~400°C) and voltages. Therefore, this technique would cause a problem in cases with deposited biological reagents on the chips. For the COC chips described in **Paper II** and **Paper III**, solvent welding was used. However, brittle membranes which easily cracked up were a problem with this sealing method. In addition, deposited reagents might be exposed to the solvent used for the welding. For this reason solvent welding was not the best alternative. Adhesive pressure sensitive tapes were used to seal the silicon and COC chips used in **Paper IV**. The adhesive on the tape did not seem to interfere with the amplification reaction. But due to hydrophobicity of the adhesive, it became difficult to fill the reaction chambers designed for spotting. Huge problems related to these tapes had to do with leakage of sample if the sealing surface of the chips was covered with PEG coating. However,

this adhesive tape would not be an option for the pumping mechanism presented in **Paper III**, as the tape would have glued itself to the bottom of the actuation chambers.

A novel non-contact pumping mechanism based on on-chip flexible COC membranes combined with actuation pins in the surrounding instrument was tested and evaluated (**Paper III**). The mechanism enabled metering, isolation and movement of nanoliter sized sample plugs in parallel reaction channels. The COC chips with integrated pumps were able to simultaneously move parallel sample plugs along the reaction channels in four different positions. Each reaction channel contained a set of 4 actuation chambers in order to obtain metering, isolation and movement of the sample plug into the detection area. The pump accuracy depended on the evaporation and deformation of the COC membranes used. Successful amplification of artificial HPV 16 oligonucleotides plugs of approximately 96 nl (detection volume of 80 nl) was obtained on premixed NASBA reaction mixture. However, these amplification results are not discussed in **Paper III**. In most of the measurements, the sample plugs were relocated from the detection area. Hence, it was no longer possible for the optical detection system to record the fluorescent signal of the amplification. This was the reason for not using the non-contact pumping mechanism for the experiments in **Paper II**. Either geometrical constrictions or valves should have been implemented within the reaction channels in order to fix the sample during measurement.

A syringe pump in combination with capillary forces was tested on the COC chips in **Paper IV**. As mentioned previously, the design of the microfluidic network affected the filling and encapsulation of bubbles, actuation and movement of the liquid plugs to the reaction chambers. Large reaction chambers were required in order to be able to perform spotting of reagents. Otherwise the reagents would spread out through the whole microfluidic network if the spotted liquid came in contact with the walls. The sample containing DMSO and sorbitol for rehydration of the mastermix showed good wetting properties of the PEG coated surfaces. The combination of the DMSO and sorbitol solution and the hydrophilic surface induced the liquid to start creeping trough out the microfluidic channels along the channel corners. In this case, the sample plug applied to the chip did not obtain static equilibrium of the meniscus, due to the high wetting properties of the sample plug on this PEG coated surface. The instability of the liquid will drive the wetting along the edges up to the very end of the channel system, as

62

long as sufficient liquid is provided in the system.[84, 213] This creeping effect was able to drain the reaction chambers during metering and movement. A capillary stop valve was introduced in the channel by spotting a hydrophobic patch (Teflon AF). The capillary valve stopped the creeping liquid behaviour and pressure differences of ~1000 Pa were required to overcome the strength of the valve in order to move the liquid. However, such capillary stop valves can produce possible gating inefficiencies, when liquids with low surface tension are used.[214]

Two custom-made optical detection instruments were developed in order to measure the NASBA reaction in nanoliter volumes on a microchip (**Paper I**, **Paper II**). For the second instrument, it was possible to obtain 56 times the excitation light intensity on the reaction channels compared to the first instrument. The increase is mainly due to a brighter light emitting diode (LED). The silicon chips had an optically smooth, reflecting and non-fluorescent surface, where the fluorescent light was spread uniformly into a hemisphere, assuming that the channel walls were 100% reflecting (**Paper I**). The detection optics would collect 8% of the excited fluorescent light. In the case of a transmitting chamber wall (polymer materials) with an opening angle of the collecting angle of $\pm$ 26°, only 5% of the excited fluorescent light was collected, as the fluorescent light was spread into a sphere instead of into a hemisphere (**Paper II**, **Paper IV**). In addition, polymer materials usually display autofluorescence. However, polymer materials may be bleached when exposed to light for longer periods of time.[96] Further, the surfaces of polymer materials is rougher in the range of 0.03 µm to 16.6 µm (**Paper IV**), while the surface roughness of the silicon chips were in the order of 1/10 of the excitation wavelength used (**Paper I**). When the surface roughness is large, the excitation and emission lights in the measurements are scattered and the optical pathway is disturbed, which may lead to unreliable measurements. However, the surface roughness varies considerably, depending on the chip material and fabrication method used. Injection moulded, hot embossed and micromachined silicon microchips usually offer lower surface roughness compared to milled and laser ablated microchips. Therefore, these rough surfaces will be less suitable as optical elements.

The solvent background signal can be drastically reduced by minimizing the optical detection volume, since the signal from a single molecule is dependent on probe volume dimensions, whilst the background scales proportionally with the probe volume.[46] For very

low concentrations of target, an increased detection volume is generally undesirable, since the background interferences increase. The various components of the NASBA mixture, either individually or in combination, can contribute to an increased value of background fluorescence, in addition to that produced from leakage from the molecular beacon. This has not been evaluated in this work. However, Obeid et al.[71] found that the combination of primers and Triton X-100 in their PCR reaction mixture contributed to the high background fluorescence, although, neither primers nor Triton X-100 showed high background when studied separately.

It is often the background noise which limits the sensitivity of an assay. The signal-to-noise ratio is the power ratio between the signal and the background noise and it should be as large as possible in order to obtain the good sensitivity. In addition to reduction of the background fluorescence of the chip material and the reagents in use, the LED and the photomultiplier tube (PMT) components of the instruments depend on temperature. Hence, the fluorescence measurements will have a small variation on a day to day basis. For a successful NASBA reaction, the signal to noise ratio was typically in the order of 1000 for the COC chips.

The first instrument which was used required manual positioning of the silicon chips (**Paper I**). It was difficult to place the microchip in the exact same position every time. This resulted in discrepancies between samples, negative controls as well as the starting point of amplified targets. In addition, variations in concentrations can explain the level of fluorescence. The error introduces a relative shift in detector readout and does not affect the amplification process itself. The results show a distinct difference between negative controls and the amplification curve. The start signal of both the 10 nl and the 50 nl reaction chambers were approximately 2-fold compared to the background signal of empty silicon chips. The fluorescence signal was amplified by a factor of 2 for both chips during the reaction, while the conventional amplification showed an increase of ~7 times. However, this is expected, as baseline offset will become more significant as the reaction volume decreases, and it will dominate at low signal levels. The ratio between the start signal and the background signal in the second instrument and the chips with 10 parallel reaction channels were in the order of 3 (**Paper II**). No crosstalk was detected between the parallel reaction channels. The experiments showed that the ratio between the final fluorescence level and the initial fluorescence level for

the amplification on the microchips was nearly constant for all sample concentrations, while it decreased with sample concentration for the conventional experiments. The overall lower ratio obtained in the microchips could be explained by the enlarged background signal, caused by autofluorescent COC and light scattering from imperfect polymer surfaces. The background signal (**Paper IV**) varies quite a lot also due to the material and backgrounds. Also, the results described in **Paper IV**, illustrates that the field of view is critical. When optimizing the detection volumes in the silicon chips, volumes from 100 nl to 600 nl were used. The optical view of the instrument was adjusted to be able to detect the whole 600 nl chamber. As a result, the signal from the experiment using 100 nl is most likely lost because of the background signal, and the straight line is due to this and not to unsuccessful amplification. It has been possible to perform NASBA at even lower detection volumes. The signal from the 200 nl detection volume is also very low. However, a certain increase is observed. The results presented show that it would be of advantage to increase the detection volume to 500 nl as the increase in signal from 500 nl to 600 nl was not significant.

5 Concluding remarks and future perspectives

To our knowledge, this work presents the very first work employing NASBA in a microchip format at the nanoliter scale. The conventional NASBA reaction was at first reduced by a factor of 2000. However, later the reaction volume on chip was in subsequent experiments increased from 10 nl to 500 nl in order to make more robust and reliable diagnostic applications. The detection limits were found to be comparable to those obtained for experiments performed in conventional routine-based laboratory systems for both oligonucleotides and cell lines. In addition, identification of different targets in one and the same clinical sample by simultaneous detection in multi-parallel reaction chambers is most likely possible and indicates that the microchip and its detection system has a potential for diagnostic use in a POC setting.

Several aspects of the development of a self-contained microchip for NASBA have been tested. The present work provides useful guidelines towards the development of a complete automatic chip performing NASBA. Still, a number of important issues remain to be studied before satisfactory results can be obtained. However, integration of self-contained sample preparation chips along with amplification and detection chips would constitute a fully automatic, laboratory independent diagnostic system. Further, the integrated diagnostic system have to validated with regard to sensitivity, risk of cross-contamination, robustness and the reliability of the system using clinical samples.

This work will be continued through two projects; MicroActive (IST-2005-017319)[215] and SmartHEALTH (FP6-2004-IST-NMP-2-016817)[216] within the EU's 6th IST Framework Programme.

References

1. Chan, A. B. and Fox, J. D. (1999) NASBA and other transcription-based amplification methods for research and diagnostic microbiology, *Rev Med Microbiol*, **10**, 4, 185 - 196

2. Keer, J. T. and Birch, L. (2003) Molecular methods for the assessment of bacterial viability, *J Microbiol Methods*, **53**, 2, 175 - 183

3. Hill, C. S. (1996) Molecular diagnostics for infectious diseases, *J Clin Ligand Assay*, **19**, 1, 43 - 52

4. Hodinka, R. L. (1998) The clinical utility of viral quantitation using molecular methods, *Clin Diagn Virol*, **10**, 1, 25 - 47

5. Reyes, D. R., Iossifidis, D., Auroux, P-A., and Manz, A. (2002) Micro Total Analysis Systems 1. Introduction, Theory and Technology, *Anal Chem*, **74**, 12, 2623 - 2636

6. Auroux, P-A., Iossifidis, D., Reyes, D. R., and Manz, A. (2002) Micro Total Analysis Systems 2. Analytical Standard Operations and Applications, *Anal Chem*, **74**, 12, 2637 - 2652

7. Vilkner, T., Janasek, D., and Manz, A. (2004) Micro total analysis systems. Recent developments, *Anal Chem*, **76**, 12, 3373 - 3385

8. Bayraktar, T. and Pidugu, S. B. (2006) Characterization of liquid flows in microfluidic systems, *Int J Heat Mass Tran*, **49**, 5-6, 815 - 824

9. Krishnan, M., Burke, D. T., and Burns, M. A. (2004) Polymerase chain reaction in high surface-to-volume ratio SiO_2 microstructures, *Anal Chem*, **76**, 22, 6588 - 6593

10. Raja, S., Ching, J., Xi, L. Q., Hughes, S. J., Chang, R., Wong, W., McMillan, W., Gooding, W. E., McCarty, K. S., Chestney, M., Luketich, J. D., and Godfrey, T. E. (2005) Technology for automated, rapid, and quantitative PCR or reverse transcription-PCR clinical testing, *Clin Chem*, **51**, 5, 882 - 890

11. Verpoorte, E. (2002) Microfluidic chips for clinical and forensic analysis, *Electrophoresis*, **23**, 677 - 712

12. Tüdos, A. J., Besselink, G. A. J., and Schasfoort, R. B. M. (2001) Trends in miniaturized total analysis systems for point-of-care testing in clinical chemistry, *Lab Chip*, **1**, 2, 83 - 95

13. Rasooly, A. (2006) Moving biosensors to point-of-care cancer diagnostics, *Biosens Bioelectron*, **21**, 10, 1847 - 1850

14. Rasooly, A. and Jacobson, J. (2006) Development of biosensors for cancer clinical testing, *Biosens Bioelectron*, **21**, 10, 1851 - 1858

15. Yager, P., Edwards, T., Fu, E., Helton, K., Nelson, K., Tam, M. R., and Weigl, B. H. (2006) Microfluidic diagnostic technologies for global public health, *Nature*, **442**, 7101, 412 - 418

16. Khandurina, J. and Guttman, A. (2002) Bioanalysis in microfluidic devices, *J Chromatogr A*, **943**, 159 - 183

17. Lee, S. J. and Lee, S. Y. (2004) Micro total analysis system (mu-TAS) in biotechnology, *Appl Microbiol Biotechnol*, **64**, 3, 289 - 299

18. Ginocchio, C. C., Kemper, M., Stellrecht, K. A., and Witt, D. J. (2003) Multicenter evaluation of the performance characteristics of the NucliSens HIV-1 QT assay used for quantitation of human immunodeficiency virus type 1 RNA, *J Clin Microbiol*, **41**, 1, 164 - 173

19. Kraus, I., Molden, T., Erno, L. E., Skomedal, H., Karlsen, F., and Hagmar, B. (2004) Human papillomavirus oncogenic expression in the dysplastic portio; an investigation of biopsies from 190 cervical cones, *Br J Cancer*, **90**, 7, 1407 - 1413

20. Molden, T., Kraus, I., Karlsen, F., Skomedal, H., Nygard, J. F., and Hagmar, B. (2005) Comparison of human papillomavirus messenger RNA and DNA detection: A cross-sectional study of 4,136 women < 30 years of age with a 2-year follow-up of high-grade squamous intraepithelial lesion, *Cancer Epidemiol Biomarkers Prev*, **14**, 2, 367 - 372

21. Cuschieri, K. S., Whitley, M. J., and Cubie, H. A. (2004) Human papillomavirus type specific DNA and RNA persistence - Implications for cervical disease progression and monitoring, *J Med Virol*, **73**, 1, 65 - 70

22. Walboomers, J. M. M., Jacobs, M. V., Manos, M. M., Bosch, F. X., Kummer, J. A., Shah, K. V., Snijders, P. J. F., Peto, J., Meijer, C. J. L. M., and Munoz, N. (1999) Human papillomavirus is a necessary cause of invasive cervical cancer worldwide, *J Pathol*, **189**, 1, 12 - 19

23. Parkin, D. M., Bray, F., Ferlay, J., and Pisani, P. (2005) Global cancer statistics, 2002, *CA Cancer J Clin*, **55**, 2, 74 - 108

24. Muñoz, N., Bosch, F. X, de Sanjosé, S., Herrero, R., Castellsagué, X., Shah, K. V., Snijders, P. J. F., and Meijer, C. J. L. M. (2003) Epidemiologic Classification of Human Papillomavirus Types Associated with Cervial Cancer, *N Engl J Med*, **348**, 6, 518 - 527

25. Jenkins, D. (2001) Diagnosing human papillomaviruses: recent advances, *Curr Opin Infect Dis*, **14**, 1, 53 - 62

26. Gulliksen, A. and Karlsen, F. (2007) Microchips for the diagnosis of cervical cancer, *Microchip-based Assay Systems: Methods and Application*, Humana Press Inc., Totowa, NJ, 1, 65 - 86

27. Cook, N. (2003) The use of NASBA for the detection of microbial pathogens in food and environmental samples, *J Microbiol Methods*, **53**, 2, 165 - 174

28. Lockhart, D. J. and Winzeler, E. A. (2000) Genomics, gene expression and DNA arrays, *Nature*, **405**, 6788, 827 - 836

29. Compton, J. (1991) Nucleic acid sequence-based amplification, *Nature*, **350**, 6313, 91 - 92

30. Leone, G., vanSchijndel, H., vanGemen, B., Kramer, F. R., and Schoen, C. D. (1998) Molecular beacon probes combined with amplification by NASBA enable homogeneous, real-time detection of RNA, *Nucleic Acids Res*, **26**, 9, 2150 - 2155

31. Tyagi, S. and Kramer, F. R. (1996) Molecular Beacons: Probes that Fluoresce upon Hybridization, *Nat Biotechnol*, **14**, 303 - 308

32. Weusten, J. J. A. M., Carpay, W. M., Oosterlaken, T. A. M., van Zuijlen, M. C. A., and van de Wiel, P. A. (2002) Principles of quantitation of viral loads using nucleic acid sequence-based amplification in combination with homogeneous detection using molecular beacons, *Nucleic Acids Res*, **30**, 6,

33. Malek, L., Darasch, S., Davey, C., Henderson, G., Howes, M., Lens, P., and Sooknanan, R. (1992) Application of NASBA isothermal nucleic-acid amplification method to the diagnosis of HIV-1, *Clin Chem*, **38**, 3, 458 - 458

34. Deiman, B., van Aarle, P., and Sillekens, P. (2002) Characteristics and applications of nucleic acid sequence-based amplification (NASBA), *Mol Biotechnol*, **20**, 2, 163 - 179

35. Greijer, A. E., Adriaanse, H. M. A., Kahl, M., Tacken, N. M. M., Oldenburg, N., Sijlmans, A., van de Crommert, J. M. G., Drekkers, C. A. J., Sillekens, P. T. G, and Middeldorp, J. M. (2001) Quantitative competitive NASBA for measuring mRNA expression levels of the immediate early 1, late pp67, and immune evasion genes US3, US6 and US11 in cells infected with human cytomegalovirus, *J Virol Methods*, **96**, 133 - 147

36. Tong, J. F., Bendahhou, S., Chen, H., and Agnew, W. S. (1994) A simplified method for single-cell RT-PCR that can detect and distinguish genomic DNA and messanger-RNA transcripts, *Nucleic Acids Res*, **22**, 15, 3253 - 3254

37. Simpkins, S. A., Chan, A. B., Hays, J., Popping, B., and Cook, N. (2000) An RNA transcription-based amplification technique (NASBA) for the detection of viable Salmonella enterica, *Lett Appl Microbiol*, **30**, 1, 75 - 79

38. Guatelli, J. C., Whitefield, K. M., Kwoh, D. Y., Barringer, K. J., Richman, D. D., and Gingeras, T. R. (1990) Isothermal, invitro amplification of nucleic acids by a multienzyme reaction modeled after retroviral replication, *Proc Natl Acad Sci USA*, **87**, 5, 1874 - 1878

39. Kievits, T., vanGemen, B., Vanstrijp, D., Schukkink, R., Dircks, M., Adriaanse, H., Malek, L., Sooknanan, R., and Lens, P. (1991) NASBA isothermal enzymatic invitro nucleic-acid amplification optimized for the diagnosis of HIV-1 infection, *J Virol Methods*, **35**, 3, 273 - 286

40. Milligan, J. F., Groebe, D. R., Witherell, G. W., and Uhlenbeck, O. C. (1987) Oligoribonucleotide synthesis using T7 RNA-polymerase and synthetic DNA templates, *Nucleic Acids Res*, **15**, 21, 8783 - 8798

41. Jin, S. and Breuer, K. S. (2003) Diffusion-limited evaporation in long microchannels, *Proceedings of IMECE03*

42. Pourahmadi, F., McMillan, W. A., Ching, J., Chang, R., Christel, L. A., Kovacs, G. T. A., Northrup, M. A., and Petersen, K. E., (2003) *Device incorporating a microfluidic chip for separating analyte from a sample*, US 6664104 B2

43. Dittrich, P. S. and Manz, A. (2006) Lab-on-a-chip: microfluidics in drug discovery, *Nat Rev Drug Discov*, **5**, 3, 210 - 218

44. Delamarche, E., Juncker, D., and Schmid, H. (2005) Microfluidics for processing surfaces and miniaturizing biological assays, *Adv Mater*, **17**, 24, 2911 - 2933

45. Verpoorte, E. (2003) Chip vision - optics for microchips, *Lab Chip*, **3**, 3, 42N - 52N

46. de Mello, A. J. (2003) Seeing single molecules, *Lab Chip*, **3**, 2, 29N - 34N

47. Dittrich, P. S. and Manz, A. (2005) Single-molecule fluorescence detection in microfluidic channels - the Holy Grail in muTAS?, *Anal Bioanal Chem*, **382**, 8, 1771 - 1782

48. Fiorini, G. S. and Chiu, D. T. (2005) Disposable microfluidic devices: fabrication, function, and application, *Biotechniques*, **38**, 3, 429 - 446

49. Schwarz, M. A. and Hauser, P. C. (2001) Recent developments in detection methods for microfabricated analytical devices, *Lab Chip*, **1**, 1, 1 - 6

50. Grow, A. E., Wood, L. L., Claycomb, J. L., and Thompson, P. A. (2003) New biochip technology for label-free detection of pathogens and their toxins, *J Microbiol Methods*, **53**, 2, 221 - 233

51. Verpoorte, E. and De Rooij, N. F. (2003) Microfluidics meets MEMS, *Proceedings of the IEEE*, **91**, 6, 930 - 953

52. van Merkerk, R. O. and van den Berg, A. (2006) More than technology alone, *Lab Chip*, **6**, 7, 838 - 839

53. www.abbottpointofcare.com/istat (2006)

54. Hughes, S. J., Xi, L. Q., Raja, S., Gooding, W., Cole, D. J., Gillanders, W. E., Mikhitarian, K., McCarty, K., Silver, S., Ching, J., McMillan, W., Luketich, J. D., and Godfrey, T. E. (2006) A rapid, fully automated, molecular-based assay accurately analyzes sentinel lymph nodes for the presence of metastatic breast cancer, *Ann Surg*, **243**, 3, 389 - 398

55. Ulrich, M. P., Christensen, D. R., Coyne, S. R., Craw, P. D., Henchal, E. A., Sakai, S. H., Swenson, D., Tholath, J., Tsai, J., Weir, A. F., and Norwood, D. A. (2006) Evaluation of the Cepheid GeneXpert (R) system for detecting *Bacillus anthracis*, *J Appl Microbiol*, **100**, 5, 1011 - 1016

56. Lee, T. M. H. and Hsing, I. M. (2006) DNA-based bioanalytical microsystems for handheld device applications, *Anal Chim Acta*, **556**, 1, 26 - 37

57. Haber, C. (2006) Microfluidics in commercial applications; an industry perspective, *Lab Chip*, **6**, 1118 - 1121

58. van den Berg, A. and Bergveld, P. (2006) Labs-on-a-chip: origin, highlights and future perspectives - On the occasion of the 10th µTAS conference, *Lab Chip*, **6**, 1266 - 1273

59. Clayton, J. (2005) Go with the microflow, *Nat Methods*, **2**, 8, 621 - 627

60. Ferrance, J. P., Wu, Q. R., Giordano, B., Hernandez, C., Kwok, Y., Snow, K., Thibodeau, S., and Landers, J. P. (2003) Developments toward a complete micro-total analysis system for Duchenne muscular dystrophy diagnosis, *Anal Chim Acta*, **500**, 1-2, 223 - 236

61. Northrup, M. A., Ching, M. T., White, R. M., and Watson, R. T. (1993) DNA amplification with a microfabricated reaction chamber, *Transducers '93 the 7th International Conference on Solid-State Sensors and Actuators*, 924 - 927

62. Zhang, C. S., Xu, J. L., Ma, W. L., and Zheng, W. L. (2006) PCR microfluidic devices for DNA amplification, *Biotechnol Adv*, **24**, 3, 243 - 284

63. Obeid, P. J. and Christopoulos, T. K. (2004) Microfabricated systems for nucleic acid analysis, *Crit Rev Clin Lab Sci*, **41**, 5-6, 429 - 465

64. Kricka, L. J. and Wilding, P. (2003) Microchip PCR, *Anal Bioanal Chem*, **377**, 5, 820 - 825

65. Auroux, P. A., Koc, Y., deMello, A., Manz, A., and Day, P. J. R. (2004) Miniaturised nucleic acid analysis, *Lab Chip*, **4**, 6, 534 - 546

66. deMello, A. J. (2001) DNA amplification: does 'small' really mean 'efficient'?, *Lab Chip*, **1**, 2, 24N - 29N

67. Liu, J., Enzelberger, M., and Quake, S. (2002) A nanoliter rotary device for polymerase chain reaction, *Electrophoresis*, **23**, 10, 1531 - 1536

68. Liu, J., Hansen, C., and Quake, S. R. (2003) Solving the "world-to-chip" interface problem with a microfluidic matrix, *Anal Chem*, **75**, 18, 4718 - 4723

69. Anderson, R. C., Su, X., Bogdan, G. J., and Fenton, J. (2000) A miniature integrated device for automated multistep genetic assays, *Nucleic Acids Res*, **28**, 12, e60 - e60

70. Obeid, P. J., Christopoulos, T. K., Crabtree, H. J., and Backhouse, C. J. (2003) Microfabricated device for DNA and RNA amplification by continuous-flow polymerase chain reaction and reverse transcription-polymerase chain reaction with cycle number selection, *Anal Chem*, **75**, 2, 288 - 295

71. Obeid, P. J. and Christopoulos, T. K. (2003) Continuous-flow DNA and RNA amplification chip combined with laser-induced fluorescence detection, *Analytica Chimica Acta*, **494**, 1-2, 1 - 9

72. Marcus, J. S., Anderson, W. F., and Quake, S. R. (2006) Parallel picoliter RT-PCR assays using microfluidics, *Anal Chem*, **78**, 3, 956 - 958

73. Liao, C. S., Lee, G. B., Liu, H. S., Hsieh, T. M., and Luo, C. H. (2005) Miniature RT-PCR system for diagnosis of RNA-based viruses, *Nucleic Acids Res*, **33**, 18,

74. Ives, J., Gerdes, J., Weigl, B., and Hayenga, J. (2003) Molecular diagnostics with a fully integrated microfluidic system, *smallTalk2003*, 36

75. Baeumner, A. J., Jones, C., Wong, C. Y., and Price, A. (2004) A generic sandwich-type biosensor with nanomolar detection limits, *Anal Bioanal Chem*, **378**, 6, 1587 - 1593

76. Esch, M. B., Locascio, L. E., Tarlov, M. J., and Durst, R. A. (2001) Detection of viable *Cryptosporidium parvum* using DNA-modified liposomes in a microfluidic chip, *Anal Chem*, **73**, 13, 2952 - 2958

77. Baeumner, A. J., Cohen, R. N., Miksic, V., and Min, J. (2003) RNA biosensor for rapid detection of viable *Escherichia coli* in drinking water, *Biosens Bioelectron*, **18**, 405 - 413

78. Baeumner, A. J., Pretz, J., and Fang, S. (2004) A universal nucleic acid sequence biosensor with nanomolar detection limits, *Anal Chem*, **76**, 4, 888 - 894

79. Zaytseva, N. V., Goral, V. N., Montagna, R. A., and Baeumner, A. J. (2005) Development of a microfluidic biosensor module for pathogen detection, *Lab Chip*, **5**, 8, 805 - 811

80. Zaytseva, N. V., Montagna, R. A., and Baeumner, A. J. (2005) Microfluidic biosensor for the serotype-specific detection of Dengue virus RNA, *Anal Chem*, **77**, 23, 7520 - 7527

81. Whitesides, G. M. (2006) The origins and the future of microfluidics, *Nature*, **442**, 7101, 368 - 373

82. Zimmermann, M., Bentley, S., Schmid, H., Hunziker, P., and Delamarche, E. (2005) Continuous flow in open microfluidics using controlled evaporation, *Lab Chip*, **5**, 12, 1355 - 1359

83. Walker, G. M. and Beebe, D. J. (2002) An evaporation-based microfluidic sample concentration method, *Lab Chip*, **2**, 2, 57 - 61

84. Goldschmidtboeing, F., Rabold, M., and Woias, P. (2006) Strategies for void-free liquid filling of micro cavities, *J Micromech Microeng*, **16**, 7, 1321 - 1330

85. Laser, D. J. and Santiago, J. G. (2004) A review of micropumps, *J Micromech Microeng*, **14**, 6, R35 - R64

86. Nguyen, N. T. and Wu, Z. G. (2005) Micromixers - a review, *J Micromech Microeng*, **15**, 2, R1 - R16

87. Rios, A., Escarpa, A., Gonzalez, M. C., and Crevillen, A. G. (2006) Challenges of analytical microsysterns, *TrAC Trends Anal Chem*, **25**, 5, 467 - 479

88. Geschke, O., Klank, H., and Telleman, P., (2004) *Microsystem engineering of lab-on-a-chip devices*, Wiley-VCH Verlag GmbH & Co, Weinheim

89. Beebe, D. J., Mensing, G. A., and Walker, G. M. (2002) Physics and applications of microfluidics in biology, *Annu Rev Biomed Eng*, **4**, 261 - 286

90. Becker, H. and Locascio, L. E. (2002) Polymer microfluidic devices, *Talanta*, **56**, 2, 267 - 287

91. Rohr, T., Ogletree, D. F., Svec, F., and Frechet, J. M. J. (2003) Surface functionalization of thermoplastic polymers for the fabrication of microfluidic devices by photoinitiated grafting, *Adv Funct Mater*, **13**, 4, 264 - 270

92. deMello, A. J. (2002) Plastic fantastic?, *Lab Chip*, **2**, 2, 31N - 36N

93. Li, P. C. H., (2006) *Microfluidic Lab-on-a-Chip for Chemical and Biological Analysis and Discovery*, CRC Press Taylor & Francis Group, Boca Raton

94. Nguyen, N-T. and Wereley, S. T., (2002) *Fundamentals and applications of microfluidics*, Artech House, Inc., Norwood

95. Ahn, C., Choi, J-W., Beaucage, G, Nevin, J. H., Lee, J-B., Puntambekar, A., and Lee, J. Y. (2004) Disposable Smart Lab on a Chip for Point-of-care Clinical Diagnostics, *Proceedings of the IEEE*, **92**, 1, 154 - 173

96. Hawkins, K. R. and Yager, P. (2003) Nonlinear decrease of background fluorescence in polymer thin-films - a survey of materials and how they can complicate fluorescence detection in mu TAS, *Lab Chip*, **3**, 4, 248 - 252

97. Senturia, S. D, (2001) *Microsystem design*, Springer Science + Business Media, Inc., New York

98. Mitchell, P. (2001) Microfluidics - downsizing large-scale biology, *Nat Biotechnol*, **19**, 8, 717 - 721

99. Dittrich, P. S., Tachikawa, K., and Manz, A. (2006) Micro total analysis systems. Latest advancements and trends, *Anal Chem*, **78**, 12, 3887 - 3907

100. Lamonte, R. R. and McNally, D. (2001) Cyclic olefin copolymers, *Adv Mater Process*, **159**, 3, 33 - 36

101. Snakenborg, D., Perozziello, G., Klank, H., Geschke, O., and Kutter, J. P. (2006) Direct milling and casting of polymer-based optical waveguides for improved transparency in the visible range, *J Micromech Microeng*, **16**, 2, 375 - 381

102. Becker, H. and Gartner, C. (2000) Polymer microfabrication methods for microfluidic analytical applications, *Electrophoresis*, **21**, 1, 12 - 26

103. Shoffner, M. A., Cheng, J., Hvichia, G. E., Kricka, L. J., and Wilding, P. (1996) Chip PCR 1. Surface passivation of microfabricated silicon-glass chips for PCR, *Nucleic Acids Res*, **24**, 2, 375 - 379

104. Cheng, J., Shoffner, M. A., Hvichia, G. E., Kricka, L. J., and Wilding, P. (1996) Chip PCR 2. Investigation of different PCR amplification systems in microfabricated silicon-glass chips, *Nucleic Acids Res*, **24**, 2, 380 - 385

105. Taylor, T. B., WinnDeen, E. S., Picozza, E., Woudenberg, T. M., and Albin, M. (1997) Optimization of the performance of the polymerase chain reaction in silicon-based microstructures, *Nucleic Acids Res*, **25**, 15, 3164 - 3168

106. Erill, I., Campoy, S., Erill, N., Barbe, J., and Aguilo, J. (2003) Biochemical analysis and optimization of inhibition and adsorption phenomena in glass-silicon PCR-chips, *Sens Actuators B*, **96**, 3, 685 - 692

107. Panaro, N. J., Lou, X. J., Fortina, P., Kricka, L. J., and Wilding, P. (2004) Surface effects on PCR reactions in multichip microfluidic platforms, *Biomed Microdevices*, **6**, 1, 75 - 80

108. Lou, X. J., Panaro, N. J., Wilding, P., Fortina, P., and Kricka, L. J. (2004) Mutation detection using ligase chain reaction in passivated silicon-glass microchips and microchip capillary electrophoresis, *Biotechniques*, **37**, 3, 392 - 398

109. Lou, X. J., Panaro, N. J., Wilding, P., Fortina, P., and Kricka, L. J. (2004) Increased amplification efficiency of microchip-based PCR by dynamic surface passivation, *Biotechniques*, **36**, 2, 248 - 251

110. Ratner, B. D. (1995) Surface modification of polymers - chemical, biological and surface analytical challenges, *Biosens Bioelectron*, **10**, 797 - 804

111. Landers, J. P. (2003) Molecular diagnostics on electrophoretic microchips, *Anal Chem*, **75**, 12, 2919 - 2927

112. Horvath, J. and Dolnik, V. (2001) Polymer wall coatings for capillary electrophoresis, *Electrophoresis*, **22**, 644 - 655

113. Giordano, B. C., Copeland, E. R., and Landers, J. P. (2001) Towards dynamic coating of glass microchip chambers for amplifying DNA via the polymerase chain reaction, *Electrophoresis*, **22**, 334 - 340

114. Kopp, M. U., Luechinger, M. B, and Manz, A. (1998) Chemical Amplification: Continous flow PCR on a chip, *Science*, **280**, 1046 - 1048

115. Khandurina, J., McKnight, T. E., Jacobson, S. C., Waters, L. C., Foote, R. S., and Ramsey, J. M. (2000) Integrated system for rapid PCR-based DNA analysis in microfluidic devices, *Anal Chem*, **72**, 13, 2995 - 3000

116. Burns, M. A., Johnson, B. N., Brahmasandra, S. N., Handique, K., Webster, J. R., Krishnan, M., Sammarco, T. S., Man, P. M., Jones, D., Heldsinger, D., Mastrangelo, C. H., and Burke, D. T. (1998) An integrated nanoliter DNA analysis device, *Science*, **282**, 5388, 484 - 487

117. Münchow, G., Dadic, D., Doffing, F., Hardt, S., and Drese, K. S. (2005) Automated chip-based device for simple and fast nucleic acid amplification, *Expert Rev Mol Diagn*, **5**, 4, 613 - 620

118. Shin, Y. S., Cho, K., Lim, S. H., Chung, S., Park, S. J., Chung, C., Han, D. C., and Chang, J. K. (2003) PDMS-based micro PCR chip with parylene coating, *J Micromech Microeng*, **13**, 5, 768 - 774

119. Alcantar, N. A., Aydil, E. S., and Israelachvili, J. N. (2000) Polyethylene glycol-coated biocompatible surfaces, *J Biomed Mater Res*, **51**, 3, 343 - 351

120. Andrade, J. D., Hlady, V., and Jeon, S. I. (1996) Poly(ethylene oxide) and protein resistance - Principles, problems, and possibilities, *Hydrophilic polymers*, American Chemical Society, 51 - 59

121. Jeon, S. I., Lee, J. H., Andrade, J. D., and Degennes, P. G. (1991) Protein Surface Interactions in the Presence of Polyethylene Oxide .1. Simplified Theory, *J Colloid Interface Sci*, **142**, 1, 149 - 158

122. Caldwell, K. D. (1997) Surface Modifications with Adsorbed Poly(ethylene oxide)-Based Block Copolymers Physical Characteristics and Biological Use, *Poly(ethylene glycol) Chemistry and Biological Applications*, American Chemical Society, San Francisco, CA, 400 - 419

123. Wang, J., Chen, Z. Y., Corstjens, P. L. A. M., Mauk, M. G., and Bau, H. H. (2006) A disposable microfluidic cassette for DNA amplification and detection, *Lab Chip*, **6**, 1, 46 - 53

124. Matsubara, V., Kerman, H., Kobayashi, M., Yamamura, S., Morita, V., Takamura, Y., and Tamiya, E. (2004) On-chip nanoliter-volume multiplex TaqMan polymerase chain reaction from a single copy based on counting fluorescence released microchambers, *Anal Chem*, **76**, 21, 6434 - 6439

125. Schneegass, I., Bräutigam, R., and Köhler, J. M. (2001) Miniaturized flow-through PCR with different template types in a silicon chip thermocycler, *Lab Chip*, **1**, 1, 42 - 49

126. Yang, J, Liu, Y, Rauch, C. B., Stevens, R. L., Liu, R. L., Lenigk, R., and Grodzinski, P (2002) High sensitivity PCR assay in plastic micro reactors, *Lab Chip*, **2**, 179 - 187

127. Lee, T. M. H., Hsing, I-M, Lao, A. I. K., and Carles, M. C. (2000) A miniaturized DNA Amplifier: Its Application in Traditional Chinese Medicine, *Anal Chem*, **72**, 17, 4242 - 4247

128. Wilson, I. G. (1997) Inhibition and facilitation of nucleic acid amplification, *Appl Environ Microbiol*, **63**, 10, 3741 - 3751

129. Borst, A., Box, A. T. A., and Fluit, A. C. (2004) False-positive results and contamination in nucleic acid amplification assays: Suggestions for a prevent and destroy strategy, *Eur J Clin Microbiol Infect Dis*, **23**, 4, 289 - 299

130. Hatefi, Y and Hanstein, W. G. (1969) Solubilization of particulate proteins and nonelectrolytes by chaotropic agents, *Proc Natl Acad Sci USA*, **62**, 1129 - 1136

131. von Hippel, P. H. and Wong, K-Y. (1964) Neutral Salts: The Generality of Their Effects on the Stability of Macromolecular Conformations, *Science*, **145**, 577 - 580

132. Norde, W. and Lyklema, J. (1992) Why proteins prefer interfaces, *The Vroman Effect*, VSP, 1 - 20

133. www.bioafrica.net (2007)

134. www.uoguelph.ca (2007)

135. Wahlgren, M. and Arnebrant, T. (1991) Protein Adsorption to Solid-Surfaces, *Trends Biotechnol*, **9**, 6, 201 - 208

136. Irvine, D. J., Mayes, A. M., Satija, S. K., Barker, J. G., Sofia-Allgor, S. J., and Griffith, L. G. (1998) Comparison of tethered star and linear poly(ethylene oxide) for control of biomaterials surface properties, *J Biomed Mater Res*, **40**, 3, 498 - 509

137. Soderquist, M. E. and Walton, A. G. (1980) Structural changes in proteins adsorbed on polymer surfaces, *J Colloid Interface Sci*, **75**, 2, 386 - 397

138. Adamson, A. W. and Gast, A. P., (1997) *Physical chemistry of surfaces*, John Wiley & Sons, Inc., New York, 6th edn

139. Beissinger, R. L. and Leonard, E. F. (1981) Plasma protein adsorption and desorption rates on quartz: approach to multi-component systems, *Trans Am Soc Artif Intern Organs*, **27**, 225 - 230

140. Lundstrom, I. and Elwing, H. (1990) Simple Kinetic-Models for Protein Exchange-Reactions on Solid-Surfaces, *J Colloid Interface Sci*, **136**, 1, 68 - 84

141. de Rosier, T. A., de la Cruz, N. B., and Wilkosz, R. K., (2001) *Method and formulation for stabilization of enzymes*, US 6294365 B1

142. Roy, I. and Gupta, M. N. (2004) Freeze-drying of proteins: some emerging concerns, *Biotechnol Appl Biochem*, **39**, 165 - 177

143. Carpenter, J. F., Prestrelski, S. J., and Arakawa, T. (1993) Separation of Freezing- and Drying-Induced Denaturation of Lyophilized Proteins Using Stress-Specific Stabilization : I. Enzyme Activity and Calorimetric Studies, *Archives of Biochemistry and Biophysics*, **303**, 2, 456 - 464

144. Prestrelski, S. J., Arakawa, T., and Carpenter, J. F. (1993) Separation of Freezing- and Drying-Induced Denaturation of Lyophilized Proteins Using Stress-Specific Stabilization : II. Structural Studies Using Infrared Spectroscopy, *Arch Biochem Biophys*, **303**, 2, 465 - 473

145. Roser, B. J., (1990) *Protection of proteins and the like*, US 4891319

146. Carpenter, J. F., Crowe, J. H., and Arakawa, T. (1990) Comparison of solute-induced protein stabilization in aqueous-solution and in the frozen and dried states, *J Dairy Sci*, **73**, 12, 3627 - 3636

147. Anchordoquy, T. J. and Carpenter, J. F. (1996) Polymers protect lactate dehydrogenase during freeze-drying by inhibiting dissociation in the frozen state, *Arch Biochem Biophys*, **332**, 2, 231 - 238

148. Lagally, E. T., Simpson, P. C., and Mathies, R. A. (2000) Monolithic integrated microfluidic DNA amplification and capillary electrophoresis analysis system, *Sens Actuators B*, **63**, 3, 138 - 146

149. Chen, D. L. and Ismagilov, R. F. (2006) Microfluidic cartridges preloaded with nanoliter plugs of reagents: an alternative to 96-well plates for screening, *Curr Opin Chem Biol.*, **10**, 3, 226 - 231

150. Linder, V., Sia, S. K., and Whitesides, G. M. (2005) Reagent-loaded cartridges for valveless and automated fluid delivery in microfluidic devices, *Anal Chem*, **77**, 1, 64 - 71

151. Seetharam, R., Wada, Y., Ramachandran, S., Hess, H., and Satir, P. (2006) Long-term storage of bionanodevices by freezing and lyophilization, *Lab Chip*, **6**, 9, 1239 - 1242

152. Garcia, E., Kirkham, J. R., Hatch, A. V., Hawkins, K. R., and Yager, P. (2004) Controlled microfluidic reconstitution of functional protein from an anhydrous storage depot, *Lab Chip*, **4**, 1, 78 - 82

153. Puckett, L. G., Dikici, E., Lai, S., Madou, M., Bachas, L. G., and Daunert, S. (2004) Investigation into the applicability of the centrifugal microfluidics development of protein-platform for the ligand binding assays incorporating enhanced green fluorescent protein as a fluorescent reporter, *Anal Chem*, **76**, 24, 7263 - 7268

154. Schena, M., Shalon, D., Davis, R. W., and Brown, P. O. (1995) Quantitative monitoring of gene-expression patterns with a complementary-DNA microarray, *Science*, **270**, 5235, 467 - 470

155. Schena, M. (1996) Genome analysis with gene expression microarrays, *Bioessays*, **18**, 5, 427 - 431

156. Ramsay, G. (1998) DNA chips: State-of-the-art, *Nat Biotechnol*, **16**, 1, 40 - 44

157. Ringeisen, B. R., Wu, P. K., Kim, H., Pique, A., Auyeung, R. Y. C., Young, H. D., Chrisey, D. B., and Krizman, D. B. (2002) Picoliter-scale protein microarrays by laser direct write, *Biotechnol Prog*, **18**, 5, 1126 - 1129

158. Koltay, P., Steger, R., Bohl, B., and Zengerle, R. (2004) The dispensing well plate: a novel nanodispenser for the multiparallel delivery of liquids (DWP Part I), *Sens Actuators A*, **116**, 3, 483 - 491

159. Steinert, C. P., Goutier, I., Gutmann, O., Sandmaier, H., Daub, M., de Heij, B., and Zengerle, R. (2004) A highly parallel picoliter dispenser with an integrated, novel capillary channel structure, *Sens Actuators A*, **116**, 1, 171 - 177

160. Breisch, S., de Heij, B., Lohr, M., and Stezle, M. (2004) Selective chemical surface modification of fluidic microsystems and characterization studies, *J Micromech Microeng*, **14**, 4, 497 - 505

161. Gutmann, O., Kuehlewein, R., Reinbold, S., Niekrawietz, R., Steinert, C. P., de Heij, B., Zengerle, R., and Daub, M. (2005) Fast and reliable protein microarray production by a new drop-in-drop technique, *Lab Chip*, **5**, 6, 675 - 681

162. de Heij, B., Daub, M., Gutmann, O., Niekrawietz, R., Sandmaier, H., and Zengerle, R. (2004) Highly parallel dispensing of chemical and biological reagents, *Anal Bioanal Chem*, **378**, 1, 119 - 122

163. Epstein, J. R., Biran, I., and Walt, D. R. (2002) Fluorescence-based nucleic acid detection and microarrays, *Anal Chim Acta*, **469**, 1, 3 - 36

164. Gast, F. U. and Fiehn, H. (2003) The development of integrated microfluidic systems at GeSiM, *Lab Chip*, **3**, 1, 6N - 10N

165. Schaeferling, M., Schiller, S., Paul, H., Kruschina, M., Pavlickova, P., Meerkamp, M., Giammasi, C., and Kambhampati, D. (2002) Application of self-assembly techniques in the design of biocompatible protein microarray surfaces, *Electrophoresis*, **23**, 3097 - 3105

166. Fang, X. H., Li, B. Q., Petersen, E., Seo, Y. S., Samuilov, V. A., Chen, Y., Sokolov, J. C., Shew, C. Y., and Rafailovich, M. H. (2006) Drying of DNA droplets, *Langmuir*, **22**, 14, 6308 - 6312

167. Fang, X. H., Li, B. Q., Petersen, E., Ji, Y., Sokolov, J. C., and Rafailovich, M. H. (2005) Factors controlling the drop evaporation constant, *J Phys Chem B*, **109**, 43, 20554 - 20557

168. Prestrelski, S. J., Arakawa, T., and Carpenter, J. F. (1993) Separation of Freezing- and Drying-Induced Denaturation of Lyophilized Proteins Using Stress-Specific Stabilization: II. Structural Studies Using Infrared Spectroscopy, *Arch Biochem Biophys*, **303**, 2, 465 - 473

169. Su, F., Chakrabarty, K., and Fair, R. B. (2006) Microfluidics-based biochips: Technology issues, implementation platforms, and design-automation challenges, *IEEE Transactions on Computer-Aided Design of Integrated Circuits and Systems*, **25**, 2, 211 - 223

170. Eijkel, J. C. T. and van den Berg, A. (2005) Water in micro- and nanofluidics systems described using the water potential, *Lab Chip*, **5**, 11, 1202 - 1209

171. Jakeway, S. C., deMello, A. J., and Russell, E. L. (2000) Miniaturized total analysis systems for biological analysis, *Fresenius J Anal Chem*, **366**, 6-7, 525 - 539

172. Squires, T. M. and Quake, S. R. (2005) Microfluidics: Fluid physics at the nanoliter scale, *Rev Mod Phys*, **77**, 3, 977 - 1026

173. Stroock, A. D., Dertinger, S. K. W., Ajdari, A., Mezic, I., Stone, H. A., and Whitesides, G. M. (2002) Chaotic mixer for microchannels, *Science*, **295**, 5555, 647 - 651

174. www.hdm-stuttgart.de (2007)

175. vanGemen, B., VanBeuningen, R., Nabbe, A., Vanstrijp, D., Jurriaans, S., Lens, P., and Kievits, T. (1994) A one-tube quantitative HIV-1 RNA NASBA nucleic-acid amplification assay using electrochemiluminescent (ECL) labeled probes, *J Virol Methods*, **49**, 2, 157 - 167

176. Tyagi, S., Bratu, D. P., and Kramer, F. R. (1998) Multicolor molecular beacons for allele discrimination, *Nat Biotechnol*, **16**, 49 - 53

177. Vet, J. A. M., van der Rijt, B. J. M., and Blom, H. J. (2002) Molecular beacons: colorful analysis of nucleic acids, *Expert Rev Mol Diagn*, **2**, 1, 77 - 86

178. Drake, T. J. and Tan, W. H. (2004) Molecular beacon DNA probes and their bioanalytical applications, *Appl Spectrosc*, **58**, 9, 269A - 280A

179. Niesters, H. G. M. (2001) Quantitation of Viral Load Using Real-Time Amplification Techniques, *Methods*, **25**, 4, 419 - 429

180. Monis, P. T. and Giglio, S. (2006) Nucleic acid amplification-based techniques for pathogen detection and identification, *Infect Genet Evol*, **6**, 1, 2 - 12

181. Fang, X. H., Li, J. W. J., Perlette, J., Tan, W. H., and Wang, K. M. (2000) Molecular beacons - Novel fluorescent probes, *Anal Chem*, **72**, 23, 747A - 753A

182. Bonnet, G., Tyagi, S., Libchaber, A., and Kramer, F. R. (1999) Thermodynamic basis of the enhanced specificity of structured DNA probes, *Proc Natl Acad Sci USA*, **96**, 6171 - 6176

183. deBaar, M. P., vanDooren, M. W., deRooij, E., Bakker, M., vanGemen, B., Goudsmit, J., and deRonde, A. (2001) Single rapid real-time monitored isothermal RNA amplification assay for quantification of human immunodeficiency virus type 1 isolates from groups M, N, and O, *J Clin Microbiol*, **39**, 4, 1378 - 1384

184. Fister, J. C., Jacobson, S. C., Davis, L. M., and Ramsey, J. M. (1998) Counting Single Chromophore Molecules for Ultrasensitive Analysis and Separations on Microchip Devices, *Anal Chem*, **70**, 431 - 437

185. Craighead, H. (2006) Future lab-on-a-chip technologies for interrogating individual molecules, *Nature*, **442**, 7101, 387 - 393

186. Bruno, A. E., Maystre, F., Krattiger, B., Nussbaum, P., and Gassmann, E. (1994) The pigtailing approach to optical-detection in capillary electrophoresis, *Trends Anal Chem*, **13**, 5, 190 - 198

187. Demchenko, A. P. (2005) The problem of self-calibration of fluorescence signal in microscale sensor systems, *Lab Chip*, **5**, 11, 1210 - 1223

188. Song, L. L., Varma, C. A. G. O., Verhoeven, J. W., and Tanke, H. J. (1996) Influence of the triplet excited state on the photobleaching kinetics of fluorescein in microscopy, *Biophys J*, **70**, 6, 2959 - 2968

189. Irawan, R., Tjin, S., Yager, P., and Zhang, D. (2005) Cross-talk problem on a fluorescence multi-channel microfluidic chip system, *Biomed Microdevices*, **7**, 3, 205 - 211

190. Ducrée, J. and Zengerle, R. (2005) FlowMap: microfluidics roadmap for the life sciences, *www.microfluidics-roadmap.com*

191. Hong, J. W. and Quake, S. R. (2003) Integrated nanoliter systems, *Nat Biotechnol*, **21**, 10, 1179 - 1183

192. Liu, R. H., Yang, J. N., Lenigk, R., Bonanno, J., and Grodzinski, P. (2004) Self-contained, fully integrated biochip for sample preparation, polymerase chain reaction amplification, and DNA microarray detection, *Anal Chem*, **76**, 7, 1824 - 1831

193. Thorsen, T., Maerkl, S. J., and Quake, S. R. (2002) Microfluidic large-scale integration, *Science*, **298**, 580 - 584

194. Hong, J. W., Studer, V., Hang, G., Anderson, W. F., and Quake, S. R. (2004) A nanoliter-scale nucleic acid processor with parallel architecture, *Nat Biotechnol*, **22**, 4, 435 - 439

195. Nguyen, D. C., Keller, R. A., Jett, J. H., and Martin, J. C. (1987) Detection of Single Molecules of Phycoerythrin in Hydrodynamically Focused Flows by Laser-Induced Fluorescence, *Anal Chem*, **59**, 17, 2158 - 2161

196. Dovichi, N. J., Martin, J. C., Jett, J. H., and Keller, R. A. (1983) Attogram detection limit for aqueous dye samples by laser-induced fluorescence, *Science*, **219**, 845 - 847

197. Leamon, J. H., Lee, W. L., Tartaro, K. R., Lanza, J. R., Sarkis, G. J., deWinter, A. D., Berka, J., and Lohman, K. L. (2003) A massively parallel PicoTiterPlate (TM) based platform for discrete picoliter-scale polymerase chain reactions, *Electrophoresis*, **24**, 21, 3769 - 3777

198. de Boer, M. A., Jordanova, E. S., Kenter, G. G., Peters, A. A., Corver, W. E., Trimbos, J. B., and Fleuren, G. J. (2007) High human papillomavirus oncogene mRNA expression and not viral DNA load is associated with poor prognosis in cervical cancer patients., *Clin Cancer Res*, **13**, 1, 132 - 138

199. Polstra, A. M., Goudsmit, J., and Cornelissen, M. (2002) Development of real-time NASBA assays with molecular beacon detection to quantify mRNA coding for HHV-8 lytic and latent genes, *BMC Infect Dis*, **2**, 1 - 10

200. Lagally, E. T., Medintz, I., and Mathies, R. A. (2000) Single-Molecule DNA amplification DNA Amplification and Analysis in an Integrated Microfluidic Device, *Anal Chem*, **73**, 3, 565 - 570

201. Belgrader, P., Benett, W., Hadley, D., Long, G., Mariella, R., Milanovich, F., Nasarabadi, S., Nelson, W., Richards, J., and Stratton, P. (1998) Rapid pathogen detection using a microchip PCR array Instrument, *Clin Chem*, **44**, 10, 2191 - 2194

202. www.cepheid.com (2007)

203. Lin, Y. C., Huang, M. Y., Young, K. C., Chang, T. T., and Wu, C. Y. (2000) A rapid micro-polymerase chain reaction system for hepatitis C virus amplification, *Sens Actuators B*, **71**, 1-2, 2 - 8

204. Oda, R. P., Strausbauch, M. A., Huhmer, A. F. R., Borson, N., Jurrens, S. R., Craighead, J., Wettstein, P. J., Eckloff, B., Kline, B., and Landers, J. P. (1998) Infrared-mediated thermocycling for ultrafast polymerase chain reaction amplification of DNA, *Anal Chem*, **70**, 20, 4361 - 4368

205. Nagai, H., Murakami, Y., Morita, Y., Yokoyama, K., and Tamiya, E. (2001) Development of a microchamber array for picoliter PCR, *Anal Chem*, **73**, 5, 1043 - 1047

206. Weigl, B. H., Gerdes, J., Tarr, P., Yager, P., Dillman, L., Peck, R., Ramachandran, S., Lemba, M., Kokoris, M., Nabavi, M., Battrell, F., Hoekstra, D., Klein, E. J., and Denno, D. M. (2006) Fully integrated multiplexed lab-on-a-card assay for enteric pathogens, *Proc. of SPIE*, **6112**, 1 - 11

207. Liu, X. J. and Tan, W. H. (1999) A fiber-optic evanescent wave DNA biosensor based on novel molecular beacons, *Anal Chem*, **71**, 22, 5054 - 5059

208. Malek, L., Sooknanan, R., and Compton, J. (1994) Nucleic Acid Sequence-Based Amplification (NASBA[TM]), *Protocols for Nucleic Acid Analysis by Nonradioactive Probes*, Humana Press Inc., Totowa, NJ, 1, 253 - 260

209. Szemes, M. and Schoen, C. D. (2003) Design of molecular beacons for AmpliDet RNA assay - Characterization of binding stability and probe specificity, *Anal Biochem*, **315**, 2, 189 - 201

210. Northrup, M. A., Benett, B, Hadley, D., Landre, P, Lehew, S., Richards, J., and Stratton, P. (1998) A miniature analytical instrument for nucleic acids based on micromachined silicon reaction chambers, *Anal Chem*, **70**, 5, 918 - 922

211. Matsubara, Y., Kerman, K., Kobayashi, M., Yamamura, S., Morita, Y., and Tamiya, E. (2005) Microchamber array based DNA quantification and specific sequence detection from a single copy via PCR in nanoliter volumes, *Biosens Bioelectron*, **20**, 8, 1482 - 1490

212. Chen, Z. Y., Wang, J., Qian, S. Z., and Bau, H. H. (2005) Thermally-actuated, phase change flow control for microfluidic systems, *Lab Chip*, **5**, 11, 1277 - 1285

213. Gong, H. Q., Ramalingam, N., Chen, L. Q., Che, J., Wang, Q. H., Wang, Y. M., Yang, X. H., Yap, P. H. E., and Neo, C. H. (2006) Microfluidic handling of PCR solution and DNA amplification on a reaction chamber array biochip, *Biomed Microdevices*, **8**, 2, 167 - 176

214. Gliere, A. and Delattre, C. (2006) Modeling and fabrication of capillary stop valves for planar microfluidic systems, *Sens Actuators A*, **130**, 601 - 608

215. www.sintef.no/microactive (2007)

216. www.smarthealthip.com (2007)

Appendix; Papers I – IV

Paper I

Articles

Real-Time Nucleic Acid Sequence-Based Amplification in Nanoliter Volumes

Anja Gulliksen,*,†,‡ Lars Solli,†,§ Frank Karlsen,† Henrik Rogne,‖ Eivind Hovig,⊥ Trine Nordstrøm,† and Reidun Sirevåg‡

NorChip AS, Industriveien 8, 3490 Klokkarstua, Norway, Department of Biology, University of Oslo, Kristine Bonnevies hus, 0316 Oslo, Norway, Department of Energy and Process Engineering, Norwegian University of Science and Technology, Kolbjørn Hejes vei 1B, 7491 Trondheim, Norway, Department of Microsystems, SINTEF Electronics and Cybernetics, Forskningsveien 1, 0314 Oslo, Norway, and Department of Tumor Biology, Norwegian Radium Hospital, Montebello, 0310 Oslo, Norway

Real-time nucleic acid sequence-based amplification (NASBA) is an isothermal method specifically designed for amplification of RNA. Fluorescent molecular beacon probes enable real-time monitoring of the amplification process. Successful identification, utilizing the real-time NASBA technology, was performed on a microchip with oligonucleotides at a concentration of 1.0 and 0.1 μM, in 10- and 50-nL reaction chambers, respectively. The microchip was developed in a silicon−glass structure. An instrument providing thermal control and an optical detection system was built for amplification readout. Experimental results demonstrate distinct amplification processes. Miniaturized real-time NASBA in microchips makes high-throughput diagnostics of bacteria, viruses, and cancer markers possible, at reduced cost and without contamination.

Applying microsystem technology to the diversity of analytical problems has become an area of enormous interest, especially in connection with the development of microfluidic chips for clinical and forensic analysis.[1] One advantage of miniaturization is sub-microliter consumption of reagents and sample. In addition, improved heat- and mass-transfer rates may give faster reaction kinetics. Miniaturization enables integration of multiple analytical steps in the same device, thus reducing the risk of carryover contamination. Hand-held lab-on-a-chip devices for point-of-care diagnostics are being developed.

A commonly used technique in molecular biology, clinical research, and evolutionary studies is enzymatic amplification of nucleic acids. The first thermostable amplification procedure published, polymerase chain reaction (PCR),[2] allowed amplification to a great number of copies of a specific region of a DNA chain in a very short time. Northrup et al.[3] initially introduced PCR in silicon microstructures in 1993. Since then, numerous publications have appeared on simplification of PCR in microsystems using different approaches.[3–15] Most of the reported PCR amplification methods use a combination of silicon and glass chips, with reaction chambers in the microliter range. Only a few reports describe PCR in nanoliter volumes or smaller. Experiments by Nagai et al.[4] have demonstrated successful PCR amplification in reaction chambers for volumes down to 86 pL. Amplifications in reaction volumes of 160 and 280 nL have been reported by Hühmer and Landers and Lagally et al., respectively.[5–8]

The main benefit of reducing sample volumes in PCR lies in enhanced thermal- and mass-transfer rates, which can significantly reduce the reaction time. Different approaches have been reported in order to obtain efficient heat transfer, such as conventional thermocyclers,[9] integrated polysilicon thin-film heaters,[3] Peltier elements,[10] infrared radiation,[5] waterbaths,[11] copper blocks,[12] and indium−tin oxide thin-film heaters.[15]

* Corresponding author: (phone) +4740403488; (fax) +4732798801; (e-mail) Anja.Gulliksen@norchip.com.
† NorChip AS.
‡ University of Oslo.
§ Norwegian University of Science and Technology.
‖ SINTEF.
⊥ Norwegian Radium Hospital.

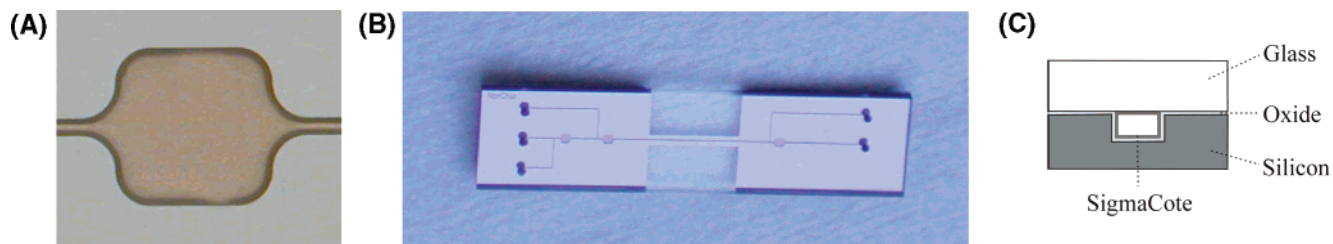(1) Verpoorte, E. *Electrophoresis* **2002**, *23*, 677−712.
(2) Saiki, R. K.; Scharf, S.; Faloona, F.; Mullis, K. B.; Horn, G. T.; Erlich, H. A.; Arnheim, N. *Science* **1985**, *230*, 1350−1354.
(3) Northrup, M. A.; Ching, M. T.; White, R. M.; Watson, R. T. *Transducers'93* **1993**, 924−927.
(4) Nagai, H.; Murakami, Y.; Morita, Y.; Yokoyama, K.; Tamiya, E. *Anal. Chem.* **2001**, *73*, 1043−1047.
(5) Hühmer, A. F. R.; Landers, J. P. *Anal. Chem.* **2001**, *72*, 5507−5512.
(6) Lagally, E. T.; Medintz, I.; Mathies, R. A. *Anal. Chem.* **2000**, *73*, 565−570.
(7) Lagally, E. T.; Simpson, P. C.; Mathies, R. A. *Sens. Actuators, B* **2000**, *63*, 138−146.
(8) Lagally, E. T.; Emrich, C. A.; Mathies, R. A. *Lab Chip* **2001**, *1*, 102−107.
(9) Waters, L. C.; Jacobson, S. C.; Kroutchinina, N.; Khandurina, J.; Foote, R. S.; Ramsey, J. M. *Anal. Chem.* **1998**, *70*, 158−162.
(10) Khandurina, J.; McKnight, T. E.; Jacobson, S. C.; Waters, L. C.; Foote, R. S.; Ramsey, J. M. *Anal. Chem.* **2000**, *72*, 2995−3000.
(11) Curcio, M.; Roeraade, J. *Anal. Chem.* **2003**, *75*, 1−7.
(12) Kopp, M. U.; Luechinger, M. B.; Manz, A. *Science* **1998**, *280*, 1046−1048.
(13) Yuen, P. K.; Kricka, L. J.; Fortina, P.; Panaro, N. J.; Sakazume, T.; Wilding, P. *Genome Res.* **2001**, *11*, 405−412.
(14) Taylor, M. T.; Nguyen, P.; Ching, J.; Petersen, K. E. *J. Micromech. Microeng.* **2003**, *13*, 201−208.
(15) Friedman, N. A.; Meldrum, D. R. *Anal. Chem.* **1998**, *70*, (14), 2997−3002.

Figure 1. (A) Photograph of a 10-nL reaction chamber, $450 \times 450 \times 50$ μm. (B) The dimensions of the outer microchip are 5000×20000 μm. The two additional reaction chambers and channels were intended for loading of different reagents but were not used in these experiments. (C) Sketch of the cross-sectional area of the microchip.

The development of PCR in microsystems has led to the integration of complex procedures relevant for performing on-chip PCR. Microchips where several analytical steps were incorporated onto a single device have been reported, including the following: cell lysis, amplification, real-time detection, and electrophoretic separation of PCR products.[4,5,8,13,14]

We have applied an alternative amplification method, termed nucleic acid sequence-based amplification (NASBA), to microchips. NASBA, initially introduced by Compton[16] in 1991, is a sensitive, transcription-based amplification system specifically designed for detecting RNA. The technology relies on the simultaneous activity of three enzymes (avian myeloblastosis virus reverse transcriptase, RNase H, T7 RNA polymerase) under isothermal conditions (41 °C), producing more than 10^9 copies in 90 min. The amplification method is particularly well suited for analyses of various kinds of RNA: genomic RNA, mRNA, rRNA, viriods, and ssDNA. In some NASBA systems, dsDNA may also be amplified, albeit very inefficiently, and only in the absence of the corresponding RNA target.[17] Based on this, the NASBA reaction has an application range including viral diagnostics, gene expression, and cell viability.[18]

NASBA is isothermal and consequently no thermocycling is needed. This is an advantage since it simplifies both the microchip design and the instrument specifications. In NASBA, the amplification is dependent on three enzymes, each catalyzing a specific reaction. Optimal stoichiometric ratio of the enzymes involved is necessary for the reaction to proceed. Thus, the amplification reaction itself is more complex in the case of NASBA than in the case of PCR, which only utilizes one enzyme. In NASBA, molecular beacon probes[19–21] hybridize to the target during the amplification, making possible real-time monitoring, which simplifies both the analytical procedure and the features of the microchip.

In this work, we report successful real-time amplification of oligonucleotides using NASBA technology in 10- and 50-nL silicon–glass reaction chambers. To our knowledge, this is the first time NASBA has been demonstrated in such a microsystem format.

(16) Compton, J. *Nature* **1991**, *350* (6313), 91−92.
(17) Deiman, B.; van Aarle, P.; Sillekens, P. *Mol. Biotechnol.* **2002**, *20*, 163−179.
(18) Leone, G.; van Schijndel, H.; van Gemen, B.; Kramer, F. R.; Schoen, C. D. *Nucleic Acids Res.* **1998**, *26* (9), 2150−2155.
(19) Tyagi, S.; Kramer, F. R. *Nat. Biotechnol.* **1996**, *14*, 303−308.
(20) Tyagi, S.; Bratu, D. P.; Kramer, F. R. *Nat. Biotechnol.* **1998**, *16*, 49−53.
(21) Tyagi, S.; Marras, S. A. E.; Kramer, F. R. *Nat. Biotechnol.* **2000**, *18*, 1191−1196.

MATERIALS AND METHODS

Microchip Fabrication. The microchips were processed by SINTEF. Chambers and channels were etched in the silicon wafers with a ⟨100⟩ crystal orientation using reactive ion etching. A 700-Å oxide layer was grown, before the silicon wafers were bonded to 525-μm-thick Pyrex glass, forming channels and chambers. The channels have cross sections of 50×50 μm. The dimensions of the 10- and 50-nL reaction chambers were $450 \times 450 \times 50$ and $1000 \times 1000 \times 50$ μm, respectively. Conically shaped holes in the Pyrex wafer were made by powder blasting by Micronit. The diameters of these holes were 430 μm on the top surface and 150 μm on the bottom surface. To prevent adsorption of template and inhibition of the enzymes, the chips were coated with SigmaCote (Sigma Chemical Co., St. Louis, MO), according to the manufacturer's instructions. Figure 1 shows photographs of a 10-nL reaction chamber (A), the whole microchip with dimensions of $5000 \times 20\,000$ μm (B), and an illustration of the cross-sectional area of the silicon–glass microchip (C). The 50-nL microchips had the same layout as the 10-nL microchips, but with larger reaction chambers. Altogether, less than 70 microchips were fabricated for both 10 and 50 nL.

Optical Detection System and Heat Regulation. An optical system for measuring fluorescence was made for excitation at 494 nm and detection at 525 nm. The instrument consisted of a sample stage and a hinged optical table, located directly above the stage. The stage was mounted on an optical bench and had micrometer screws for *x*-, *y*-, and *z*-alignment of the sample.

Figure 2 shows a diagram of the optical geometry of the instrument. A high-intensity blue light-emitting diode (LED) (Marl International Ltd.) excited the fluorophores from above at a 23° angle to the reaction chamber. The excitation light was filtered and focused onto the reaction chamber. Emitted fluorescent light was collected by two lenses (Melles Griot, Santa Clara, CA) perpendicular to the reaction chamber and guided through a prism (Melles Griot), a dichroic beam splitter (Chroma Technology Corp, Brattleboro, VT), a filter (Chroma Technology Corp.), and finally into the photomultiplier tube detector (Hamamatsu). The data collection and preparation of the detected signal was processed on a laptop computer using LabView 5.11 software (National Instruments, Austin, TX). A schematic overview of the experimental setup is shown in Figure 3A. Figure 3B shows a photograph of the actual detection unit.

The intensity of the fluorescent light (3.5 pW) is extremely low compared to the excitation light (1 mW). Typically a filter transmits ~1/10 000 of unwanted light, which is insufficient to
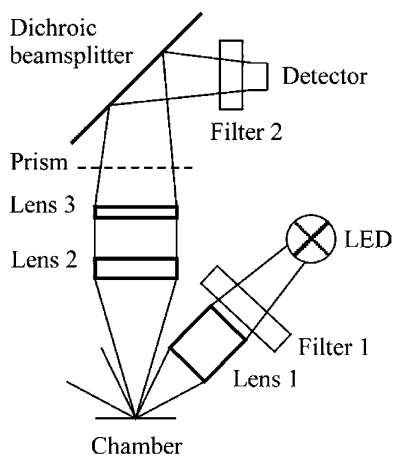
Figure 2. Sketch of the optical geometry. Blue light is emitted from the LED as shown in the diagram. Filter 1 is a bandwidth filter (465–500 nm). Lens 1 focuses the light onto the reaction chamber. The lens has a focal length of 10 mm and a diameter of 6 mm. Lens 2 (focal length, 17 mm; diameter, 14 mm) and lens 3 (focal length, 55 mm; diameter, 14 mm) collect and guide the fluorescent light from the fluorophores to a prism and dichroic beam splitter. The latter projects the light onto filter 2 (500–545 nm), which is mounted in front of the detector.
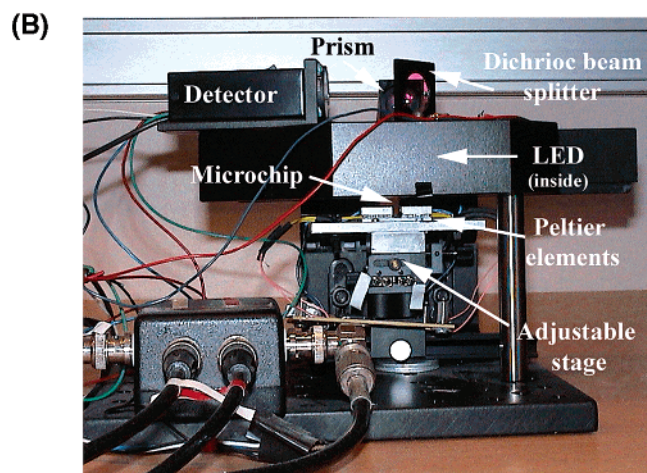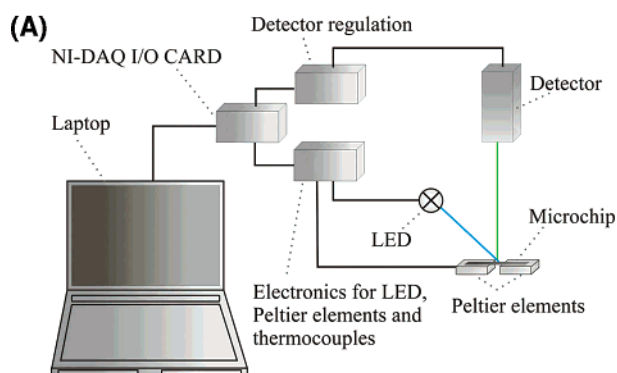
Figure 3. (A) Diagram of the experimental setup. (B) Photograph of the optical module.

separate the fluorescence from the LED light. Consequently, reflection or scattering of the excitation light into the direction of the optical path of the detector must be avoided. The 23° angle between the LED and the reaction chamber surface eliminates such reflections. To eliminate scattering, the surface in the

reaction chamber was made optically smooth, which means a surface roughness less than 1/10 of the wavelength of the light employed. The roughness in the reaction chambers in the silicon−glass chips was measured with a WYKO white light interferometer (Veeco Instruments Inc., Woodbury, NY) and found to be less than 40 nm and thus within the limits of optical smoothness.

To control the temperature of the chip, an aluminum chip holder was mounted on top of a Peltier element (Marlow Industries Inc., Dallas, TX). A thermocouple was integrated in the aluminum block with a feedback circuit to the Peltier element. The temperature system was controlled externally on a laptop computer with incorporated digital PID controllers (National Instruments) for regulation. The temperature precision of the system was within 41.0 ± 0.1 °C. A commercial Fluke temperature calibration apparatus (Fluke, Everett, WA) was used to calibrate the system with thermocouples and a platinum resistance sensor. Measurements were performed both on the aluminum block and on top of a dummy chip without glass. The Fluke temperature calibration unit measured absolute temperatures to within ± 0.1 °C. The overall temperature accuracy of the system was ± 0.3 °C, after calibration.

A limited number of disposable microchips were fabricated. Commercially available glass capillaries (Drummond Scientific Co, Broomall, PA) were used for temperature calibration, sample alignment, and testing of the data collection system. For these purposes, solutions containing active fluorophores in addition to the NASBA reaction mixture were applied to the glass capillaries. The glass capillaries had a capacity of 5 μL with an inside diameter and outside diameter of 447 and 940 μm, respectively. During measurements, only 2 mm of the capillary was illuminated; this corresponds to a detection volume of 300 nL.

Additionally, conventional 20-μL NASBA reactions were performed in polypropylene tubes. The amplification was performed in a Biotek FL600 reader (MWG Biotech AG). The experiments were carried out in order to compare the experimental results from the microchips and the glass capillaries with conventional methods. The Biotek FL600 reader had a temperature variance of 41 ± 1 °C. Both the custom-made instrument with integrated thermal control and optical detection and the Biotek FL600 reader had an excitation wavelength at 494 nm and an emission wavelength at 525 nm.

Sample Material. A positive control for human papillomavirus (HPV) 16, from the HPV Proofer kit (NorChip AS, Klokkarstua, Norway) was used as sample material. In addition, an artificial 118-bp single-stranded DNA (ssDNA) 5′-GATTAGACATTTCA-GCATACGCATAATCGGCCGGCTTCGCCTAGGCATATCCTT-TGCATGCTACTATATGGGACGATACGACCAAATGCCA-GTCAGATAGCACAGTAGCAGCGATTAA-3′ (NorChip AS) was used to test NASBA in nanoliter volumes.

NASBA. The NASBA reaction was performed in microchips and glass capillaries with volumes of 10, 50, and 300 nL. For performance comparison, conventional amplification was carried out in 20-μL polypropylene tubes.

Primers and molecular beacon probes for the HPV 16 were provided with the HPV Proofer kit (NorChip AS). Primers and probes for the 118-bp ssDNA were not included in the original kit. The following sequences were used in the amplification process of the ssDNA: primer 1 (5′-AATTCTAATACGACTCAC-

TATAGGGAGAAGGGCTGCTACTGTGCTATCTGA-3′), primer 2 (5′-GACATTTCAGCATACGCATA-3′). and molecular beacon probe (5′-FAM-GCGGCATCCTTTGCATGCTACTATA GCCGC-dabsyl-3′) (NorChip AS).

The reagents were mixed according to the manufacturer's instructions. It should be pointed out that manual mixing of reagents may lead to some relative shifts in the negative and positive baseline signals presented in the plots due to concentration variations of reagents. Depending on the application and target of interest, the reactants were optimized. For HPV 16, the final concentration of the molecular beacon was 0.42 μM, whereas for the ssDNA the concentration was 0.21 μM. As a negative control, water was added to the reaction mixture instead of target DNA. In addition to the regular kit reagents, yeast tRNA (Sigma Chemical Co.) was added to the reaction mixture to a final concentration of 4 μg/mL. To reduce the surface adsorption of enzymes and targets, tRNA was used as a dynamic coating. The surfaces of the silicon chips may inhibit the amplification reaction and were treated with surface agents to reduce nonspecific adsorption of the NASBA reagents. As previously described, both the silicon−glass chips and the glass capillaries were coated with SigmaCote to prevent adsorption.

Reagent solution (10 μL) from the kit and 5 μL of sample material (0.1 and 1.0 μM) were mixed and heated to 65 °C for 5 min. The mixture was subsequently cooled to 41 °C, after which the enzymes were added and the resulting solution was kept at 41 °C for 5 min. A Hamilton glass syringe, with a disposable sequencing pipet tip attached to it, was used to apply the sample to a chip. The solution was drawn into the hydrophilic microchip by capillary forces. The inlet holes were subsequently covered with wax to avoid evaporation of the sample. The chip was incubated in the chip holder on top of the Peltier elements at 41 °C. Approximately 10 min was needed to inject the reaction mixture into the reaction chambers and to align the microchip. The microchip was only used once due to a high risk of contamination if the microchips were to be used in subsequent experiment.

The same approach that was used for the microchips was utilized to coat, fill, and seal the disposable glass capillaries. The pipets were completely filled with reaction mixture and placed on the aluminum block on top of the Peltier elements underneath the optical detection system. The custom-built instrument detected only a 2-mm cross section of the glass capillary, corresponding to a reaction volume of 300 nL.

RESULTS AND DISCUSSION

The main objective of these experiments was to demonstrate the NASBA procedure in microchips with nanoliter reaction volumes. Due to the limited number of silicon−glass microchips, which passed the quality control, it was decided to test only one kind of sample in the 10-and 50-nL reaction chambers. Table 1 lists the experiments performed in microchips, glass capillaries, and polypropylene tubes. The results of the nanoliter-scale amplification reactions were compared to conventional NASBA performed in polypropylene tubes (20 μL).

The reactions presented in Figures 4−7 started after 10 min, due to the time consumed for addition of enzymes and injection of sample into the microchip and alignment in the instrument. Figures 4 and 5 demonstrate results for real-time NASBA per-

Table 1. Overview of the Figures Presented and the Experiments Performed

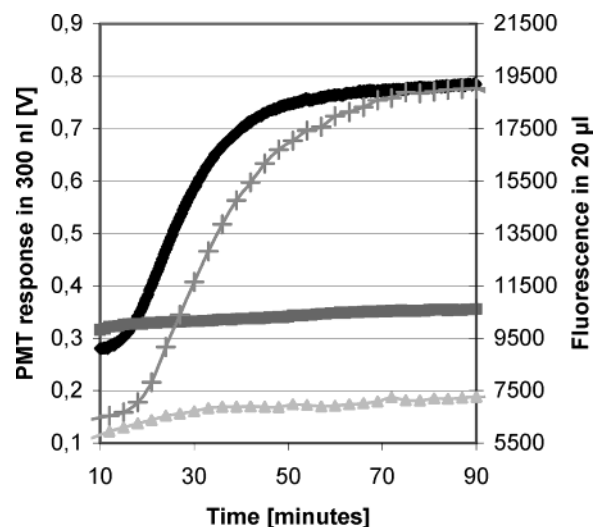| Figure	reaction chamber	chamber volume	sample material
4	glass capillary	300 nL	ssDNA
	polypropylene tube	20 μL	ssDNA
5	glass capillary	300 nL	HPV 16
	polypropylene tube	20 μL	HPV 16
6	microchip	50 nL	ssDNA
	polypropylene tube	20 μL	ssDNA
7	microchip	10 nL	HPV 16
	polypropylene tube	20 μL	HPV 16

Figure 4. Real-time NASBA of ssDNA performed in glass capillaries and in conventional polypropylene tubes: ◆, 0.1 μM ssDNA in 300 nL; ■, negative control in 300 nL; +, 0.1 μM ssDNA in 20 μL; ▲, negative control in 20 μL.

formed in glass capillaries and in the conventional Biotek FL600 reader, using 0.1 μM ssDNA and 1 μM HPV 16 as sample material, respectively. The results using negative controls are presented in each case.

A comparison of the curves shown in Figures 4 and 5, for 300 and 20 μL, displays a high degree of conformity in performance. The graphs demonstrate the characteristic shape of a real-time amplified reaction, and there is a clear difference between the amplification and the negative control. The exponential phase for detection starts at the same time for both 300- and 20-μL volumes. However, there is a significant difference in the signal level for the HPV 16 compared to that of the ssDNA caused by concentration variations of the molecular beacons. Using ssDNA as target, the signal levels obtained for both glass capillaries measured in the custom-made instrument and in the conventional reader demonstrate a 3-fold increase from start to end point. The increase of the conventional amplification of HPV 16 is ~7 times the base signal, whereas in the glass capillaries the increase is 5 times (Figure 5). This is expected, as noise will become more significant as the reaction volume decreases and will dominate at low signal levels.

Figure 6 shows results from experiments using ssDNA in silicon−glass microchips with 50-nL reaction chambers, and in 20-μL polypropylene tubes using the conventional reader. The ssDNA concentration was 0.1 μM. For illustration purposes, the
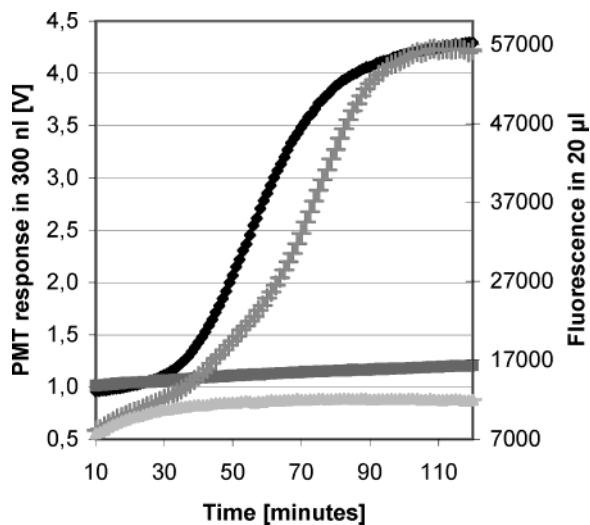
Figure 5. Real-time NASBA of HPV 16 oligonucleotides performed in glass capillaries and in conventional polypropylene tubes: ◆, 1.0 μM HPV 16 in 300 nL; ■, negative control in 300 nL, + 1.0 μM HPV 16 in 20 μL; ▲, negative control in 20 μL.
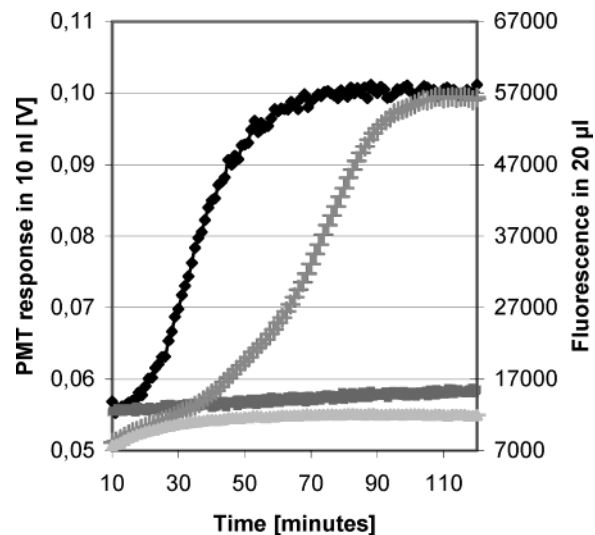

Figure 7. Real-time NASBA of HPV 16 oligonucleotides performed in a 10-nL reaction chamber and in conventional polypropylene tubes: ◆, 1.0 μM HPV 16 in 10 nL; ■, negative control in 10 nL, + 1.0 μM HPV 16 in 20 μL; ▲, negative control in 20 μL.
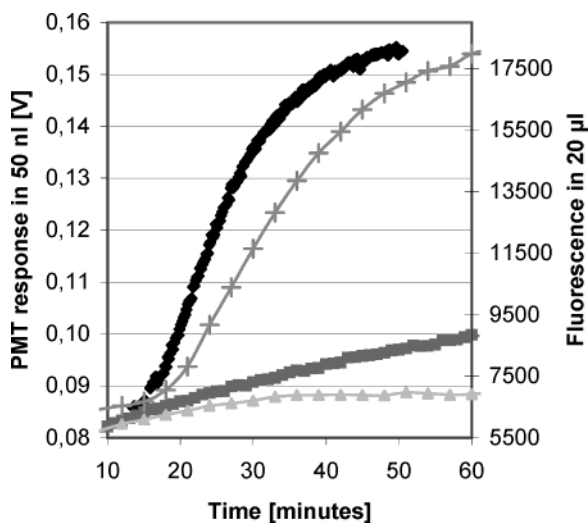
Figure 6. Real-time NASBA of ssDNA performed in a 50-nL reaction chamber and in conventional polypropylene tubes: (◆, 0,1 μM ssDNA in 50 nL; ■, negative control in 50 nL, + 0.1 μM ssDNA in 20 μL; ▲, negative control in 20 μL.

negative control was adjusted by a factor of 0.45 in the figure. As shown in Figure 4, the conventional amplification signal increases 3 times from the starting level. In 50 nL, the signal increases by a factor of 2. The discrepancy between the negative control and the starting point of the amplified target was anticipated, as it was difficult to repeatedly place the microchip manually in exactly the same position every time. The error introduces a relative shift in the detector readout and does not affect the amplification process itself. The results show a distinct difference between the negative control and the amplification curve. The amplification curve displays the expected shape and time dependency.

Figure 7 shows the results of the amplification of HPV 16 performed in a silicon−glass microchip with a 10-nL reaction chamber and in the conventional polypropylene tubes. For the 10-nL reaction volume, the signal was amplified by a factor of 2 from 0.055 to 0.100 V. The fluorescence signal in the con-

ventional reaction volume was increased 7 times and is the same as presented in Figure 5. The 10-nL amplification curve has a different progress further to the left in the chart compared to the conventional curve. Several factors can result in the observed shape of the curve. Such factors could be due to higher target concentration[17] and concentration variations, because the target of interest was acquired from different samples. In addition, the heat transfer in silicon is significantly faster than in glass or polypropylene and can result in reduced amplification times.

Another challenge related to microchip miniaturization is surface treatment. In microsystems, the surface-to-volume ratio is several orders of magnitude larger than in conventional systems. Preliminary experiments performed with no surface treatment of the silicon−glass structures gave negative results. Therefore, if the surface is not treated to prevent adsorption, the large surface area can disturb and even inhibit the whole process as in this case. Shoffner et al.[22] emphasized the need of surface treatment to be able to perform PCR in silicon−glass structures. Enzymes are complex molecules consisting of hydrophilic, hydrophobic, and charged areas in a vital three-dimensional structure, and the surface properties of the reaction chamber can cause the enzymes to adsorb to the surface. The major subprocesses constituting the overall protein adsorption are changes in the state of hydration, redistribution of charged groups, and rearrangements in the protein structure. It is therefore important to obtain a surface with hydrophilic properties similar to that of the enzyme exterior.[23] The surface property in microsystems used for the NASBA reaction, which contains three enzymes, is therefore extremely important. Downscaling the reaction volume also effects the fluid dynamics of the system. The surface tension can be treated chemically to create either hydrophilic or hydrophobic behavior with specific liquids.[24]

(22) Shoffner, M. A.; Cheng, J.; Hvichia, G. E.; Kricka, L. J.; Wilding, P.: *Nucleic Acids Res.* **1996**, 375−379.
(23) Norde, W.; Lyklema, J. *The Vroman Effect, VSP* **1992**, 1−20.
(24) Ratner, B. D. *Biosens. Bioelectron.* **1995**, *10*, 797−804.

CONCLUSION

The experimental results have shown it is possible to detect real-time NASBA amplification in 10-nL volumes by utilizing a custom-made microfabricated device and an optical detection system under process control. This is a reduction of the conventional 20-μL reaction volumes by a factor of 2000. Furthermore, real-time NASBA was performed on two different target sequences at the nanoliter level. The performance of the NASBA reaction for the silicon−glass microchip was in agreement with the conventional method. But to obtain amplification in silicon−glass microchips, addition of small quantities of carrier molecules and surface treatment were required.

Miniaturization makes it possible to integrate processes such as amplification and detection within the same microchip. Integration of an additional function such as sample preparation will result in even shorter analysis time and in addition reduce the possibility for contamination. The results from these experiments will be applied in future work toward an automated μ-TAS system for clinical diagnosis.

Paper II

Parallel nanoliter detection of cancer markers using polymer microchips

Anja Gulliksen,*[ab] Lars Anders Solli,[c] Klaus Stefan Drese,[d] Olaf Sörensen,[d] Frank Karlsen,[ae] Henrik Rogne,[f] Eivind Hovig[g] and Reidun Sirevåg[b]

A general multipurpose microchip technology platform for point-of-care diagnostics has been developed. Real-time nucleic acid sequence-based amplification (NASBA) for detection of artificial human papilloma virus (HPV) 16 sequences and SiHa cell line samples was successfully performed in cyclic olefin copolymer (COC) microchips, incorporating supply channels and parallel reaction channels. Samples were distributed into 10 parallel reaction channels, and signals were simultaneously detected in 80 nl volumes. With a custom-made optical detection unit, the system reached a sensitivity limit of 10^{-6} µM for artificial HPV 16 sequences, and 20 cells µl^{-1} for the SiHa cell line. This is comparable to the detection limit of conventional readers, and clinical testing of biological samples in polymer microchips using NASBA is therefore possible.

Introduction

Several studies have demonstrated that the presence of the human papilloma virus (HPV) is a prerequisite for the development of cervical cancer, the second most common cancer in women.[1,2] Screening of cervical cancer is mainly done by cytological testing. However, this method has both poor reproducibility and specificity, as well as limited sensitivity.[3] Therefore, new diagnostic methods have been developed. The present on-line technology identifies high-risk HPV mRNA transcripts employing real-time nucleic acid sequence-based amplification (NASBA).[4–7] Briefly, NASBA is an isothermal (41 °C) method specifically designed for amplification of any single-stranded RNA and DNA sequence, by using three different enzymes simultaneously. The use of a specific and sensitive technology, such as NASBA, for detection of high-risk HPV types, makes it possible to meet the increasing demands for diagnostic precision and prognostic information, and to prevent incorrect diagnosis based on subjective decisions.

We present experimental evidence of real-time NASBA detection in cyclic olefin copolymer (COC) microchips, with 80 nl detection volumes. The sample is automatically distributed into 10 parallel reaction channels for simultaneous detection, making it possible to specifically amplify and detect several different targets with high sensitivity on just one sample. The work presented here is part of a project towards a fully automated and disposable diagnostic microsystem with integrated sample preparation and detection modules for virus and bacteria identification. Shorter handling time, combined with reduced reagent and sample consumption, will be benefits of this system compared to conventional methods (Fig. 1).

Materials and methods

Microchip fabrication

Microchips, incorporating supply channels, reaction channels and microfluidic actuation systems, were injection molded in COC polymer.[8] A photograph of the microchip is shown in Fig. 2(a). An actuation system was implemented on the microchip for liquid plug movement. However, the actuation mechanism is not described here, as it was not applied to these experiments. A description of the design and actuation functions of the chips is presented elsewhere.[9]

The microchips were oxygen plasma activated prior to coating with 5% (w/v) polyethylene glycol (PEG) in methanol (Sigma Chemical Co, St. Louis, MO). A cotton linter filter (Schleicher & Schuell BioScience GmbH, Relliehausen, Germany) was placed in the waste chamber, and the chips were sealed by welding a 75 µm COC membrane to the substrate. To block out background fluorescence from the thermal pads in the instrument, gold (25 nm) was sputtered on the back of the chip.

Optical detection system

The optical detection system was redesigned from an earlier prototype,[10] to increase light intensity and reduce component costs (Fig. 2(b)). Light emitting diodes (LED) (Lumileds, San Jose, CA), with 130 mW centred at 470 nm, excited the fluorophores from above at an angle of 26° to the plane of the chip surface. Hence, the excitation light is reflected away from the light path of the detection unit. Scattered excitation light entering the detection unit was reduced by a bandpass filter (Chroma Technologies Corp, Brattleboro, VT), 465 nm–500 nm, and collimated through a lens (Melles Griot, Santa Clara, CA), Ø12.5 mm/f30 mm. An off-axis fresnel lens, Ø50 mm/f25 mm, focused the collimated light onto the reaction chambers. Fluorophores, excited at 494 nm and emitting at 525 nm, were activated and the light was collected in the center of the fresnel lens, passed through a lens, Ø25 mm/f100 mm, a prism (Melles Griot), a bandwidth filter, 500 nm–545 nm, and an aperture, before being detected by a photomultiplier-tube (PMT) (Hamamatsu, Shizuoka, Japan). A 2 × 2 mm^2 area of the reaction channel was illuminated by the LED, corresponding to a detection volume of 80 nl (400 × 2000 × 100 µm^3).

*anja.gulliksen@norchip.com
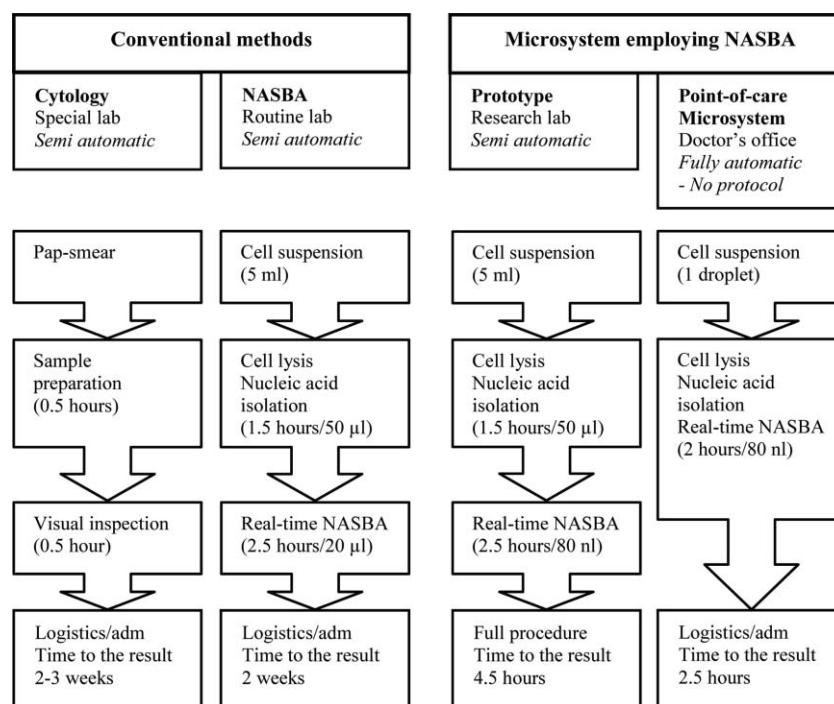
Fig. 1 Comparison of conventional methods and a point-of-care microsystem for detection of cervical cancer. The false negative results for cytology is 69% for the first time tests. Employing NASBA, the false negative result is reduced to 23%. The time scale is approximate, since the analysis can be performed using different methods and instruments.
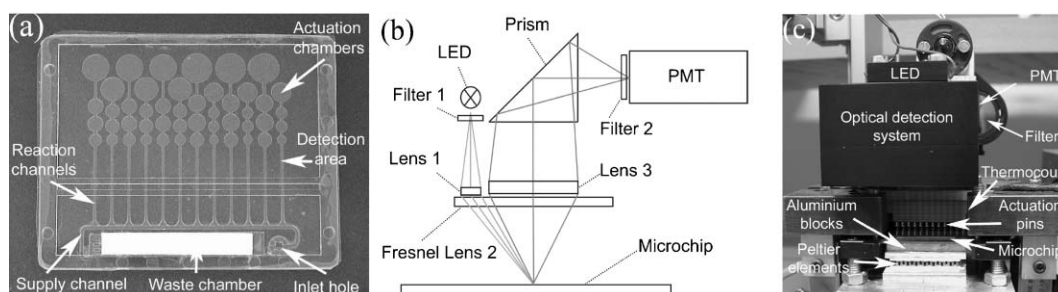
Fig. 2 (a) A photograph of the COC microchip with dimensions of 50 × 40 mm. (b) Sketch of the optical geometry. (c) Photograph of the major components in the instrument.

Sequential measurements of the reaction chambers were performed by automatically moving the chip underneath the optical unit. Each channel was measured for 1 s on each scanning cycle, using a digital lock-in system operating at 1 kHz. A complete chip cycle took 90 s. Data were collected and processed using MATLAB (The MathWorks Inc., Natick, MA). Fig. 2(c) shows a photograph of the instrument set-up.

Instruments

Peltier elements (Marlow Industries Inc., Dallas, TX) with aluminum blocks mounted on top formed the chip holder. A thermal pad was placed on the blocks for thermal contact to the chip. A thermocouple was integrated into the chip holder, with feedback to the Peltier elements. Temperature regulation was controlled externally by the use of MATLAB. The system was calibrated with a commercial temperature calibration instrument (Fluke, Everett, WA) and platinum resistance sensors, both with an accuracy of ± 0.1 °C. Temperature calibrations were performed both on the aluminum block, and on top of a dummy microchip, without a membrane. The overall temperature accuracy of the system was within ± 1 °C.

The instrument was equipped with a movable chip holder for alignment of the polymer microchip, automatic actuation and optical positioning. The servomotors (Omron Electronics, Kyoto, Japan) were regulated by a physical signaling sublayer (PLS) (Saia-Burgess Electronics AG, Murten, Switzerland), programmed with PG 5 (Saia-Burgess Electronics AG). All communications were run through a serial line (RS232) and controlled by MATLAB.

Results from the two outermost channels on the microchip were excluded in this work, because of a design fault in the instrument.

For comparison, sample solutions were also tested using microplates in a conventional microplate reader, Lambda

FL600 (Bio-Tek Instruments, Winooski, VT). The total detection volume of the Lambda FL600 was 20 µl.

Sample material

The SiHa cell line, with 1–2 copies of integrated HPV 16 DNA per cell, was used as a model system.[11–13] The cells were obtained from the American Type Culture Collection (ATCC, Manassas, VA) and maintained in Dulbecco's modified Eagles medium (DMEM), supplemented with 10% fetal bovine serum (FBS), 2 mM L-glutamine and 25 µg m^{-1} gentamycin. The cells were incubated at 37 °C in a 5% CO_2 atmosphere, trypsinated, counted in a Bürker chamber, and lysed in lysis buffer (bioMérieux, Boxtel, the Netherlands), before the nucleic acids were isolated and extracted using a NucliSens Extractor (bioMérieux).[14]

In addition, artificial HPV 16 sequences, from the PreTect® HPV-Proofer kit (NorChip AS, Klokkarstua, Norway) were used as targets in the reaction. To define the lower detection limit of the system, dilution series were tested. Serial dilutions ranging from 10^{-10} µM to 10^{-1} µM were tested using the artificial HPV 16 sequence, whereas the SiHa cell line was tested over a range from 2×10^{-2} cells µl^{-1} to 2×10^{3} cells µl^{-1}. SiHa cell line samples (250 cells µl^{-1}) have been previously used as positive controls for detection of HPV 16 in biopsies from cervical cones[6,17] in conventional microplates.

NASBA procedures

All reagents required to perform the NASBA amplification and the HPV detection were supplied as part of the PreTect® HPV-Proofer kit. The final concentration of the reaction mixture: 40 mM Tris-HCl (pH 8.5), 70 mM KCl, 12 mM $MgCl_2$, 5 mM DTT, 1 mM dNTP, 2 mM ATP, 2 mM CTP, 2 mM UTP, 1.5 mM GTP, 0.5 mM ITP, 0.2 µM of each primer, 0.4 µM molecular beacon probe (FAM/Dabsyl), 375 mM sorbitol, 0.119 g l^{-1} BSA, 15% (v/v) DMSO, 6.4 U AMV RT, 32 U T7 RNA polymerase and 0.08 U RNase H.

The reagent mixture except for the enzymes (26 µl) and sample material (13 µl) were mixed manually and heated on a conventional block heater at 65 °C for 2 min. The mixture was subsequently incubated at 41 °C for 2 min, after which the enzymes (13 µl) were added. This mixture was then immediately applied to the microchip and distributed into 10 parallel reaction channels. To ensure that all individual reaction channels were filled, one actuation chamber on each channel was punctured before the addition of the mixture to the microchip. This caused the reaction channels to be filled due to capillary forces. Excess reaction mixture was drawn into the waste chamber and absorbed by the filter, completely separating the fluids in individual reaction channels. Chip movement, process control and measurements were handled by the instrument.

For comparison, the ten-fold serial dilutions of the artificial HPV 16 sequence and of the SiHa cell line were tested, both in the microchip and in the conventional system. Reaction mixtures were prepared in the same way for both systems. The reaction volume for the conventional system was 20 µl.

For negative controls, water for molecular biology (DNase or RNase not detected, Sigma Chemical Co.) was added instead of sample material. All experiments were run for 2.5 h at 41 °C.

Calculations

Experimental results were processed with a dedicated NASBA regression calculation program, PreTect Data Analyzer (NorChip AS), based on polynomial regression algorithms. The final fluorescence level was divided with the initial fluorescence level and all reactions with a ratio larger than 1.7 were considered positive. Time-to-positivity (TTP)[15,16] was chosen as the point of onset for exponential increase. The average slopes were calculated from the data between 10 and 80% increase in initial fluorescence level. The detection limit of the microchips was defined as the lowest concentration tested where all 10 reaction channels were positive.

Results and discussion

Identification of the HPV 16 sequence and the SiHa cell line utilizing real-time NASBA was successfully performed in polymer microchips with a detection volume of 80 nl. Fig. 3 shows the result obtained from one microchip experiment using a SiHa cell line and a HPV 16 sequence. The graphs are clearly positive, and reveal the same sigmoid curvature as when samples were tested using regular 20 µl volumes and conventional readers.[5,10,16]
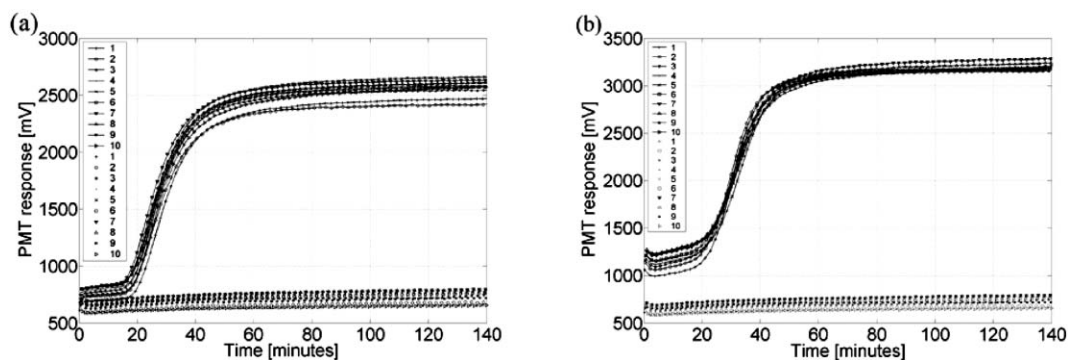
Fig. 3 A (a) SiHa cell line sample (2000 cells µl^{-1}) and a (b) HPV 16 sequence sample (0.1 µM) tested on a microchip. Solid lines characterize positive amplification reactions while no lines represent negative controls. The key numbers indicate the reaction channels on the microchip from left to right.

To characterize the amplification reactions, several different parameters were evaluated: the fluorescence ratio, time-to-positivity (TTP), the average slope of the linear part of the curve, the number of positive amplifications, the number of polymer microchips and microplate reactions tested. The values shown in Table 1 represent the average values and the standard deviations of all the positive samples tested within the different dilution series. In comparison, the standard deviations of: the fluorescent ratio, the TTP and the average slope for an individual microchip ranged from (0.1–0.5), (0.0–14.5) and (1.2–19.6), respectively. For most experiments, the standard deviations, between parallel reaction channels on one microchip, are in the lower part of the range.

A comparison of the NASBA results from the HPV 16 sequence and from the SiHa cell line, shows that all parameters display the same trend for microsystems as for conventional methods, except for the ratio between the final and initial fluorescence levels. This ratio is nearly constant for the microchip experiments, but decreases with sample concentration for the conventional experiments. The fluorescense level is determined by the concentration of molecular beacons in the reaction mixture. Theoretically, if the amplification reaches full reactant consumption, the final fluorescense level should be independent of sample concentration, but reached at different times. The overall lower ratio obtained in the microchips could be explained by the enlarged background noise, caused by autofluorescent COC and light scattering from imperfect polymer surfaces. The auto-fluorescence of the microchips was measured to ~ 300 mV. Adsorption of reagents to the chamber wall will also contribute to background noise.

The results for the microchips correlate well with the conventional methods (Table 1). When concentrations are reduced, TTP increases, and the average slope decreases, because reagents need more time to find and interact with the targets. Small amounts of target give less amplified material at the beginning of the reaction, and hence the TTP increases. However, very high sample concentrations may slow down the reactions, because of enzymatic inhibition.

The custom-made optical detection system was found to have a detection limit of 10^{-6} μM for the artificial HPV 16 sequence, and 20 cells μl^{-1} for the SiHa cell line material. These values are the same as for the conventional Lambda FL600 reader (Table 1). It was possible to detect even lower concentrations in both systems, but the results were inconsistent, most likely due to stochastic sampling effects. The detection limit of the NASBA reaction is dependent on the target of interest, the quality of the RNA samples, and influenced by the design of the primers and the molecular beacon probe. Negative control experiments were run to check for contamination. Because the microchips were only used once, false positive results are only possible if the premixed reaction mixture is contaminated. False negative results could theoretically only arise from contamination with inhibiting agents during microchip fabrication.

The experimental results, based on experiments from 140 microchips $\times$ 10 individual reaction channels, including negative controls, are summarized in Table 1. Several factors influence the experimental results and are reflected in the

Table 1 NASBA performed on microchips and conventional microplates. The detection volumes were 80 nl and 20 μl, respectively. Serial dilutions of an artificial HPV 16 sequence and a SiHa cell line were tested for both systems. The table shows the average and standard deviations of all values measured in all experiments. A line represents no positive reaction detected

Concentration	Ratio				TTP/min				Average slope: Microchips /mV min^{-1}; Conventional/Fluorescence units min^{-1}				No. of positive reactions/Total no. of reactions	No. of positive reactions/Total no. of reactions
	80 nl Microchips	20 μl Conventional			80 nl Microchips	20 μl Conventional			80 nl Microchips	20 μl Conventional			80 nl Microchips	20 μl Conventional
HPV 16 sequence /μM														
10^{-1}	2.8 ± 0.3	6.5 ± 0.2			13.9 ± 4.6	14.0 ± 0.8			45.6 ± 10.4	111.2 ± 19.3			40 / 40	6 / 6
10^{-2}	3.1 ± 0.4	6.7 ± 0.3			14.7 ± 4.0	11.8 ± 1.5			43.5 ± 9.5	96.3 ± 28.3			40 / 40	6 / 6
10^{-3}	2.7 ± 0.4	6.5 ± 0.3			9.0 ± 2.1	15.3 ± 1.8			46.0 ± 17.7	113.1 ± 33.6			30 / 30	6 / 6
10^{-4}	2.8 ± 0.3	5.2 ± 1.1			22.2 ± 4.5	23.8 ± 4.7			35.1 ± 17.9	94.4 ± 58.9			30 / 30	6 / 6
10^{-5}	2.6 ± 0.4	4.8 ± 1.2			22.6 ± 7.4	25.1 ± 3.7			29.9 ± 13.7	84.1 ± 38.3			30 / 30	12 / 12
10^{-6}	2.5 ± 0.5	3.8 ± 0.8			25.3 ± 3.6	26.3 ± 5.5			19.6 ± 9.2	42.7 ± 11.4			30 / 30	12 / 12
10^{-7}	2.1 ± 0.3	1.8 ± 0.1			37.1 ± 12.7	33.8 ± 7.4			17.3 ± 11.8	15.7 ± 1.5			33 / 70	2 / 12
10^{-8}	1.9 ± 0.3	—			43.8 ± 7.1	—			9.9 ± 3.6	—			6 / 60	0 / 12
10^{-9}	2.3 ± 0.9	—			81.0 ± 38.2	—			15.0 ± 6.3	—			2 / 60	0 / 12
10^{-10}	—	—			—	—			—	—			0 / 50	
SiHa cell line/cells μl^{-1}														
2×10^{3}	2.9 ± 0.3	4.9 ± 0.6			16.9 ± 2.7	29.3 ± 1.3			42.6 ± 6.2	80.1 ± 6.8			40 / 40	6 / 6
2×10^{2}	2.8 ± 0.4	3.8 ± 1.2			18.9 ± 3.4	29.3 ± 4.0			40.6 ± 14.5	52.5 ± 24.8			40 / 40	6 / 6
2×10^{1}	2.9 ± 0.3	3.7 ± 1.2			30.7 ± 9.3	33.3 ± 7.9			37.5 ± 11.1	44.0 ± 16.8			39 / 40	5 / 6
2×10^{0}	2.8 ± 0.5	3.0 ± 0.4			38.0 ± 26.1	39.8 ± 1.1			35.1 ± 15.5	28.0 ± 7.2			60 / 70	2 / 6
2×10^{-1}	2.7 ± 0.5	—			70.1 ± 39.1	—			39.3 ± 15.0	—			4 / 50	0 / 6
2×10^{-2}	—	—			—	—			—	—			0 / 30	0 / 6

calculated standard deviations. The results show that when the sample concentration of the input target decreases, the standard deviation increases. This could be caused by nonspecific surface binding of the target or pipetting skills. Particularly, nonspecific surface binding is more pronounced for the microchips than for regular microplates, because of a larger surface-to-volume ratio. For the present microchips, this is of great importance, because only three of the four walls forming the reaction chambers were coated with PEG. Experiments with uncoated microchips show complete inhibition of the reaction (data not shown). The PEG coating was in some cases damaged when the membrane was welded to the microchip, at treatment which may change the surface structure and lead to increased nonspecific binding and scattering of the excitation light. Also, BSA acts as a dynamic coating, reducing nonspecific binding of reagents to the channel walls. Volume variations in the pipetting affects the standard deviations for both microchips and microplates. Thus, reagents for individual microchips were mixed separately for each experiment, while for the conventional reactions only two reaction solution were mixed to perform all the experiments. Hence, the exact time for addition of enzymes and insertion of the microchip into the instrument varied between experiments. Also, stochastic sampling variation at lower molecular concentrations may affect the standard deviation.

The microchips used in these experiments had a large dead volume due to the design of the channel network. However, a reduction of dead volume may easily be obtained with a revised design.

Conclusions

Detection of cancer markers using real-time NASBA has been successfully demonstrated. To our knowledge, these are the first results showing detection of mRNA using real-time NASBA within such a microsystem. The detection limits are comparable to those obtained for experiments performed in conventional routine-based laboratory systems, demonstrating that the microchip and its detection system has a potential for diagnostic use in a point-of-care setting.

Future microchips could contain more reaction channels, and be combined with multiplexing of several different targets in each of the channels. Simultaneous detection of different targets is possible to identify with multi-parallel reaction channels having integrated different reagents in the channels. The benefits of the present system are reduced reagent consumption, combined with multi-parallel target testing, using only one sample. Hence, less sample material is required, since in many cases the amount of sample material is limited. Finally, an integration of this microchip, with an integrated sample preparation microchip, would constitute a fully automatic, laboratory independant diagnostic system, resulting in an overall time and cost reduction of the whole analysis.

Anja Gulliksen,[*ab] **Lars Anders Solli,**[c] **Klaus Stefan Drese,**[d] **Olaf Sörensen,**[d] **Frank Karlsen,**[ae] **Henrik Rogne,**[f] **Eivind Hovig**[g] **and Reidun Sirevåg**[b]

[a] NorChip AS, Industriveien 8, 3490 Klokkarstua, Norway.
E-mail: anja.gulliksen@norchip.com; Fax: +47 32 79 88 01;
Tel: +47 40 40 34 88
[b] University of Oslo, Dept. of Molecular Biosciences, 0316 Oslo, Norway
[c] NTNU, Dept. of Energy and Process Engineering, 7491 Trondheim, Norway
[d] IMM, Fluidik und Simulation, 55129 Mainz, Germany
[e] Buskerud University College, Kongsgata 51, 3019 Drammen, Norway
[f] SINTEF ICT, Dept. of Microsystems & Nanotechnology, 0314 Oslo, Norway
[g] Norwegian Radium Hospital, Dept. of Tumor Biology, Montebello, 0310 Oslo, Norway

References

1 J. M. M. Walboomers, M. V. Jacobs, M. M. Manos, F. X. Bosch, J. A. Kummer, K. V. Shah, P. J. Snijders, J. Peto, C. J. Meijer and N. Muñoz, *J. Pathol.*, 1999, **189**, 12–19.
2 N. Muñoz, F. X. Bosch, S. de Sanjosé, R. Herrero, X. Castellsagué, K. V. Shah, P. J. F. Snijders and C. J. L. M. Meijer, *N. Engl. J. Med.*, 2003, **348**, 518–527.
3 D. Jenkins, *Curr. Opin. Infect. Dis.*, 2001, **14**, 53–62.
4 J. Compton, *Nature*, 1991, **350**, 6313, 91–92.
5 G. Leone, H. van Schijndel, B. van Gemen, F. R. Kramer and C. D. Schoen, *Nucleic Acids Res.*, 1998, **26**, 9, 2150–2155.
6 I. Kraus, T. Molden, L. E. Ernø, H. Skomedal, F. Karlsen and B. Hagmar, *Br. J. Cancer*, 2004, **90**, 7, 1407–1413.
7 K. S. Cuschieri, M. J. Whitley and H. A. Cubie, *J. Med. Virol.*, 2004, **73**, 65–70.
8 H. G. Elias, *An introduction to polymer science*, 1997, VCH, NY.
9 K. S. Drese, O. Soerensen, L. Solli and A. Gulliksen, *smallTalk2003*, The Microfluidics, Microarrays and BioMEMS conference, July 13–16, 2003, San Jose, CA, USA, p. 69, Association for Laboratory Automation, http://www.labautomation.org.
10 A. Gulliksen, L. Solli, F. Karlsen, H. Rogne, E. Hovig, T. Nordstrøm and R. Sirevåg, *Anal. Chem.*, 2004, **76**, 9–14.
11 S. Syrjanen, P. Partanen, R. Mantyjarvi and K. Syrjanen, *J. Virol. Methods*, 1988, **19**, 225–238.
12 A. Mincheva, L. Gissmann and H. zur Hausen, *Med. Microbiol. Immunol.*, 1987, **176**, 5, 245–256.
13 H. B. Heiles, E. Genersch, C. Kessler, R. Neumann and H. J. Eggers, *Biotechniques*, 1988, **6**, 10, 978–981.
14 R. Boom, J. A. Sol, M. M. M. Salimans, C. L. Jansen, P. M. E. Wertheimvandillen and J. Vandernoordaa, *J Clin. Microbiol.*, 1990, **28**, 3, 495–503.
15 H. G. M. Niesters, *Methods*, 2001, **25**, 419–429.
16 M. P. de Baar, M. W. van Dooren, E. de Rooij, M. Bakker, B. van Gemen, J. Goudsmit and A. de Ronde, *J. Clin. Microbiol.*, 2001, **39**, 4, 1378–1384.
17 I. Kraus, NorChip AS, Norway, personal communication.

Paper III

A non-contact pump mechanism for parallel movement of nanoliter sized liquid plugs using flexible diaphragms

Lars A Solli,[*a,b] Anja Gulliksen,[b,c] Liv Furuberg,[d] Olaf Sörensen,[e] Frank Karlsen,[b,f] Lars R Sætran,[a] Henrik Rogne[d‡] and Klaus S Drese[e]

[a] Dept. of Energy and Process Engineering, Norwegian University of Science and Technology, Kolbjørn Hejes vei 2, N-7491 Trondheim, Norway.
[b] NorChip AS, Industriveien 8, N-3490 Klokkarstua, Norway. Fax: +47 3279 8801; Tel: +47 3279 8800, E-mail: lars.solli@norchip.com
[c] Dept. of Biology, University of Oslo, Kristine Bonnevies hus, N-0316 Oslo, Norway.
[d] Dept. of Microsystems, SINTEF ICT, Forskningsveien 1, P.O. Box 124 Blindern, N-0314 Oslo, Norway.
[e] Institut für Mikrotechnik Mainz GmbH, Carl-Zeiss-Strasse 18-20, 55129 Mainz, Germany.
[f] Institute for Microsystems Technology, Vestfold University College, P.O. Box 2243, N-3103 Tønsberg, Norway.

A novel non-contact pump mechanism for metering and movement of nanoliter sized liquid plugs in parallel channels has been developed. This work presents one part of the development of a lab-on-a-chip technology platform for point-of-care diagnostics. The cyclic olefin copolymer microchip has twelve parallel reaction channels with four pumps each, which are able to simultaneously move twelve sample plugs four steps in total. The combination of on-chip flexible diaphragms and actuation pins in a surrounding instrument constitute the pumps. We present results on the functioning and precision of the membrane pumps. Effects related to the membrane material, channel geometry, wall pinning, and pump chamber geometries are examined. The risk of cross contamination is drastically reduced between and within subsequently analyzed chips. However, evaporation of liquid reduces the pump quality and the inaccuracy in the positioning indicates the need for improvements of membrane material.

Introduction

Medical diagnostics based on microfluidic systems are currently being proposed for a variety of applications.[1-3] Microsystem solutions provide low-cost tests with rapid results using disposable microchips. The chips are inserted into automated instruments which can be used by non-qualified personnel. The goal is to create instruments where a sample (*e.g.* blood or saliva) can be inserted into a chip and the diagnostic results are displayed in a panel shortly after. The sample has to be guided through the microfluidic chip where all necessary reactions must take place, by the means of a micropump.[4]

An advantageous option for lab-on-a-chip systems is the ability to divide the sample into discrete independently controllable nanoliter sized liquid plugs. Transporting samples in liquid plugs bears some advantages over the usual continuous-flow systems. A

1

microfluidic operation can be reduced to a set of repeated basic operations, *i.e.*, moving one plug over one unit of action area. This method also facilitates utilization of the recirculating flow pattern[5] within the plug to minimize the time of both mixing and heat transfer.

The group of Burns *et al.*[6] reported in 1998 a plug-based integrated device for amplification and separation of DNA, where the movement of the plugs was based on external pneumatic control combined with on-chip vents and hydrophobic patches. Usually, external pneumatic control is handled by a pressure source or a syringe, while on-chip solutions might use ferrofluid as a dynamic plunger.[7] Several other transport methods in microscale segmented gas-liquid flow systems have been investigated, *e.g.* thermocapillary pumping,[8] electrowetting,[9] and thermopneumatic.[10]

We are in the process of developing a fully automated lab-on-a-chip device with no operating protocols for detecting human papillomavirus (HPV) cervix cancer markers.[11,12] This on-line technology identifies high-risk HPV mRNA transcripts employing real-time nucleic acid sequence-based amplification (NASBA).[13-16] The microfluidic chip consists of two parts: A sample preparation chip (not reported here), which concentrates and extracts nucleic acids from a patient sample, and a NASBA chip, which amplifies and detects mRNA. This work documents a solution for the pumping mechanism in the NASBA chip.

In the NASBA chip, the injected sample containing mRNA will be split into several plugs, for simultaneous analysis of different HPV viruses, along with negative, positive (artificial oligos), and human U1A sample control.[17] Each of the plugs will be metered to have a well-defined volume. Subsequently, the plugs are pushed through the chip, in parallel channels. Each sample plug must be halted three times at exact channel positions for mixing with dried reagents and finally also at an optical window for detection of a possible NASBA amplification. Capillary forces are utilized for pulling the sample into the chip and draining the excess sample into the waste chamber. In addition a pump mechanism is needed for metering and positioning the plugs.

The risk of cross contamination between on-chip reaction channels must be avoided, as well as contamination of instrument parts which severely will endanger sequential chip analysis. Thus, a non-contact pump mechanism that exclusively works on one reaction channel each, is preferred. We present a pump mechanism based on on-chip chambers with lids that are initially pressed down by pins actuated by the handling system. When the pins are lifted, the plug is pulled towards the expanded chamber. A similar mechanism has previously been used to inject sample from on-chip reservoirs.[18]

2

This paper presents a lab-on-a-chip system for plug-based real-time NASBA detection in cyclic olefin copolymer (COC) microchips with 95 nl plug volumes. It reports on experiments on the controllability of plug metering and positioning, using the chip membrane as pumps, whereas the previous work[12] showed optical detection of artificial HPV 16 sequences and SiHa cell line samples using the NASBA technology in the same microchip.

## Materials and methods

Microchip fabrication

The microchips were fabricated using injection moulding[19] of COC polymer (Grade 8007, Topas Advanced Polymers GmbH, Germany). The mould insert was manufactured with ultra precision milling of nickel. The microchips were oxygen plasma activated prior to coating with 0.5% (w/v) polyethylene glycol (PEG, P2263, Sigma-Aldrich Co.) in methanol.

The chip (see Fig. 1a.) is a 2 mm thick COC substrate embodying on one side the microstructures and on the other side pockets for thermal control. The sealing foil is a 75 μm thick COC membrane acting as a top cover for the microstructures (not visible in the figure). The membrane was sealed to the substrate using solvent bonding with cycloolefin. The COC is hydrophobic of nature and the PEG-coated COC is hydrophilic of nature. A cotton linter filter (Schleicher & Schuell BioScience GmbH, Relliehausen, Germany) was placed in the waste chamber to provide a driving force to drain the excess sample.

Diaphragm pumps chamber design

The inlet, located at the lower right hand side of the chip in Fig. 1a, is connected to a waste chamber through the supply channel. The supply channel has a cross-section of 550×550 μm². The waste chamber has venting to the outside atmosphere. Perpendicular to the supply channel are twelve parallel closed-end reaction channels, with a cross-section of 400×100 (width×depth) μm². The reaction channels have four rounded chambers each, called actuation chambers, at their end. These four chambers work as diaphragm pumps, which will transport the liquid in four steps into the reaction channel. In order to test liquid sample transport compared to actuation chamber sizes, four different sets of chambers are designed on one chip (see Fig. 1a. From left to right: Channels 1, 3, 5 and 2, 4, 6 and 7, 9, 11 and 8, 10, 12 are equal). It was found that channels 8, 10 and 12 resulted in the best

plug positioning over the three reaction sites, where the mixing and the optical read-out are located. The chamber diameters of the four chambers in these channels were 1.5, 1.84, 1.84 and 3.26 mm (see Fig. 1b).
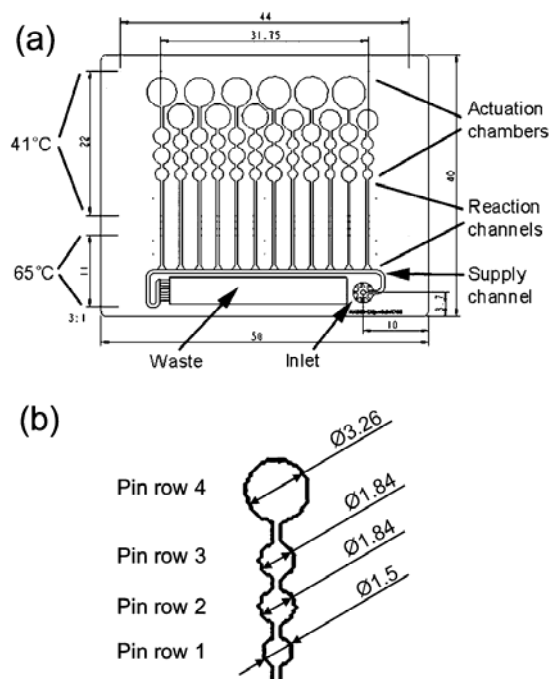

Fig. 1   Illustrations of the NASBA microchip. All dimensions are in millimetres. (a) The two thermal pockets are displayed as the light grey areas as pointed to by the 41˚C and the 65˚C text, respectively. The waste chamber has an opening in the end close to the inlet. The delta shaped areas that connect the reaction channels with the supply channel are present to ease the filling procedure due to smoother corners. The inlet is designed to maintain the liquid plug in position above the inlet area, ensuring successful filling. (b) Segment of the actuation chambers of the reaction channel to the very right in Fig. 1a. Each channel has four individual diaphragm pump chambers; one for metering and three for movement. In total the chip has 48 chambers in twelve separate channels. The four chambers are located on horizontal lines as represented by the pin row numbers.

Mechanical actuation

The pump principle is illustrated in Fig. 2a. Volume is increased by the release of a deflected diaphragm. The liquid plug enters a new equilibrium position downstream the channel. The actuation mechanism consists of 48 spring-loaded pins (GSS-3 series, Interconnect Devices, Inc., KS, USA) with a rounded tip and a head diameter of 1.96 mm, assembled in two blocks. The upper block in Fig. 2b contains the pins for row 2, 3 and 4 (see Fig. 1b). The rows are in a staircase formation. The block is mounted to a robotic shaft

4

movable in the longitudinal axis of the pins. The staircase formation of the pin rows and the springs enable the ability to release the pumps in pin row 2 simultaneously, followed by pin row 3 and 4, by elevating the block in three steps. The second block in Fig. 2b contains the first pin row and is mounted on a magnetic actuator. This allows faster response time of the pin actuation. This was originally intended to aid the mixing of the dried chemicals into the liquid sample, but this is not reported in this work. Fig. 2c illustrates how the pin deflects the membranes of the four actuation chambers. As the illustration shows the pin head is larger than chamber 1, 2 and 3, *i.e.* the pin will not hit the bottom in these chambers.
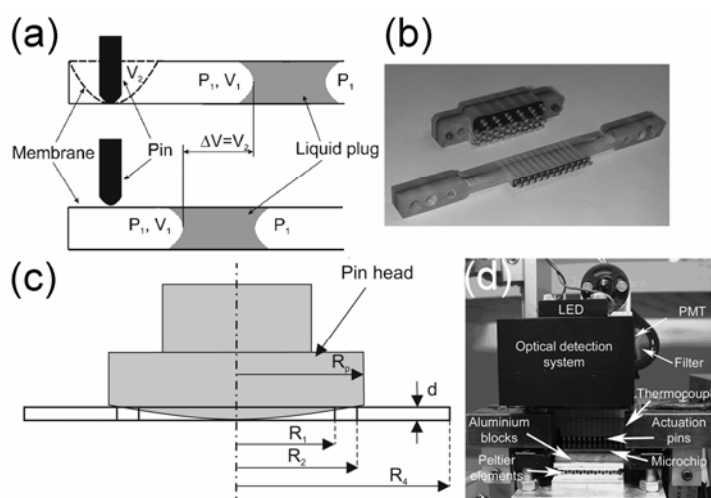
Fig. 2 (a) Principle sketch of the pin actuation. Both sketches illustrate a cross-section of a reaction channel with a sample plug in equilibrium and an actuation chamber at the left end. The upper sketch displays a pin which is pushing the membrane down in the actuation chamber, thus creating a displaced volume. The lower sketch presents a situation where the pin has been elevated. When revealing the displaced volume, the pressure in the confined volume at the end of the reaction channel decreases. Thus, the pressure in front and rear of the plug are no longer in equilibrium and the plug will move to the left to again resituate in equilibrium. (b) Photograph of the two blocks that contain the pin rows. (c) Illustration of a pin head in chambers 2, 3 and 4. d is the depth of the chambers and R_p, R_1, R_2 and R_4 are the radii of the pin head, chamber 1, chamber 2 (and 3) and chamber 4, respectively. The height of the spherical cap that constitutes the tip of the pin equals the depth of the chambers d. (d) Photograph of the major components in the custom-made instrument.

Instrument

Fig. 2d displays a photograph of the major components in the instrument. The parts that compose the optical system are described in Gulliksen *et al.*[12] The instrument further comprises two Peltier elements (Marlow Industries Inc., Dallas, TX) with aluminum blocks

mounted on top to form the chip holder. A thermal pad was placed on the blocks for thermal contact to the chip. A thermocouple was integrated into the chip holder, with feedback to the Peltier elements. The system was calibrated with a commercial temperature calibration instrument (Fluke, Everett, WA) and platinum resistance sensors, both with an accuracy of ± 0.1°C. Temperature calibrations were performed both on the aluminum block, and on top of a dummy microchip, without a membrane. The overall temperature accuracy of the system was within ± 1°C.

The instrument was equipped with a chip holder movable in two axes for pin elevation and optical positioning. The servomotors (Omron Electronics, Kyoto, Japan) were regulated by a physical signaling sublayer (PLS) (Saia-Burgess Electronics AG, Murten, Switzerland), programmed with PG 5 (Saia-Burgess Electronics AG).

All communications were run through a serial line (RS232) and controlled externally by MATLAB.

Experimental procedure

Liquid sample material

The sample material used in the experiments is a NASBA mixture (PreTect® HPV-Proofer kit (NorChip AS, Norway)). See Gulliksen *et al.*[12] for details about the sample. This solution does not contain any targets, so no amplification will be present in the experiments. The sample proved to have wettable characteristics to both the non-coated lid surface and the PEG-coated microchannel surface. The sample liquid exhibited a contact angle of 56.4˚ and 25˚ on the COC and the PEG-coated COC, respectively, when investigated with the sessile drop method. The surface tension in air of the liquid was 35 mN m^{-1}, when investigated with the pendant drop method. All the measurements were conducted in room temperature with the DROP instrument (University of Oslo, Norway).

Metering and isolation of sample plugs

Metering is accomplished by the combination of capillary forces and the first set of pumps. As capillary forces pull the liquid sample through the supply channel, the cross-section difference between the supply channel and the reaction channels ensures that liquid is also pulled into the reaction channels. The capillary pressure across a meniscus in a microchannel with a lid of different wetting behaviour, can be expressed as:[20]

$$\Delta P = \gamma \cos\left(\theta_{chip}\right)\left(\frac{2d+w}{dw}\right) + \gamma \cos\left(\theta_{lid}\right)\left(\frac{w}{dw}\right). \tag{1}$$

Here, w is the width, d is the depth, γ is the surface tension of the liquid and θ_{chip} and θ_{lid} are the contact angles of the chip and the lid, respectively. By inserting θ_{chip}=25˚, θ_{lid}=56.4˚ and γ=35 mN m^{-1}, Eq. 1 yields ΔP = 669.5 Pa. The reaction channels have initially an atmospheric pressure of 101325 Pa, thus the volume change is about 0.66%. The upstream closed volume in actuation channel 12 is at this stage calculated to be 1683 nl, hence the sample will enter ~11 nl into the channel. Subsequently, the first pin row is elevated and the liquid is pulled a distance into the reaction channel, defined by the first diaphragm pump. Further, the filter drains the excess sample in the supply channel, and the rear meniscus of the sample snaps off liquid at the intersection with the reaction channels, leaving separated sample plugs in the reaction channels. The filling- and draining process of the supply channel is a continuous procedure.
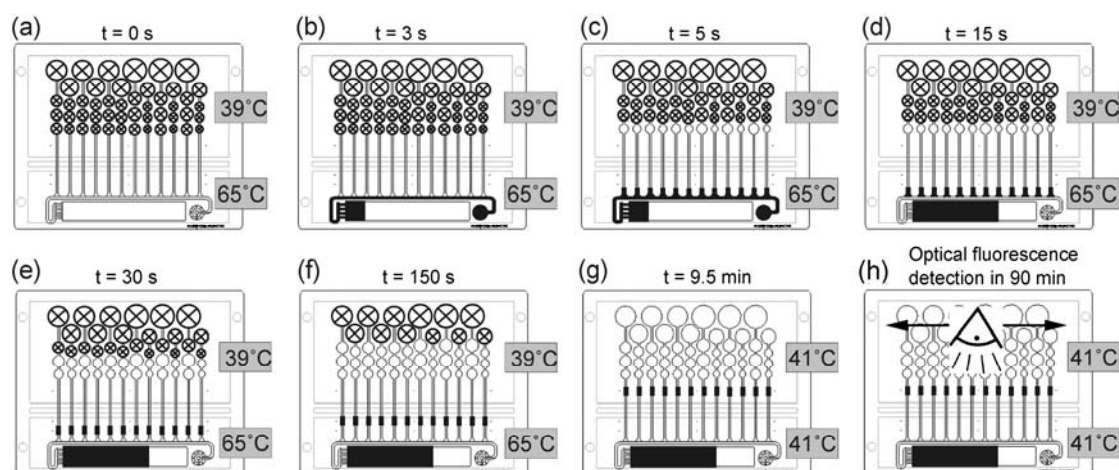
Principle of the NASBA chip

The principle of the whole NASBA procedure is presented step-by-step with timeline in Fig. 3a-h. The chip is in the initial state when all the chamber diaphragms are pressed down (a). Sample is introduced and pulled into the chip by capillary forces (b), plugs are metered (c) and excess sample is drained by the filter (d). The twelve sample plugs are moved to the two dried reagent spots (e and f), and finally to the last combined reagent and optical detection site (g), where the NASBA detection starts (h). The NASBA procedure requires heating in two steps. Initially a temperature of 65˚C is needed for denaturation of the nucleic acids. Subsequently the temperature is lowered to 41˚C for the amplification to take place (see Fig. 3). The first two reaction sites are at 65˚C. The reaction mixture containing enzymes in the last reaction site must not exceed 42˚C. In order to assure a certain safety margin, this part of the chip was only heated up to 39˚C, while the other was kept at 65˚C (see Fig. 3a-f).

Experimental

In order to saturate the humidity inside the chip, a 2 µl part of the sample was pre-injected into the chip and kept in the inlet area for approximately 5 minutes at the initial chip temperature of 65˚C/39˚C (see Fig. 3a). This procedure was implemented to reduce evaporation of sample and minimize its consequences such as sample displacement and

volume loss. Next, a sample volume of 25 μl was applied to the inlet hole by a pipette. Capillary forces moved the sample into the chip and the elevation of the first pin row moved a defined sample volume into the twelve parallel reaction channels. The supply channel was subsequently drained by the filter, leaving 12 isolated sample plugs in each reaction channel. No dried analytes were present in the reaction sites during the experiments of this paper. This part will be presented in future work.

Optical monitoring of plug positioning in parallel channels is conducted with a DV-camera (Sony DCR-TRV30E) placed above the instrument. All pictures are taken five seconds after the pin elevation. Data for the plug movement are produced by measuring covered distances on larger paper reprints. The accuracy of the measurements is given from the pixel size on the reprints, which is about 43 μm on the microchip.


Fig. 3   Schematic illustrations displaying the NASBA chip procedure step-by-step. A circle with a cross inside indicates that the membrane of the particular actuation chamber is pushed down. The grey boxes denote the temperature of the Peltier elements. The sample liquid is shown in black. Here, the four sets of actuation chambers are considered identical in order to emphasize the topical principle, hence, the equal sample movement. The timeline is included above each figure. (a) The chip in its initial position. All four pins impress the membranes into the actuation chambers. (b) Sample is applied to the inlet and the supply channel is filled due to capillary forces. (c) The first set of pins is elevated and sample is metered into the reaction channels. (d) The supply channel is drained into the waste chamber, leaving separated sample plugs in the reaction channels. (e) The second row of pins is elevated and the sample plugs are moved onto their first reaction site. (f) The third row of pins is elevated and the sample plugs are moved onto the second reaction site. (g) The fourth row of pins is withdrawn and the sample plugs are moved onto the third reaction site. (h) The NASBA amplification

Results and discussion

Metering and movement of plugs, including heating procedure were conducted in 12 different microchips. The pictures in Fig. 4 show a typical result from one reaction channel. Parallel metering and movement were performed successfully in all twelve channels on each chip. However, in order to have realizable statistics, only channel 12 in the different chips was investigated.

The metering volume in the experiments produced plugs of sample volumes of 95.6±17.1 nl. Fig. 5 displays experimental data of the plug movement. Each middle point of the plug samples is monitored in the three movement steps to the three reaction sites. The positions are measured from the start of the reaction channel. The inset in Fig. 5 demonstrates the reproducibility of the actuation method. The error bars represent standard deviation based on the 12 reaction channels. The first reaction site has a mean position with standard deviation of 2.08 ± 0.27 mm, the second 4.21 ± 0.38 mm and the third 9.85 ± 0.44 mm.
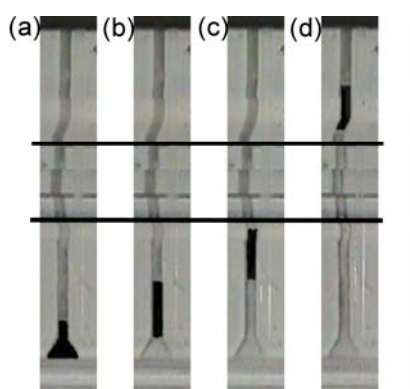
Fig.4   Picture series showing a typical result of a plug sample in reaction channel 12 displaced by the diaphragm pumps. The plug is coloured black for visualization purposes. The channels and plugs appear skewed in the images, because only their shadow is visible on the grey cover of the Peltier element. The horizontal lines represent the edges of the temperature zones. (a) Plug in metering position. (b) Plug moved to reaction site 1. (c) Plug moved to reaction site 2. (d) Plug moved to reaction site 3.
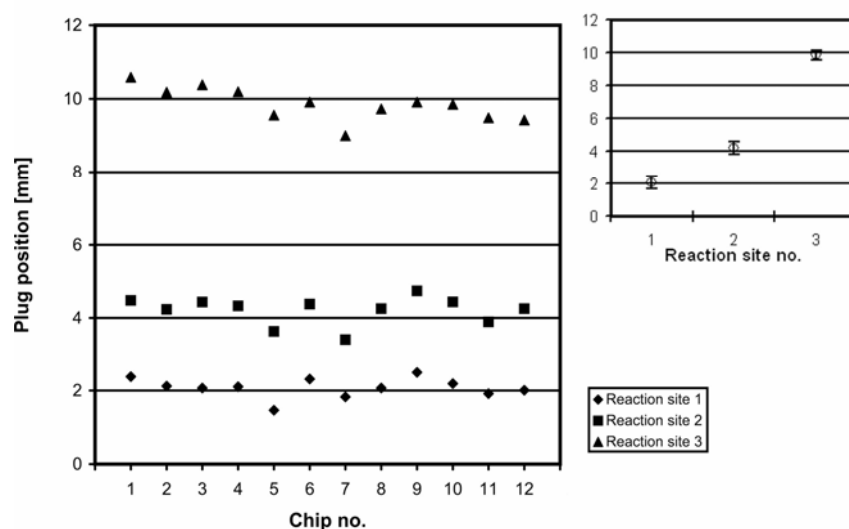
Fig. 5   Graph showing plug positions of 12 different microchips. All points denote centre points of plugs in reaction channel 12. Inset: The open circles represent the average values of the middle position of the plug in the reaction sites. Standard deviations are included in the figure.

The measured effective pump volumes of the chambers are presented in Fig. 6. The graph shows pump volumes of actuation chamber 2, 3 and 4 of reaction channel 12. The data are collected by measuring the distance between the upstream meniscus of the plug before and after pin elevation. The second actuation chamber has a mean pump volume with standard deviation of 73.1 ± 11.3 nl, the third 82.9 ± 7.5 nl and the fourth 223.9 ± 11.9 nl. The horizontal lines in Fig. 6 represent calculated pump volumes; based on the volume of a spherical cap (height of 70 μm) for chamber 2 and 3 and a truncated cone (with radius of truncated area of 40 μm) for chamber 4. The latter model was chosen because in this case, the main part of the deflected diaphragm exhibits a linear shape, *i.e.* not curved as the deflection in the chambers comparable in size with the rounded pin head. The approximated values are 93.2 nl for actuation chamber 2 and 3, and 285 nl for actuation chamber 4. The experimental data of chamber 2 and 3 differ in average pump volumes by 13.4%, although the chambers are equal in size. Further, the estimated data diverge from the experimental by 27.5%, 12.4% and 27.3% for pump volumes 2, 3 and 4, respectively. Investigations showed that the observed deviations are caused by two main effects.

10
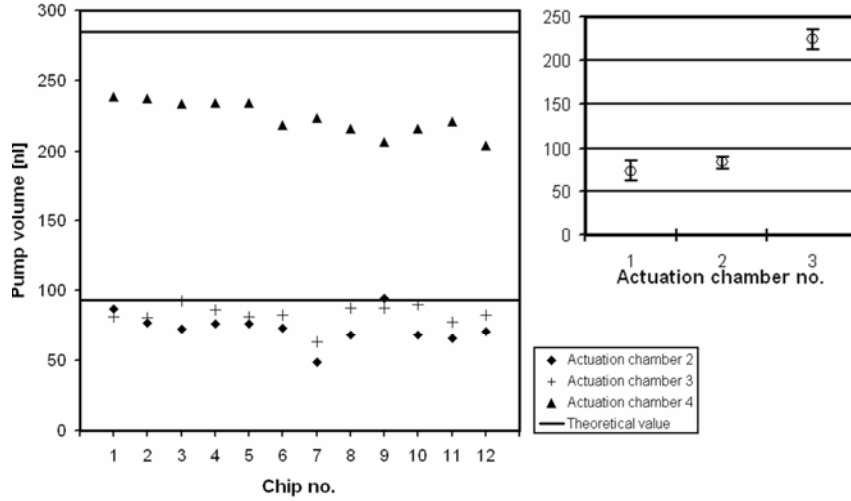
Fig. 6 *Graph showing pump volumes of actuation chamber 2, 3 and 4. The horizontal lines represent estimated pump volumes. Inset: The open circles represent the average values of the pump volume. Standard deviations are included in the figure.*

The following sections will explain the apparent difference in pump volumes between chamber 2 and 3, the theoretical overestimation of pump volume, together with the noise in the pump volume data.

First, due to the larger width of the entrance of the reaction channel (1.59 mm) compared to its overall width (0.4 mm), the pump volume deviation between actuation chamber 2 and 3 is caused by the difference in capillary pressure of the plug in the metering position (see Fig. 4a). The pressure over the front- and the back meniscus of the whole plug ΔP_{plug}, is given by:

$$\Delta P_{plug} = \Delta P_{front} - \Delta P_{back}. \tag{2}$$

By substituting Eq. 1 into Eq. 2, yields the following relation

$$\Delta P_{plug} = 2\gamma \cos\left(\theta_{chip}\right)\left(\frac{1}{w_f} - \frac{1}{w_b}\right), \tag{3}$$

where w_f and w_b are the widths of the front meniscus and back meniscus of the plug, respectively. By inserting the measured values, Eq. 3 yields $\Delta P = 594.4$ Pa. The reaction channels have initially an atmospheric pressure of 101325 Pa, thus the volume change are

11

about 0.59%. The downstream closed volume in actuation channel 12 is at this stage calculated to 1624 nl, and given the assumptions above the effect of actuation chamber 2 is ~10 nl less than chamber 3. This is in reasonable agreement with measured pump volumes in Fig. 6, as the corrected pump volumes of chamber 2 and 3 becomes comparable.

Secondly, the estimated pump volume of all chambers is reduced compared to the experimental data due to evaporation of the sample plugs. The experiments show a reduction in the measured total sample volume from the first position to the third position. The plug volumes were 89.3 ± 13 nl, 86 ± 13 nl and 81.9 ± 13 nl when leaving reaction site 1, 2 and 3, respectively. Hence, the sample has lost a volume of 3.3 nl in 2 minutes on 65˚C and 4.1 nl in 7 minutes where the temperature was reduced from 65˚C to 41˚C (see Fig. 3e and f), due to evaporation from both ends of the plugs. Further, evaporation increases the partial vapour pressures in the downstream closed side of the channel and thus expands its volume. The experiments reveal that the plugs, when in position of the two first reaction sites for mixing with dried reagents (in 2 minutes (Fig. 3e) and 7 minutes (Fig. 3f), respectively), are moved downstream before actuation of the following diaphragm pump. The data exhibits a variable behaviour, an expansion of the closed volume of 1.2 ± 3.8 nl and 7.3 ± 9.1 nl, during the elapsed time at the 2nd and the 3rd reaction sites, respectively. The evaporation effect is not quantified any further.

The variations within the experimental data are believed to be caused mainly by hysteresis effects. These are energy barriers which the fluidic interfaces must overcome before its liquid edge can advance further.[21] The channel surface was investigated using a white light interferometer (WYKO NT-2000, Veeco Instruments Inc., NY, USA). The RMS (root mean square) value of the surface roughness on the PEG coating was measured to be 0.5 μm. The measurements were conducted in a 400×450 μm^2 area inside the reaction channels. The data also show a maximum value of 1.55 μm. Pinning of menisci in microchannels with RMS roughness less than 1 nm has been observed.[22] Other possible hysteresis attributes are heterogeneous coating, chemical liquid-surface interactions and contamination such as dust in the channels.[21] These attributes are not investigated further. The effect of hysteresis is believed to have a distinct influence on liquid movement in this case of the gradually increasing volume caused by evaporation, rather than the movement due to the fast expansion of volume caused by the elevated diaphragms. Hence, it is likely to assume that the plugs are not in equilibrium positions when the diaphragm pumps are actuated, causing the pumps to achieve less than estimated.

12

A total number of six diaphragms were also investigated in the WYKO, for inspection of effects from the direct impact of the pins and plastic deformations due to deflection. The diaphragms were examined both before and after pin actuation. A gold layer with a thickness of a few nanometres was sputtered onto the membrane in order to realize the measurements. A typical result is shown in Fig. 7. The measurements showed a noteworthy plastic deformation in only one of the inspected diaphragms of approximately 2.5 nl, which is considered an insignificant contribution to the position inaccuracy. All diaphragms, however, showed a convex shape of 10±2 μm before actuation, but exhibited irregular convex shapes of 5±1.5 μm after actuation. This is due to different applied pin pressure and alignment. The unequal deformation may cause approximately 6.3 nl difference in the mid sized pumps, which are considered to be significant contribution to the variance of the pump volumes.
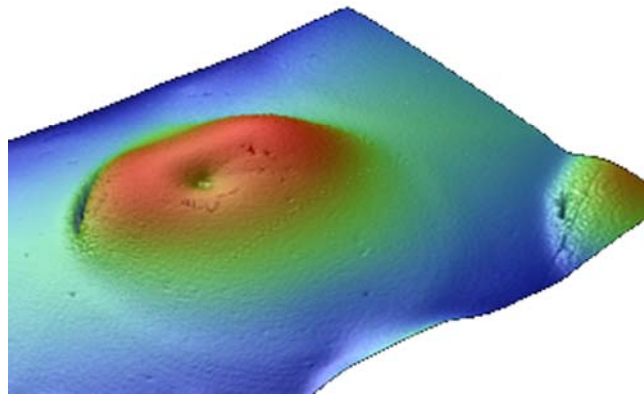
Fig. 7   Picture showing a typical WYKO visualization of a membrane after pin actuation. Parts of two adjacent chambers are visible to the right and below of the main chamber.

Conclusion and further work

A novel non-contact pumping mechanism consisting of flexible diaphragms and pins has been developed. The on-chip pumps successfully performed metering and movement of nanoliter sized liquid plugs in parallel channels, demonstrating that the pump mechanism has a potential for use in lab-on-a-chip applications.

The benefits of this system are the reduction of cross contamination risks between the twelve on-chip analysis channels, and also between the instrument parts and sequentially analysed chips. In addition, the pumps mechanism employs low-cost manufacturing, which facilitates disposable chips.

The range of the pumps may be optimized by adjusting the chamber sizes, so desired sample positions can be reached. However, the results proved that the effect of the pumps is reduced due to evaporation of the sample plugs and noise is generated from deformations of the diaphragms. Future microchips could contain valves such as geometrical restrictions in the channels combined with hydrophobic patches to aid position restriction of the plugs, while the membrane material must be changed into a more robust one. Careful design criteria must be pursued in order to decrease the evaporation, as *i.e.* reduction of on-chip dead volume to increase the efficiency of the vapour saturation.

Acknowledgements

Notes and references

‡   *In memoriam* – Dr. Henrik Rogne (1969-2006)

1   E. Verpoorte, *Electrophoresis*, 2002, **23**, 677-712.

2   B. H. Weigl, R. L. Bardell and C. R. Cabrera, *Adv. Drug Delivery Rev.*, 2003, **55**, 349-377.

3   P. C. H. Li, *Microfluidic Lab-on-a-Chip for Chemical and Biological Analysis and Discovery*, Taylor & Francis Group, Boca Raton, FL, 2006.

4   D. J. Laser and J. G. Santiago, *J. Micromech. Microeng.,* 2004, **14**, R35-R64.

5   J. L. Duda and J. S. Vrentas, *J. Fluid Mechanics*, 1971, **45**, 247-260.

6   M. A. Burns, B. N. Johnson, S. N. Brahmasandra, K. Handique, J. R. Webster, M. Krishnan, T. S. Sammarco, P. M. Man, D. Jones, D. Heldsinger, C. H. Mastrangelo and D. T. Burke, *Science*, 1998, **282**, 484-487.

7   O. Sörensen, K. S. Drese and S. Hardt, Proceedings of the 7th International Conference on Miniturized Chemical and Biological Analysis Systems, Squaw Valley, October 5-9, 2003.

8   M. A. Burns, C. H. Mastrangelo, T. S. Sammarco, F. P. Man, J. R. Webster, B. N. Johnson, B. Foerester, D. Jones, Y. Fields, A. R. Kaiser and D. T. Burke, *Proc. Natl. Acad. Sci. USA*, 1996, **93**, 5556-5561.

9   G. Beni and M. A. Tenan, *J. Appl. Physics*, 1981, **52** (10), 6011-6015.

10   K. Handique, D. T. Bruke, C. H. Mastrangelo and M. A. Burns, *Anal. Chem.*, 2001, **73** (8), 1831-1838.

11   A. Gulliksen, L. A. Solli, F. Karlsen, H. Rogne, E. Hovig, T. Nordstrøm and R. Sirevåg, *Anal. Chem.,* 2004, **76** (1), 9-14.

12   A. Gulliksen, L. A. Solli, K. S. Drese, O. Sörensen, F. Karlsen, H. Rogne, E. Hovig and R. Sirevåg, *Lab Chip,* 2005, **5**, 416-420.

13   J. Compton, *Nature,* 1991, **350** (6313), 91–92.

14   G. Leone, H. van Schijndel, B. van Gemen, F. R. Kramer and C. D. Schoen, *Nucleic Acids Res.*, 1998, **26** (9), 2150–2155.

15   I. Kraus, T. Molden, L. E. Ernø, H. Skomedal, F. Karlsen and B. Hagmar, *Br J Cancer*, 2004, **90** (7), 1407–1413.

16   K. S. Cuschieri, M. J. Whitley and H. A. Cubie, *J Med Virol*, 2004, **73**, 65–70.

17   P. T. G. Sillekens, W. J. Habets, R. P. Beijer and W. J. van Venrooij, *EMBO J.*, 1987, **6** (12), 3841-3848.

18   D. Solignac and M. A. M. Gijs, *Anal. Chem.,* 2003, **75**, 1652-1657.

19   H. G. Elias, *An introduction to polymer science*, Wiley-VHC, NY, 1997.

20   S.-H. Lee, C.-S- Lee, B.-G. Kim and Y.-K. Kim, *J. Micromech. Microeng.,* 2003, **13**, 89-97.

21   A. W. Adamson and A. P. Gast, *Pysical Chemistry of Surfaces,* John Wiley & Sons, Inc., New York, NY, 6th edn., 1997.

22   S. Jin and K. S. Breuer, Proceedings of the 2003 ASME International Mechanical Engineering Congress & Exposition, Washington, DC USA, November 16–21, 2003.

Paper IV

Towards the development of an isothermal amplification microchip

Anja Gulliksen,*[a,b] Michal Mielnik,[c] Bente F. Hoaas,[a] Eivind Hovig,[d] Frank Karlsen,[a] Henrik Rogne,[c,‡] and Reidun Sirevåg[b]

[a] NorChip AS, Industriveien 8, 3490 Klokkarstua, Norway. Fax: +47 3279 8801; Tel: +47 3279 8800; E-mail: anja.gulliksen@norchip.com
[b] University of Oslo, Dept. of Molecular Biosciences, 0316 Oslo, Norway
[c] SINTEF ICT, Microsystems & nanotechnology, Gaustadalléen 23, 0373 Oslo, Norway
[d] The Norwegian Radiumhospital, Inst. for Cancer Research, Dept. of Tumor Biology, Montebello, 0310 Oslo, Norway
[e] NTNU, Dept. of Energy and Process Engineering, 7491 Trondheim, Norway

At nanoliter volumes, any enzymatic reaction faces obstacles not observed at the macroscale, due to an altered surface area-to-volume ratio as well as other effects. A microchip requires further considerations, as chip material and manufacturing process are important parameters. Also, for a point-of-care chip, it is important to have reactants stably stored on-chip. In this study, we have addressed elements for optimal solutions, and have found that for deposition and storing of dried nucleic acid sequence-based amplification (NASBA) reagents, it is necessary to add protectants such as *e.g.* polyethylene glycol (PEG) and trehalose to recover enzyme activity upon rehydration. The standard NASBA reagents consist of a mastermix and enzymes, and were only stable when dried separately on macroscale. The times for diffusion/rehydration of modified molecular beacons in dried mastermix and FITC-labelled mouse IgG in the dried enzyme solutions were ~ 60 seconds and ~ 10 minutes in 500 nl chambers, respectively. Microchips with native cyclic olefin copolymer (COC) surfaces showed large adsorption of fluorescent labelled mouse IgG, while PEG coated surfaces showed adequate protein resistance and were found to be the most biocompatible surface coating for NASBA. Hot embossed microchips provided the lowest surface roughness and background fluorescence, and were found to be the most suitable microchips for performing NASBA. Successful amplification on chip in 500 nl reaction chambers was obtained for spotted and dried enzymes when 0.5% PEG was applied. However, successful amplification of a spotted and dried mastermix upon rehydration on a microchip has not been obtained.

Introduction

To perform molecular diagnostics on clinical samples, stock reagents are required, in addition to specifically targeted reagents. In the case of microchips, the reagents are typically introduced as aqueous solutions either via connections to large syringe pumps

or through large local reservoirs on chip.[1, 2, 3, 4] The challenge when reagents and samples are introduced to microsystems through supporting devices, such as tubing and syringes, is that this can inhibit the final analytical assay.[5] Incompatible surface materials of the tubing and the syringes can be major obstacles for sensitive assays, as *e.g.* proteins/enzymes often adsorb to the surface and are hence removed from solution. Additionally, many such supporting devices are unlikely to be disposable items. Hence, along with the question of contamination, it is important to consider the effects of surfaces repeatedly exposed to reagents and washing procedures. External reagent and sample supplies cause large and unwanted dead volumes which may influence the performance of the microchips. Furthermore, approaches utilizing external supplies tend to prevent development of complete automatic microsystems. A self-contained system, in which all reagents are stored on chip, benefits from minimal handling by the user, enabling the analysis to be performed by non-skilled personnel. Accordingly, the risk of human error is minimized. However, both liquid reagents and dried reagents have been introduced as plausible solutions for long-term storage of reagents on chip.[4, 6, 7, 8, 9, 10, 11]

Molecular diagnostics employ reagents which vary extensively with regard to stability. Normally, these diagnostic tests contain enzymes which are often considered as the most critical component of the assay. Most enzymes are unstable in aqueous systems at room temperature over time, and are often stored either frozen, or in liquid phase at -20°C or -70°C. However, by applying protectants, the reagents can be stable at room temperature for periods of up to several months.[12, 13] In most cases, long-term stability of enzymes is obtained by freeze-drying. Although freeze-drying is regarded as a gentle method in order to retain enzyme activity, the physical processes induce stress on the molecules, potentially resulting in loss of function. Therefore, it is important to include protectants which prevent denaturation during freezing (cryoprotectants) as well as drying (lyoprotectants).

In this paper, we have explored approaches for integration of the reagents for the isothermal amplification of mRNA by nucleic acid sequence-based amplification (NASBA)[14] towards the development of a self-contained disposable microchip. NASBA contains two main reagent stock solutions; the nucleotide ion-adjusted master mixture hereafter termed mastermix, and the enzymes. The most critical issue with respect to long-term storage/drying/freezing is to control stabilization of the three labile NASBA enzymes (AMV-RT, RNase H and T7 RNA polymerase). It is essential that the enzymes remain

2

active in the microchip in order to obtain successful amplification reactions after rehydration. We found that it is possible to amplify spotted and dried enzymes on a microchip, when the enzyme solution contains 0.5% PEG. Successful amplification of spotted and dried mastermix on microchips still remains. However, as amplification was demonstrated on macroscale, it is likely that the parameters for amplification may be tuned sufficiently to permit amplification of dried mastermix on microchips.

Experimental conditions

Fabrication of the microfluidic devices

Several different test chips were manufactured. To perform experiments for optimization of the detection volume and for drying of the NASBA reagents, silicon microchips were manufactured (at SINTEF) by means of deep reactive ion etching (DRIE), see Figure 1a and Figure 1b. A standard Bosch DRIE was performed on 4'' wafers. The depth of all cavities was 0.15 mm. A 1000 Å thick oxide layer was grown, before the microchips were sealed using a 3M™ Polyolefin Microplate sealing tape (HJ Bioanalytic, Germany).

(a)　　　　　　　　　　　　　　　　(b)
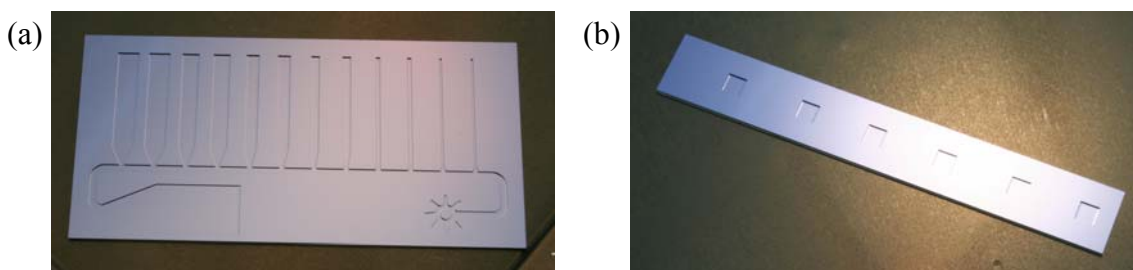
Figure 1 Silicon microchips fabricated using DRIE. (a) Silicon microchip for optimizing the detection volume. The outer dimension of the microchip was 17.0 mm × 34.1 mm. All channels on the microchip were 0.15 mm deep. The channels perpendicular to the supply channel (from right to left) were in pairs 0.33 mm, 0.67 mm, 1.00 mm, 1.33 mm, 1.67 mm and 2.00 mm wide, which corresponded to detection volumes of 100 nl, 200 nl, 300 nl, 400 nl, 500 nl and 600 nl, respectively. The illuminated area during detection was 2.0 mm × 2.0 mm. (b) Silicon microchip with six 500 nl chambers (1.85 mm × 1.85 mm × 0.15 mm) used for preliminary drying experiments of the NASBA reagents. The outer dimensions of the microchip were 5.0 mm × 34.1 mm.

Injection moulded cyclic olefin copolymer (Grade 8007, Topas Advanced Polymers GmbH, Germany) chips[15] were employed for evaluation of biocompatible

coatings in relation to the NASBA reagents and for measurements of background fluorescence (Figure 2a).

Two additional COC microchip designs were fabricated to test the drying of NASBA reagents on chip (Figure 2b). The COC chips were processed (by IMM, Mainz, Germany) in standardized sized COC (Grade 5013, Topas Advanced Polymers GmbH, Germany) plates, using computer numerical controlled (CNC) milling. The chips were milled with a 200 μm mill, a rotation of 12,000 rpm and a feed rate of 90 mm/minute. The chips could easily be mounted in a standard aluminium frame (IMM) with interconnection by means of fluidic interfaces. The depth of the channels and chambers was increased to 0.20 mm to allow enlarged detection volumes. The reaction chambers were designed for 300 nl and 500 nl detection volumes.
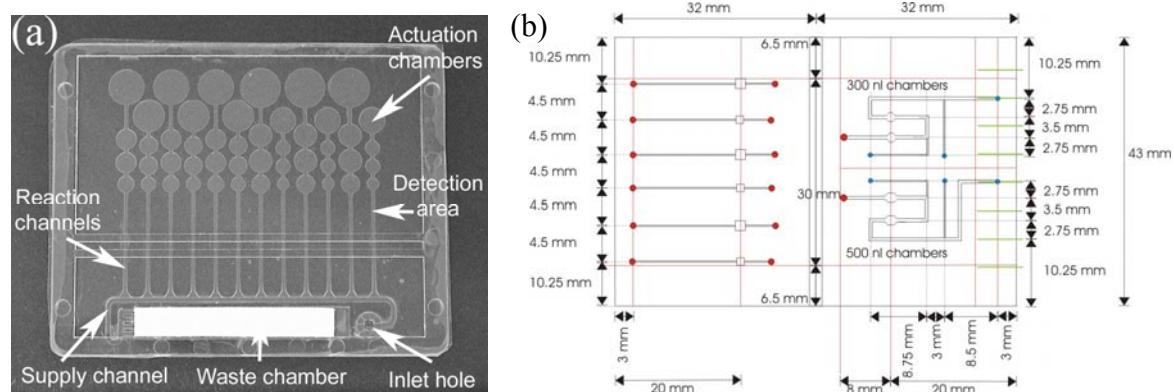

Figure 2 COC microchips. (a) The injection moulded COC microchip has been presented in detail in previous work.[15] The outer dimensions of the COC microchip were 50 mm × 40 mm and had a detection volume of 80 nl in the reaction channels. (b) COC microchips designed for spotting and drying of the NASBA reagents. The microchip to the left contained 3 single chambers of 300 nl and 3 single chambers of 500 nl. Each chamber had fluidic connection ports on the left side for individual fluidic control. The chip to the right had two chambers in series of either 300 nl or 500 nl. Venting channels and fluidic connection points were integrated on the chip at the left side for fluidic control.

After initial experiments, an improved design of the two milled COC microchips was realized using various fabrication methods (Figure 3). In addition to milling, the new COC (Grade 5013) microchips were prepared by both hot embossing and laser ablation. The die for the hot embossed chips was CNC milled into stainless steel and subsequently polished before the defined pattern of the die was transferred to the COC substrate. The substrate was pre-heated to 220°C. The temperature was kept constant for 120 seconds, the die was pressed into the chip using a force of 4 000 N. Subsequently, the COC substrate

4

was cooled to 85°C and the hot embossed chips removed. The whole process lasted about 45 minutes.

The laser ablated chips were manufactured using an excimer laser with a wavelength of 193 nm and a lens with a 4 times reduction, and a mask. For the laser ablated chip in Figure 3e, the energy density was 0.1 J/cm² with a pulse frequency of 40 Hz and a feed rate of 100 mm/minute. For ablating the 200 μm deep reaction chambers of the chips shown in Figure 3f, a negative mask was used with a stationary laser beam having a pulse frequency of 1500 Hz and an energy density of 0.3 J/cm².

The dimensions of the reaction chambers were set to 1.6 mm × 1.6 mm × 0.2 mm, corresponding to a volume of 500 nl. The corners of the reaction chambers were rounded to ensure complete filling by capillary forces. The width and depth of the supply channels were 0.2 mm.
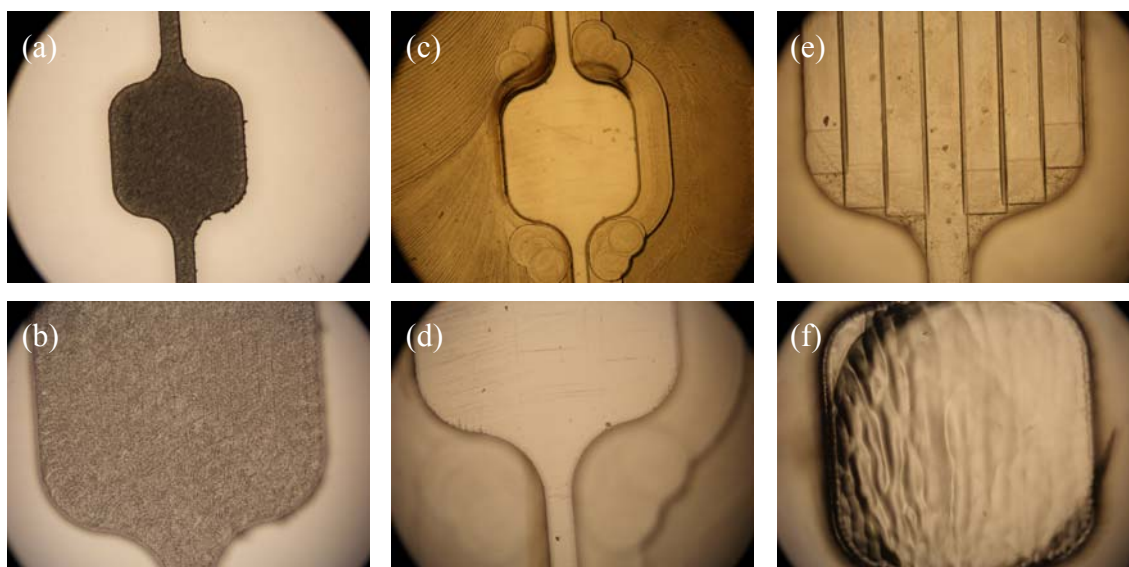
Figure 3 The images show the results of reaction chambers fabrication in COC microchips by means of milling, hot embossing and laser ablation. The surface topography was profoundly influenced by the fabrication method. Images (a) and (b) show milled reaction chambers. Hot embossed reaction chambers are shown in (c) and (d). (e) and (f) show reaction chambers laser ablated with a traversing laser beam and a stationary laser beam, respectively.

Coating of the microchips

Injection moulded microchips were dip-coated in either 5 mg/ml poly(2-ethyl-2-oxazoline)-benzophenone (PEtOx-BP) or 10 mg/ml poly(dimethyl acrylamide)-benzophenone (PDMAA-BP) (IMTEK, Germany). Both substances were cross-linked to the surface using UV at 365 nm. Isopropanol was used for rinsing, before the chips were

dried under nitrogen. The coating of the microchips with PEtOx-BP and PDMAA-BP was performed at IMTEK (Freiburg, Germany).

Polyethylene glycol (PEG, P2263) (0.5%) in methanol (Sigma Aldrich Norway AS, Norway) was also used for coating of the microchips. The PEG consisted of 2 molecules of polyethylene glycol with a molecular weight in the range of 7 000 – 9 000 g/mol, each joined internally through a homobifunctional aromatic hydrophobic spacer.

The microchips were cleaned in deionized water in an ultrasonic bath for 20 minutes prior to O_2 plasma activation and coating. For the injection moulded microchips, 18 µl of 0.5% PEG in methanol was added to the inlet hole, where after the liquid wetted the complete network of channels and chambers. For the other chips, the PEG solution was loaded directly into each reaction chamber. However, the liquid volume was reduced from 2 µl to 500 nl for these chips. When the methanol of the 0.5% PEG solution evaporated from the cavities of the microchips at room temperature, the surface of the walls was covered with PEG.

The milled and hot embossed microchips were further spotted with 0.5 % Teflon 1600 AF (DuPont, Canada) to make hydrophobic "valves" in order to control the sample. A Nanoject II (Drummond Scientific Company, Broomall, PA) was employed to dispense two droplets with the volume of 27.6 nl. The first droplet was dispensed and dried before the second droplet was added.

Surface roughness

White light interferometry was used to measure the surface roughness of the fabricated microchips (WYKO NT-2000, Veeco Instruments Inc., Woodbury, NY).

Instrumentation and data acquisition

A custom-built instrument with integrated optical detection, heat regulation and automatic chip positioning was used to detect the fluorescent signal of the NASBA reactions on the microchips. The optical detection unit recorded for 1 second on each scanning cycle, using a digital lock-in system operating at 1 kHz. Data were sampled at a frequency of 100 kHz. A more detailed description of the instrument and data acquisition is given elsewhere.[15]

A conventional microtitre plate reader, Lambda FL600 (Bio-Tek Instruments, Winooski, VT) was used to test the standard microtitre plate amplification reactions. The total detection volume of the reaction mixtures was 20 µl.

The fluorescent molecular beacon probes were excited at 494 nm and the photo multiplier tube (PMT) detected emission at 525 nm with both instruments. For the NASBA reactions, the ratio of the final fluorescence level to the initial fluorescence level was determined. All reactions with a ratio larger than 1.7 were considered positive. Time-to-positivity (TTP)[16, 17] was chosen as the point of onset for exponential increase of signal.

Background fluorescence

Autofluorescence was measured on the thermopad (Therm-A-GAP G974, Chomerics, UK) which was mounted on top of the Peltier elements to secure good heat transfer to the microchips. For comparative studies, a 1 mm thick graphite sheet, a silicon wafer with a <100> crystal orientation, a gold sputtered silicon wafer and injection moulded COC microchips were also measured.

A selection of sealing tapes were evaluated with regard to autofluorescence; 3M™ Polyolefin Microplate sealing tape (HJ Bioanalytic, Germany), ABI Prism™ Optical Adhesive Cover (Applied Biosystems, Oslo, Norway), iCycler iQ™ Optical Quality Sealing Tape (Bio-Rad Laboratories, Oslo, Norway) and Absolute™ QPCR seal (ABgene, Epsom, UK). The tapes were adhered on bits of silicon wafers and fluorescence recorded at 10 different positions for 2.5 hours. An average of all values in all positions was calculated and rounded off to the closest 50 mV.

The pressure sensitive tapes, ABI Prism™ Optical Adhesive Cover and 3M™ Polyolefin Microplate sealing tape were utilized to seal the injection moulded microchips for the amplification reactions. For all other chips, only the 3M™ Polyolefin Microplate sealing tape was used.

Biological material

Two model systems were used in these experiments; artificial human papillomavirus (HPV) type 16 oligonucleotide sequences, and the CaSki cell line, which contains the HPV type 16. The artificial HPV 16 sequences were acquired from the PreTect HPV-Proofer kit (NorChip AS, Klokkarstua, Norway).

The CaSki cells were grown in a Rosewell Park Memorial Institute (RPMI) 1640 media supplemented with 2 mM L-glutamine, 1mM sodium pyruvate, 10 mM 4-(2-hydroxyethyl)-1-piperazineethanesulfonic acid (HEPES), 10% fetal calf serum (FCS) and antibiotics. The cells were incubated at 37°C, trypsinated, counted in a

Bürker chamber and lysed in lysis buffer (bioMérieux, Boxtel, the Netherlands) before the nucleic acids were manually isolated and extracted using NucliSens® miniMAG™ (bioMérieux).

Isolation and extraction of nucleic acids using a selection of elution liquids

The manual NucliSens® miniMAG™ extraction kit (bioMérieux) contained lysis buffer, magnetic silica beads, wash buffers, and miniMAG™ elution buffer, and was used in the sample preparation. In addition to the kit elution buffer, 7 other elution liquids were tested for isolation and extraction of the nucleic acids from the CaSki cells, see Table 1. The various concentrations of DMSO and sorbitol were obtained by diluting with miniMAG™ elution buffer.

The RNA concentration in the extract was measured in two parallels on a MBA 2000 spectrophotometer from Perkin Elmer (Wellesley, MA). When testing the NASBA for biocompatibility with these extracts, some adjustments had to be made to the mastermix and enzymes solutions. Table 1 shows the elution liquids and the NASBA mixtures used for biocompatibility testing of the nucleic acid extracts.

Table 1 NASBA mixtures for biocompatibility tests of the nucleic acid extracts.

Mixture	Elution liquids	Composition of the NASBA mixtures
Mix 1	miniMAG™ elution buffer, water, 60% DMSO, 15% DMSO, 1.5 M sorbitol, 375 mM sorbitol, 60% DMSO + 1.5 mM sorbitol, and 15% DMSO + 375 mM DMSO	Regular mix - DMSO in the reagent sphere diluent, sorbitol in the enzyme diluent
Mix 2	60 % DMSO	The reagent sphere was dissolved in 120 mM Tris-HCl buffer, sorbitol in the enzyme diluent
Mix 3	60 % DMSO + 1.5 M sorbitol	The reagent sphere was dissolved in 120 mM Tris-HCl buffer, the enzyme sphere was dissolved in water
Mix 4	1.5 M sorbitol	DMSO in the reagent sphere diluent, the enzyme sphere was dissolved in water
Mix 5	15 % DMSO	The reagent sphere was dissolved in reagent sphere diluent which had been diluted 1:1.33 with 120 mM Tris-HCl buffer, sorbitol in the enzyme diluent
Mix 6	375 mM sorbitol	DMSO in the reagent sphere diluent, the enzyme sphere was dissolved in enzyme diluent which had been diluted 1:1.33 with water
Mix 7	15 % DMSO + 375 mM sorbitol	The reagent sphere was dissolved in reagent sphere diluent which had been diluted 1:1.33 with 120 mM Tris-HCl buffer, the enzyme sphere was dissolved in enzyme diluent which had been diluted 1:1.33 with water

Rehydration and diffusion measurements

A Leica DM RXA epifluorescent microscope equipped with Leica TCS 4D confocal unit (Leica Microsystems, Germany) was used to follow the rehydration and diffusion of the fluorescent molecules added to the mastermix and the enzyme solution prior to spotting and drying of these reagents on the COC chips. The imaging of the reaction chambers was performed via an HC PL Fluotar objective with 5-fold magnification and NA = 0.15. The low magnification was necessary in order to image the entire reaction chamber within the field of view of the microscope. As a consequence, the depth-wise resolution of the measurements was limited, with optical slice thickness ~ 100 μm. An Omnichrome Series 43 ArKr laser was used for sample illumination. The fluorescence filters were set for FITC detection, with excitation peak at 488 nm and emission at > 510 nm. Sequences of images at a plane 150 μm above the bottom wall of the chambers were acquired in 6 and 12 seconds time intervals.

For the present experiments, a mastermix containing molecular beacons without quenchers (fluorophores only) were spotted (10 droplets of 27.6 nl) with a Nanoject II (Drummond Scientific Company, Broomall, PA) onto the milled COC chips and dried at room temperature for 1 day. In this manner, the mastermix was fluorescent without the need for actual amplification, and its rehydration from solid state and diffusion into the sample could be monitored. The sample (1.5 μl) was a solution of 15% DMSO and 375 mM sorbitol.

In contrast to the mastermix, the enzymes did not contain any fluorescent components. In order to permit fluorescence detection of the rehydration and diffusion process of the dried enzymes, an antibody FITC-labelled mouse IgG isotype control (Southern Biotech, Birmingham, AL) was added to the enzyme solution prior to spotting and drying in the reaction chambers. A lyophilized enzyme sphere was dissolved in 2 % PEG and 100 μg/ml IgG-FITC and spotted in 5 droplets of 27.6 nl with the Nanoject II. The microchip was dried at room temperature until the following day. The dried enzymes were dissolved in 1.5 μl master mix (where the molecular beacon was replaced by one of the primers), sample, and water correcting for the volume of the dried enzymes.

Adsorption measurements

Native COC surfaces and PEG coated surfaces were investigated with regard to protein adsorption. The adsorption measurements were performed in milled microchips with

500 nl reaction chambers. The microchips were prepared as described above, by ultra-sonication and O_2 plasma activation. PEG was applied to coat half of the reaction chambers.

A solution of 0.5 mg/ml FITC-labelled mouse IgG isotype control (Southern Biotech, Birmingham, AL) was applied (5 µl) at the inlet hole of the microchips. The inlet and outlet holes were sealed using the 3M™ sealing tape. Subsequently, the microchips were placed on a heating block at 41˚C for 2.5 hours. Water (500 µl) was flushed through the chips to remove unbound IgG-FITC molecules; before non-specifically bound mouse IgG-FITC was measured using a Leica DM RXA epifluorescent microscope equipped with a Leica TCS 4D confocal unit. The reaction chambers were filled with water to ease visualization during measurement.

NASBA procedures

All reagents required to perform the HPV detection employing NASBA were supplied by the PreTect HPV-Proofer kit.[15] In addition to the standard kit reagents, protectants were added to stabilize the enzymes during the drying experiments; polyethylene glycol 8 000 (PEG), trehalose, polyvinylpyrrolidone 40 000 (PVP) and bovine serum albumin (BSA) from Sigma Aldrich. Additionally, sorbitol, dimethoxy sulfoxide (DMSO) and Tris-HCl buffer (Sigma Aldrich) were added separately in the drying experiments.

The PreTect HPV-Proofer kit consisted of lyophilized enzyme spheres (AMV-RT, RNase H and T7 RNA polymerase) and lyophilized reagent spheres containing most of the amplification reagents. Additionally, a specific enzyme diluent (with sorbitol) and reagent sphere diluent (with DMSO) was added to dissolve the lyophilized spheres. Primers, fluorescent molecular beacon probes (FAM/Dabcyl or FAM/BHQ), KCl, BSA and water were added to the reagent sphere solution resulting in the mastermix. The ratio of mastermix, enzymes and sample in a final standard NASBA reaction were 2:1:1.

Enzyme stability at high temperatures

In the first experiment, 6 lyophilized enzyme spheres were incubated at 65˚C for several time periods; 0, 15, 30, 60, 90 and 120 minutes. The lyophilized enzyme spheres were subsequently dissolved with the standard enzyme diluent, after which standard procedure was followed.

In a second experiment, the enzyme solutions were added to the mastermix and sample before the incubation step at 65˚C for 3 minutes. The temperature was then adjusted to 41˚C before measurements. The resulting fluorescence of the reaction mixtures was detected using the Lambda FL600 reader in both experiments.

Protectants and inhibition of the NASBA reaction

Dilution series of the four protectants, trehalose, PEG 8 000, PVP 40 000 and BSA were tested for biocompatibility with regard to the NASBA reaction, according to the scheme presented in Table 2. First, the dilution series was tested with 0.1 µM HPV 16 oligonucleotide as sample material. Subsequently, the CaSki cell line was tested for the optimal concentration of protectants obtained in the HPV 16 oligonuceotide experiments. The protectants were mixed with the sample material itself. Standard procedures were followed for mixing of the NASBA reaction.

Table 2 Protectants tested for biocompatibility with regard to the NASBA reaction.

Protectant	Final concentrations (0.1 µM HPV 16)	Final concentration (CaSki)
Trehalose	5, 10, 25, 50, 75, 100 [mM]	10 [mM]
PEG 8000	0.5, 0.75, 1, 2.5, 5, 7.5, 10 [%]	1 [%]
PVP 40 000	0.5, 0.75, 1, 2.5, 5, 7.5, 10 [%]	1 [%]
BSA	5, 10, 25, 50, 100, 150, 300, 500 [µg/ml]	50 [µg/ml]

A reduction of the amount of enzyme applied in the NASBA mixture was performed to evaluate the response of possible enzyme inactivation occurring in the microchips. In a standard reaction, 5 µl of enzyme solution (final concentrations: 6.4 U/reaction AMV-RT, 0.08 U/reaction RNase H, 32.0 U/reaction T7 RNA polymerase) was added. In this experiment, the volume of enzyme solution was varied between 0.5 – 5 µl. Water was added to maintain the correct concentration of the other reagents.

Subsequently, the robustness of the NASBA reaction was evaluated by altering the concentrations of the mastermix and the enzymes. The amount of reagent sphere diluent and enzyme diluent transferred to the lyophilized spheres was adjusted so that the final concentration in the reaction mixture corresponded to 0.5, 1.5, 2 and 4 times the standard concentration. In all experiments, the Lambda FL600 reader was employed.

Drying of the NASBA reagents with protectants - macroscale

Two drying schemes were investigated: (1) The mastermix and the enzyme solutions were mixed together before drying. (2) The mastermix and the enzyme solutions were dried separately.

The standard diluents of the PreTect HPV-Proofer kit contain DMSO and sorbitol, which were difficult to dry. Therefore, the DMSO (mastermix diluent) and the sorbitol (enzyme diluent) were replaced by 120 mM Tris-HCl (pH 8) and water containing dilution series of protectants, respectively. The DMSO and sorbitol were mixed with the sample and not dried, except in one case.

The reagents were dried on the backside of the injection moulded COC chips which had been coated with 0.5% PEG in methanol, (Figure 2a). After two days of drying in the dark at room temperature, the reagents were dissolved in the same amount of water as the liquid volume from which they were dried, and subsequently transferred to a microtitre plate. Samples (HPV 16 oligonucleotides and CaSki cell line) containing DMSO and sorbitol were added, and the standard NASBA procedure was followed.

Premixed NASBA reagents for evaluation of coatings and optimal detection volume on chip

In these experiments, 24 µl mastermix and 12 µl sample material (0.1 µM HPV 16 and CaSki) were mixed manually and heated on a conventional heating block at 65°C for 3 minutes. The mixture was subsequently incubated at 41°C for 3 minutes, after which the enzyme solution (12 µl) was added. The final mixture was then immediately applied to the injection moulded COC or silicon microchips, which distributed the liquid into the parallel reaction channels. The reaction channels were filled completely, due to capillary forces. The reactions on the microchips were recorded in the custom-made instrument.

Detection of dried NASBA reagents on chip

For the drying and rehydration experiments, two microchip designs were fabricated, see Figure 2b. The first chip contained only 1 reaction chamber, whilst the second chip had two chambers in series. Mastermix and enzymes were spotted in separate reaction chambers at room temperature using the Nanoject II dispenser. A volume corresponding to the required amount of reagents for 1 µl sample sizes was spotted sequentially into the chambers. For the mastermix solution, 10 droplets of 55.2 nl were

dispensed, whilst 5 droplets of 55.2 nl were spotted with enzymes. The spotted liquid was allowed to dry for approximately 30 seconds between each deposited droplet. In this manner, a well-defined cake of reagents was deposited on the bottom surface of the reaction chambers. After spotting, the chips with dried reagents were stored at room temperature for at least two days.

For the single chamber chip with spotted and dried enzymes, 24 µl mastermix, 12 µl sample material (0.1 µM HPV 16) and 12 µl 60% DMSO + 375 mM sorbitol solution were mixed manually and heated on a conventional heating block at 65˚C for 3 minutes. The mixture was subsequently incubated at 41˚C for 3 minutes. The microchip with dried enzymes was placed on a heating block for 30 minutes at 41˚C, before 1 µl mixture was applied to the chip through the inlet hole. The inlet holes and outlet holes were sealed using 3M™ sealing tape.

The procedure for the single chamber chips with deposited mastermix reagents was similar to that used with the deposited enzyme on chip. The 24 µl mastermix was exchanged by 12 µl enzyme solution and 12 µl water, while the amount of sample material and DMSO + sorbitol was maintained. Samples of 1 µl were added to the chips. The chips were then sealed prior to measurement.

The microchip with chambers in series contained deposited mastermix in the first chamber, and enzymes in the following chamber. The chip was mounted within an aluminium frame from IMM (Germany), equipped with connectors to a syringe pump (Harvard Apparatus PHD 2000). When 1 µl sample (15% DMSO + 375 mM sorbitol and 0.1 µM HPV 16 oligonucleotide) was applied, the sample filled up the first chamber containing the mastermix, which consequently was rehydrated. After 3 minutes at 65˚C, the temperature was kept at 41˚C for 3 minutes. The syringe pump was employed (10 µl/minute), lowering the pressure in the channel towards the chamber containing the enzymes. Reaching a pressure approximately 1000 Pa below atmospheric pressure, the hydrophobic valve was no longer capable of retaining the liquid, and the sample was moved to the second chamber, containing the enzymes. The chip was disassembled from the aluminium frame, sealed with 3M™ at the inlet/outlet holes and placed in the custom-made instrument for detection for 2.5 hours.

Results and discussion

In this work, aspects pertaining to the development of an isothermal amplification microchip employing NASBA have been investigated. A selection of materials, chip designs, fabrication methods and coatings were tested for optimal combined performance. Similarly, the performance after drying and rehydration of the NASBA reagents was examined, using both conventional microtitre plates (macroscale) and microchips.

Background fluorescence

Many materials fluoresce naturally, which in the case of fluorescence detection methods can interfere with the emission spectrum of the fluorophores used for detection of the sample. In these experiments, we measured the autofluorescence of a selection of backgrounds and sealing tapes in order to select the components having the lowest background fluorescence, in order to minimize the noise in the custom-made instrument. However, fluorescence measurements will unavoidably have small variations on a day to day, basis due to the temperature dependencies for both the LED and the PMT.

Table 3 shows the level of fluorescence of the backgrounds, sealing tapes, silicon wafers and injection moulded COC chips. COC substrates are considered to exhibit minimal autofluorescence compared to other polymers.[18] The fluorescence level of the thermopad was originally ~200 mV. After long-term usage, the level of fluorescence increased to ~500 mV. The smooth surface of the thermopad showed signs of being worn-out, which most likely caused the excitation light to be scattered into the optical detection pathway, and thus generating more noise. Table 3 shows the ~150 – 350 mV PMT response for graphite, silicon and gold surfaces. These are all materials which are non-fluorescent and should only produce the background signal. The graphite sheet was very soft and could easily be scratched, contributing to scattering. Gold surfaces reflect better than a native silicon surface, which can explain the differences between these two materials.

Unlike the materials discussed above, polymer substrates usually possess fluorescent properties. For these materials, bleaching is a factor that has to be accounted for.[18, 19] This phenomenon was observed for several of the sealing tapes and the COC chips (Figure 2a) tested in these experiments. Polymer materials that were exposed to light for longer periods of time had a lower fluorescence level, than if they

14

were stored in the dark as was the case for the iCycler Optical tape. The rest of the sealing tapes were found to have more or less constant levels of fluorescence over time.

Table 3 Background fluorescence of chip backgrounds, sealing tapes, silicon and COC chips. The PMT response was measured for 2.5 hours in the custom-made instrument. The table shows the average value of the measurements rounded off to the closest 50 mV.

Material	PMT response [mV]
Thermopad	~200 – 500
Graphite	~300
Silicon wafer	~150
Gold sputtered on a silicon wafer	~350
API Prism optical cover / silicon	~200 – 350
iCycler - BioRad Optical tape / silicon	~850 – 1450
3M™ Polyolefin Microplate sealing tape / silicon	~250
ABgene AB-1170 / silicon	~300
COC chip / API Prism / graphite	~650
COC chip / solvent bonded COC membrane / graphite	~650
COC chip / solvent bonded COC membrane / thermopad	~550 – 750
COC chip / solvent bonded COC membrane / gold	~350 – 650

First, the ABI Prism tape was tested with premixed NASBA reagents for amplification on the COC microchip due to low fluorescence level. During the measurements, however, small bubbles were created in the whole reaction mixture and no amplification was observed. Additional experiments with pure water were also found to create bubbles. Most likely, the adhesive on the tape reacted with the liquids within the channel structures. However, good amplification performance was obtained with the 3M sealing tape, and was thus used for all following experiments. The 3M sealing tape exhibited the same autofluorescence level as the ABI Prism tape on the COC chips.

COC microchips with gold layers on the rear side of the chip were measured to have a wide range in signal level. Thicker layers of gold gave higher PMT responses. This was probably caused by increased reflection of light from these chips, resulting in noise. In evaluating the combinations of COC chips and background, no significant differences were found. We therefore elected to continue with the 3M™ sealing tape and the thermopad background.

Surface roughness

In order to obtain chips of high quality, several microchip designs were fabricated, using different methods. WYKO was used to measure the surface properties of the fabricated injection moulded, milled, laser ablated and hot embossed COC chips. Table 4 shows that the surface roughness increased in the following order: injection moulding < hot embossing < milling < laser ablation.

Table 4 Surface properties of the fabricated test chips for the drying and rehydration of the NASBA reagents. The values of the surface roughness depend on the size, place and resolution of the measured area. These values are therefore only an indication of typical surface roughness obtained by the different production methods. (Ra – average surface roughness, Rq – root-mean square surface roughness, Rz – average of the 10 largest peaks and valleys, Rt – the largest difference between a peak and a valley) The background signal was rounded off to the closest 50 mV.

Fabrication technique	Surface roughness without PEG [µm]	Depth of reaction chambers [µm]	PMT response [mV]
Empty pad			~50
Injection moulded chips COC	Ra:0.08 Rq. 0.09 Rz: 0.5 Rt: 0.6	~100	~150*
Milling COC	Ra: 0.8 Rq: 1.0 Rz: 9.2 Rt: 11.9	~200	~250
Laser ablation I Traversing laser beam COC	Ra: 3.5 Rq: 4.3 Rz: 30.1 Rt: 32.2	~280	~700
Laser ablation II Stationary laser beam COC	Ra: 16.6 Rq. 20.3 Rz: 88.9 Rt: 89.2	~220	~650
Laser ablation II Stationary laser beam COP	Ra: 6.2 Rq. 7.1 Rz: 27.9 Rt: 33.6	~180	~1000
Hot embossing, polished die COC	Ra: 0.03 Rq: 0.08 Rz: 1.4 Rt: 1.7	~230	~200

* The injection moulded chip thickness in the detection area was 1.4 mm, compared to 1.8 mm for the rest of the chips. The background was measured in the first actuation chambers in the 10 channels in the middle of the chip.

16

Injection moulding is time consuming and expensive, and therefore was not an option for fabrication of the test chips. The depth of the reaction chambers varies with fabrication technology (Table 4), indicating that this parameter should be optimized for next generation chips. The depth difference will influence the PMT response, due to thickness of the bulk polymer exposed to the detection. This part of the background signal was investigated employing the custom-made instrument. The largest contribution to background signal was found in the laser ablated chips, which also had the highest surface roughness. Hot embossed chips showed the lowest background level. Surprisingly, the level of background signal was not much lower than for the milled microchips. As seen in Figure 3a and Figure 3b, the reaction chamber surface of the milled chips was not transparent and appeared more like a diffuser. The injection moulded chips displayed the lowest background fluorescence of all chips tested. However, this was not only related to minimal surface roughness, but also due to the fact that the chips were 0.4 mm thinner than the rest of the chips. A decision was made to continue with hot embossed chips.

Efficiency of the elution liquids for isolation and extraction of nucleic acids

Sorbitol and DMSO are critical as they increase the specificity, sensitivity and yield of the NASBA reaction.[20, 21, 22] Both substances are difficult to dry and store on chip. Sorbitol makes glassy surfaces, hindering instant rehydration of reagents, while DMSO is an organic solvent. Two alternative methods for introducing these components to the final reaction mixture were tested, eliminating the need for on-chip storage. First, the DMSO and sorbitol solutions were used to elute nucleic acids from the silica particles in the sample preparation step. Secondly, the eluted nucleic acid sample could be mixed with the DMSO and sorbitol solutions after the sample preparation. Within a microfluidic system, the latter solution would require a mixing device prior to the distribution of the sample into the reaction chambers. Both approaches were tested using the manual miniMAG™ extraction kit (bioMérieux).

CaSki cells were lysed and isolated according to the manufacturer's protocol before the different combinations of DMSO and sorbitol were used as elution liquids. In the first run; miniMAG™ kit elution buffer, 60% DMSO, 1.5 M sorbitol and 60% DMSO + 1.5 M sorbitol were tested. In the second experiment; miniMAG™ kit elution buffer, pure water, 15% DMSO, 375 mM sorbitol and 15% DMSO + 375 mM sorbitol were tested. The concentration of RNA in the extracts was measured and calculated by the spectrophotometer. As can be seen from Table 5, the kit elution buffer with 15%

DMSO gave the highest yield of RNA. One of the parallel tests using the kit elution buffer provided a similar yield of RNA. The variation in concentration between the two kit elution buffers from experiment 1 and 2 may be explained by two different CaSki samples were tested. In the first experiment, 1.5 M sorbitol showed high levels of RNA, while the elution liquid containing DMSO showed low levels of RNA. However, in the second experiment, 15% DMSO gave the best result. Obviously, the elution with DMSO was dependent on concentration of DMSO. Pure water showed surprisingly low levels of RNA, as water in many cases is used as elution liquid.

Table 5 Elution of nucleic acids from CaSki cells with miniMAG™ elution buffer, water, DMSO, sorbitol and mixtures of DMSO and sorbitol. [CaSki (1:100): "++" TTP < 90 minutes, Ratio > 6, "+" TTP < 150 minutes, Ratio > 1.4 and < 6, "-" no amplification]

Elution liquid	Spectrophotometer [μg/ml]	NASBA results
miniMAG™ elution buffer parallel 1, Mix 1	60.0 ± 3.4	++
miniMAG™ elution buffer parallel 2, Mix 1	45.6 ± 4.5	++
Water (RNase and DNase free), Mix 1	28.8 ± 2.3	++
60% DMSO, Mix 1	26.4 ± 1.1	-
60% DMSO, Mix 2*		++
15% DMSO, Mix 1	60.8 ± 4.5	++
15% DMSO, Mix 5*		++
1.5 M sorbitol, Mix 1	43.2 ± 0.0	+°
1.5 M sorbitol, Mix 4*		-
375 mM sorbitol, Mix 1	27.2 ± 1.1	+
375 mM sorbitol, Mix 6*		-
60% DMSO + 1.5 M sorbitol, Mix 1	17.2 ± 0.6	-
60% DMSO + 1.5 M sorbitol, Mix 3*		-
15% DMSO + 375 mM sorbitol, Mix 1	31.6 ± 4.0	-
15% DMSO + 375 mM sorbitol, Mix 7*		-

* The reaction mixtures are adjusted to obtain correct final concentration

° TTP is later than regular NASBA reaction

The extracts were also tested in the NASBA reaction. In addition to the standard mastermix and enzyme solutions, new solutions were made in order to obtain 15% DMSO and 375 mM sorbitol in the final reaction mixture. Table 5 shows that the extract with 60% DMSO was not amplified in the standard reaction mixture (Mix 1, Table 1). This was probably due to the high concentration of DMSO in the reaction mixture. However, the same extract was amplified very well in Mix 2, which was

adjusted to obtain a 15% final concentration of DMSO. The extract eluted with 15% DMSO was amplified in both Mix 1 and Mix 5. The extract eluted with 1.5 M sorbitol was also amplified in Mix 1. However, the TTP was higher than for the standard reactions. No amplification was detected in Mix 4, although the final concentration of sorbitol was adjusted to 375 mM. Elution with 375 mM sorbitol gave poor results for both Mix 1 and for the corrected Mix 6. None of the extracts with both DMSO and sorbitol were amplified in any of the 4 combinations, Mix 1, Mix 3 and Mix 7. From these results, we concluded that one may use DMSO (both 15% and 60%) for elution of nucleic acids. However, the reaction mixture needed adjustment to a final concentration of 15% DMSO in order to achieve amplification. Sorbitol was not preferable for any elution purposes. Based on the results described above, it was decided to mix the DMSO and sorbitol solutions in the sample after sample preparation.

Diffusion measurements

Dried mastermix

A solution of 15% DMSO and 375 mM sorbitol was applied to the reaction chamber containing the dried mastermix. The rehydration process of the dried mastermix was monitored by acquiring confocal laser scanning microscopy (CLSM) images in 12 second time intervals, taken at a plane 150 μm above the bottom wall of the reaction chamber. The temporal evolution of the rehydration and the diffusion processes are shown in Figure 4.
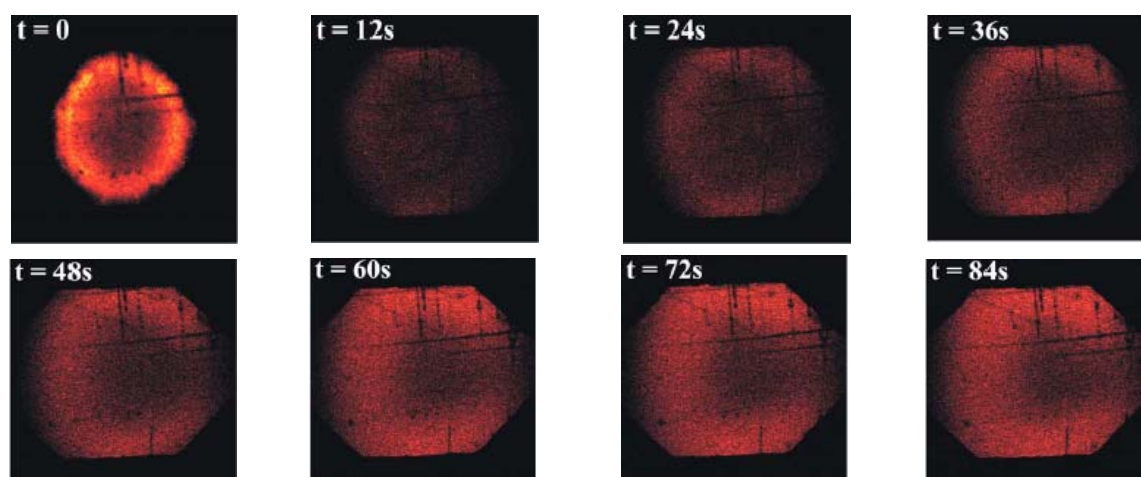
Figure 4 Rehydration of dried mastermix, temporal evolution. The time between frames was 12 seconds. The dissolving solution contains 15% DMSO and 375 mM sorbitol. The image at t = 0 was taken prior to any liquid entering the reaction chamber, i.e. at dry conditions, with the focal plane at the plane of the dried spot; hence the high image intensity. All images during rehydration were taken at a plane 150 μm above the bottom wall of the chamber.

As can be seen from Figure 4, the rehydration and diffusion of the fluorescent species was essentially completed after 60 seconds. After that time, no significant changes in the fluorescent signal from the solution (neither with regard to intensity nor homogeneity) were observed. In order to assess the results presented in Figure 4 in more detail, it is instructive to consider the diffusion length (Equation 1) for the molecular beacons at a time scale comparable to the one found in the experiments. The diffusion length, L, *i.e.* the distance a suspended particle travels through a liquid during a given time, t, can be expressed as:

$$L \approx \sqrt{2Dt} \qquad\qquad\qquad 1$$

where D is the Stokes – Einstein diffusion coefficient for a solid spherical particle suspended in an aqueous solution, given by:

$$D = \frac{kT}{3\mu\pi d_p} \qquad\qquad\qquad 2$$

Here, k is the Boltzmann constant, T is the absolute temperature, μ is the dynamic viscosity and d_P is the particle diameter. The exact dimension of the molecular beacons is not known. In order to estimate their size, we compare the mass of the molecular beacons to the mass of the enzymes, for which the size range is known. The mass of the molecular beacons contained in the mastermix is approximately 10 kDa. In comparison, the mass of the enzymes is between 17 kDa and 160 kDa.[23] A small protein, assuming a spherical shape, has a diameter of approximately 2 nm, while large proteins are in the range of 6 – 8 nm.[24] Considering the enzymes with a mass of 160 kDa to be large proteins, and assuming a spherical shape, this implies a diameter of approximately 7 nm. Assuming that the proteins and molecular beacons have similar mass density, the size of the molecular beacons can be estimated to be $d_{MB} \approx 2.8$ nm. In this case, the diffusion length during a time period of 60 seconds (estimated from Equation 1) yield a distance of 136 μm. Or, vice versa, the time required for the particles to reach the imaging plane of the measurements (*i.e.* a diffusion distance of 150 μm) could be approximated to 70 seconds.

Although the estimate given above is crude, it indicates that the diffusion time for the molecular beacons roughly corresponds to the experimentally observed time needed to obtain a homogeneous suspension of mastermix in the DMSO and sorbitol solution. This

implied that the dissolution process was diffusion-limited. Rehydration itself was rapid, occurring nearly instantaneously as compared to the time scale of diffusion.

Rehydration and sample mixing within approximately 1 minute is acceptable for the NASBA reaction and detection procedure on chip. Based on the experiments presented herein, it was concluded that no active mixing mechanisms were necessary for the rehydration and dissolution of the mastermix.

Dried enzymes

Fluorescently labelled IgG was mixed with the enzymes and dried in the reaction chambers. The antibody was chosen because of its molecular weight of 150 kDa. The molecular weights of the NASBA enzymes were 17.6 kDa, 107 kDa and 160 kDa for RNase H, T7 RNA polymerase and AMV-RT, respectively. As the enzymes with the largest size would have the lowest diffusion rate, we modeled the largest enzyme. A solution containing DMSO, sorbitol and mastermix was used for rehydration. Sequences of images at a plane 150 μm above the bottom wall of the chamber were acquired. The rehydration and diffusion processes of the dried enzymes are shown in Figure 5 and Figure 6. In Figure 5, the temporal evolution of the beginning of the rehydration process at 6 second time intervals is shown, while Figure 6 show time intervals of 1 minute.
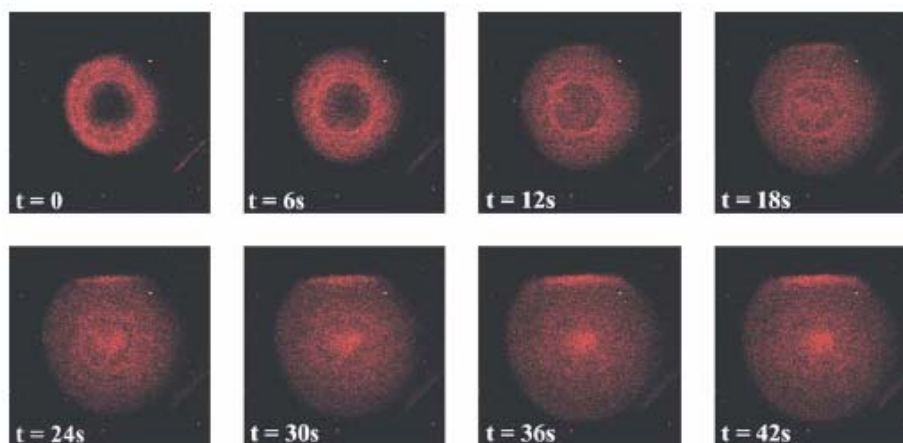
Figure 5 Rehydration of dried enzymes, temporal evolution. The time between frames was 6 seconds. The dissolving liquid was a solution containing DMSO, sorbitol and mastermix. The dried spot was inside a 500 nl chamber. All images were taken with the focal plane positioned 150 μm above the bottom wall of the reaction chamber.
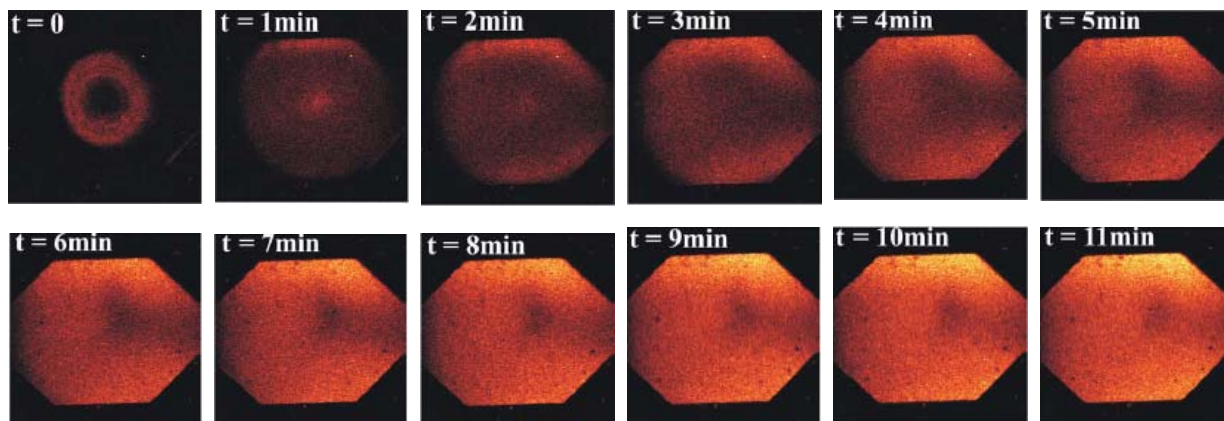
Figure 6 Rehydration of dried enzymes, temporal evolution. The time between frames was 1 minute. The dissolving liquid was a solution containing DMSO, sorbitol and mastermix. The dried spot was inside a 500 nl chamber. All images were taken with the focal plane positioned 150 µm above the bottom wall of the reaction chamber.

It was evident from the images in Figure 5 and Figure 6 that the rehydration and diffusion processes for the dried enzymes was significantly slower than that for the dried mastermix. By inspection of Figure 6, rehydration and diffusion of the fluorescent species was essentially completed after approximately 10 minutes, as no significant changes in the fluorescent signal from the solution (neither with regard to intensity nor homogeneity) were observed. Because it was not possible in these measurements to isolate the rehydration process from the diffusive mixing, an estimate of the diffusion length of the fluorescent species was made. In the present case, the fluorescent tracer was the antibody IgG with a mass of 150 kDa, *i.e.* a large protein. As indicated previously, it was assumed that the IgG was spherical and had a size of approximately 7 nm. By applying Equation 1 and Equation 2, the time required to reach the imaging plane (*i.e.* diffusion length of 150 µm) was estimated to be approximately 180 seconds. The comparably longer time required to achieve a homogeneous suspension observed in the present experiments, may be an indication that the rehydration process of the enzymes was slower than their diffusion into the bulk liquid. During drying and storage, it is common that hard films may appear at the surface of the dried reagents, which may hinder instantaneous rehydration.

Dissolution of the enzymes is thought to be the final step on a completed amplification chip, prior to detection of the fluorescent signal. Microscopic inspection of the reaction chamber after rehydration revealed that no residue of the dried material was left on the chamber wall. Therefore, the optical detection of the amplification process may be performed in the same chamber as the dissolution of the enzymes. Since this process is

time-consuming, requiring approximately 90 minutes before unambiguous decision about presence/absence of the targeted species can be reached, the ~10 minutes required for enzyme dissolution may be acceptable. Furthermore, the amplification may possibly commence immediately upon contact between the sample and the enzymes, before the enzymes are completely dissolved. If this is the case, the loss of time due to slow dissolution diminishes.

Rapid mixing can be achieved by moving the sample droplet. It is also likely that sample movement or oscillation in the reaction chamber may promote faster rehydration of the dried species. This might enhance the dissolution of the dried reagents, and especially the enzymes. On the other hand, taking into account the low mechanical strength of the enzymes, mechanical agitation to promote mixing may be undesirable with respect to the biochemical functionality.

Adsorption measurements

In general, protein adsorption is a major obstacle in many fields of technology within medicine, biotechnology and food processing. Protein adsorption is triggered by chemical and physical phenomena related to the surface properties of materials and the surrounding medium in contact with the proteins. The amount of protein that a given surface will adsorb depends on the solution which it is in contact with, especially the protein content of that solution, the amount of other proteins present, the prior history of the surface with respect to protein contact, as well as other conditions, such as flow.[25] In microsystem technology, where the surface area-to-volume ratios are significantly larger than in macroscale systems, special attention towards protein adsorption is required.[26, 27, 28] Other components of the reaction mixture may be adsorbed at surfaces as well. However, in the present experiments only a model system for proteins was considered.

The IgG-FITC molecules were used as a model system for protein adsorption. Figure 7 shows that the native COC surface adsorbs large quantities of fluorescent IgG in comparison to the PEG coated surface. While the fluorescently labelled IgG molecules were uniformly adsorbed over the whole surface of the reaction chamber of the native COC, the PEG coated reaction chamber showed only smaller areas with high intensity of fluorescence, attributable to adsorbed IgG-FITC. The high intensity seen at the lower sidewall of the PEG coated chamber is probably due to insufficient washing of the reaction

chamber along the edge. Aside from this phenomenon, the PEG coated surface showed good protein resistance.
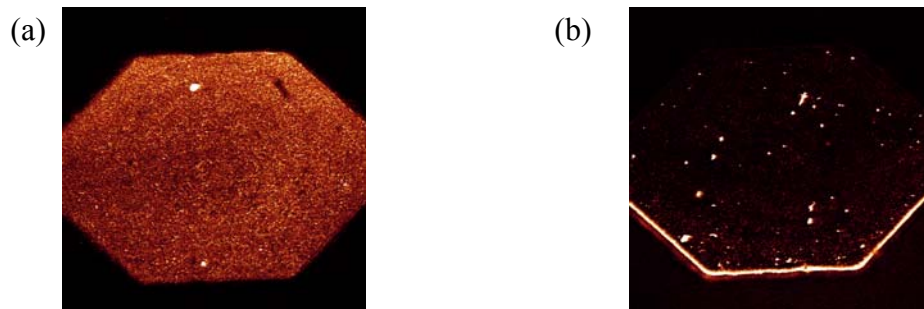
Figure 7 Adsorption of fluorescently labelled mouse IgG on native COC and PEG coated COC surfaces. The pictures were taken after incubation at 41°C for 2.5 hours followed by a washing step with water. It was assumed that the adsorbed proteins were not removed during the washing step, as adsorbed proteins do not desorb, or desorb very slowly (hours).[26] (a) Native COC surface which were only plasma activated. (b) PEG coated COC surface.

Coating of COC chips

The adsorption measurement revealed the importance of the surface properties related to protein adsorption. As the NASBA reaction is dependent on three enzymes working simultaneously during the amplification, an optimal surface is important. The three types of coating (PEtOx-BP, PDMAA-BP and PEG) were tested using the injection moulded COC chip for a biocompatibility comparison. Previous results (data not shown) have revealed that ideal model systems, like oligonucleotides, are more easily amplified than cell line samples and clinical samples. Therefore, all coatings were tested on both oligonucleotides and cell lines (CaSki). The detection volume in all cases was 80 nl.

The data presented in Table 6 show that the HPV 16 oligonucleotides were easily amplified on chip with all coatings tested. Amplification of the CaSki cells, on the other hand, was not as successful. PEG was the only coating which resulted in 10 out of 10 positive amplification reactions. Only 6 channels got positive amplification reactions for the chips coated with PEtOx-BP. Table 6 shows that with the PDMAA-BP coating, only 2 of 10 reaction channels resulted in positive amplification reactions.

PEG showed the best biocompatibility with regard to the NASBA reaction. PEG is commonly considered the most effective polymer for protein resistant surfaces, because of its unique solution properties and its molecular conformation in aqueous solution.[29] Previous experiments using PEtOx-BP and PDMAA-BP coatings have been

shown to have very low protein adsorption properties, even lower than PEG (IMTEK, data not shown). This was the reason why these compounds were tested. However, the ability of a surface coating to reject proteins depends on the nature of the proteins.

Table 6 Testing biocompatibility of the three coatings; PDMAA-BP, PEtOX-BP and PEG.

Coating	0.1 µM HPV 16 oligonucleotides	CaSki 1:1
PDMAA-BP	10 / 10	2 / 10
PEtOX-BP	10 / 10	6 / 10
PEG	10 / 10	10 / 10

In the present case, the PEG coating was physically adsorbed to the polymer chip surface due to its hydrophobic anchor. The hydrophobic-hydrophobic interaction prevented the PEG to be dissociated from the surfaces when filled with sample. Simultaneously, the PEG chains were oriented into the sample solution with the ability to reject proteins. It would be preferable to use covalently linked coatings, such as the PEtOx-BP and the PDMAA-BP, as they would provide a more stable surface chemistry.

Optimizing the detection volume

Silicon chips with detection volumes of 100 nl, 200 nl, 300 nl, 400 nl, 500 nl and 600 nl were used to evaluate different detection volumes.

Figure *8* shows a typical result obtained by performing a NASBA reaction in these chips.

For the 100 nl detection volumes, there were no positive amplification reactions. The 200 nl detection volumes had a signal increase but the reaction kinetics were different from that observed in the larger detection volumes (300 nl to 600 nl). The injection moulded COC chip in Figure 2a had a detection volume of 80 nl and amplified the same 0.1 µM HPV 16 oligonucleotide very well. The COC chips were coated with PEG, whilst the silicon chips had SiO_2 surfaces. Shoffner *et al.*[30] reported that SiO_2 surfaces did not inhibit the amplification of PCR reactions. However, the NASBA reaction uses other enzymes than the PCR reactions and they might be more susceptible to adsorption to a SiO_2 surface. Also, ions such as Mg^{2+} (which is an important co-factor for enzyme activity) can get trapped on these kinds of surfaces.[28] Hence, an imbalance of the enzymes and ions could result in the inhibition of the reaction. Another explanation of the

negative result for the 100 nl detection volume, could be that the optical view of the instrument was adjusted to be able to detect the whole 600 nl chamber. As a result, the signal from the 100 nl detection volume, is most likely lost in the background signal and the straight line is not due to unsuccessful amplification. The signal of the 200 nl detection are also influenced by the background signal.

The results presented in
Figure *8* show that it would be advantageous to increase the detection volume to 500 nl. The increase in signal from 500 nl to 600 nl is not as significant.
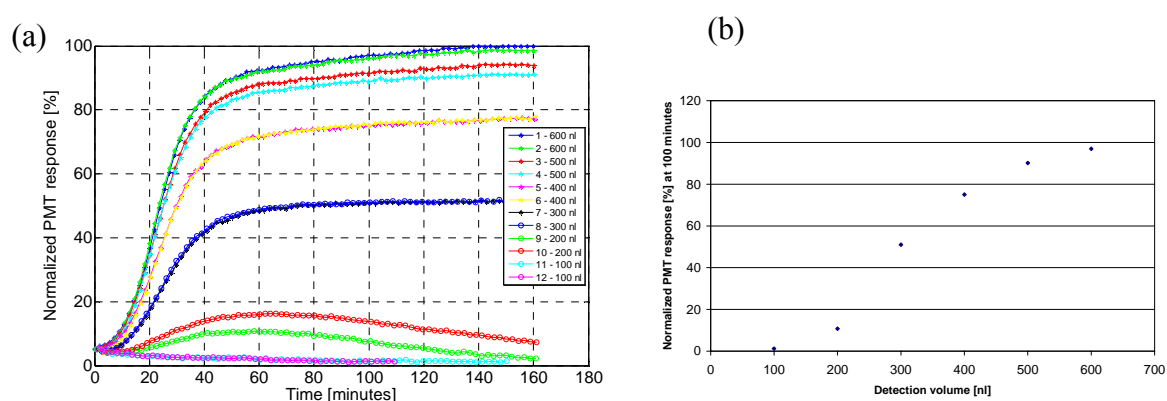
Figure 8 (a) Amplification curves for a silicon chip with 100 nl, 200 nl 300 nl, 400 nl, 500 nl and 600 nl detection volumes. The reaction mixture was premixed with 0.1 µM HPV 16 oligonucleotide as sample. (b) Normalized PMT response [%] versus detection volume at 100 minutes.

**Preliminary microfluidic tests and generation of bubbles**

In order to verify that the new fabricated chips performed as expected, and to evaluate the efficiency of the dried reagents on chip, premixed NASBA reactions were first performed in the silicon chips with single chambers (Figure 1b), as well as milled, laser ablated and hot embossed chips. The volume of the reaction chambers tested was 500 nl.

The DRIE etched silicon chips contained only reaction chambers and no supply channels. Sealing of these chambers using the 3M™ tape without air bubbles proved difficult. Only in a few cases, when a volume larger than the chamber itself was applied, was no air bubbles trapped. However, during measurement it became evident that the sealing of these chips was not tight, as gas bubbles were generated within the chambers when heated to 41˚C for a prolonged period of time. When bubbles expel reagents from the reaction chambers, they will adversely affect the temperature uniformity and the signal of the measurement. For optical detection in microfluidic

systems, the light is often unintentionally reflected at the surface of the entrapped bubbles, and thereby influencing the signals monitored.[31] No positive amplification reactions were obtained with the DRIE etched silicon chips.

Additionally, several problems were encountered with regards to fluidic handling of the very first milled chips due to the design and fabrication method. The reaction chambers were quadratic and had connection to two thin supply channels. The first supply channel was coupled to an inlet hole designed for the sample to enter the chip, while the second ensured connection with a syringe pump for fluidic handling. The sample only filled the channel by capillary forces, before it stopped due to the 90° angle of the supply channel on the reaction chamber wall. This structure created a burst valve and a syringe pump was needed to pull the liquid into the reaction chambers. In what way, the meniscus entered the chamber in a way that clearly affected how the chambers were filled with sample. In most cases, the meniscus was pinned within the chambers, leaving large air bubbles in the corners, Figure 9a. This hysteresis effect is likely to be related to roughness or impurities on the surface. As the milled chips have a high surface roughness (Table 4), this is the likely explanation for the entrapped air bubbles. Additionally, the first milled chips contained debris that was difficult to remove, and which could also have an impact on the incomplete filling. Due to the surface roughness, liquid was also lost during transportation between the reaction chambers. It was not possible to oscillate the sample within the chamber to remove the air bubbles, as the liquid only wetted the areas already being wet. The main reason for gas bubbles in microchips is that air is trapped while filling of the device with liquid for the first time.[31] The most direct approach to avoid gas trapping is to select a geometry that allows a perfect filling with wetting liquids by capillary action alone. Generation of bubbles may, however, evolve due to degassing of the liquid, out-gassing of the walls or leakages within the microchip.

A new design was made for the COC microchips, improving the transition between the supply channels and the reaction chambers. In earlier work with silicon microchips,[32] smoother and rounded corners were used in order to achieve complete capillary filling of the reaction chambers. This design was adapted, and new COC microchips manufactured by milling, laser ablation and hot embossing were produced. Table 7 shows the results of the amplification of premixed NASBA reagents in these microchips.
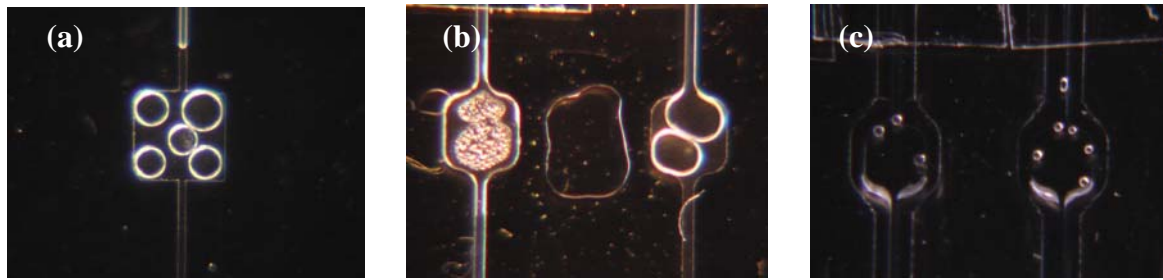
Figure 9 Generation of bubbles in COC microchips. All pictures were taken after 2.5 hours detection. (a) Milled COC chips with trapped air bubbles. (b) The sample was leaking in between the sealing tape and the milled COC chip. (c) Bubble generation in a hot embossed microchip.

Table 7 Amplification of premixed NASBA reagents in COC chips fabricated using milling, laser ablation and hot embossing. The first 4 columns are single chamber chips tested with regards to NASBA amplification, while the last column shows amplification in a COC two chamber chip where the sample plug was moved from the first chamber to the second chamber for detection.

Fabrication method	Milling	Laser ablation	Hot embossing	Serial - Hot embossing
Number of chips	2	4	3	1
Positive results	5	12	16	2
Negative results	3*	9*	2*	0

* Negative results - due to bubble generation within the reaction chamber which expelled the reaction mixture from the detection area.

It was established that leakage was a major factor for the generation of bubbles within the reaction chambers. Leakage between the microchip and the sealing tape was due to excess of the PEG coating on the sealing surface of the chips, resulting in a sealing tape that would not stick to the surface. Thus, most of the reaction chambers were drained completely during measurement, Figure 9b. The leakage and the draining of the reaction chambers ended when the volume of PEG coating was reduced from 2 µl per reaction chamber to 500 nl.

Leakage alone was not the only explanation for the generation of bubbles. The surface roughness of the chips affects how the sample wets the channels and the chambers. One assumption is that PEG does not cover the rough surfaces as well as the smooth surfaces. Nucleation points for the gas bubbles at the surface could therefore be due hydrophobic areas of uncoated COC chips which trap small air bubbles during filling of the chips. The milled and laser ablated chips had rough surfaces and a lot of problems with bubbles, compared to the injection moulded chips where bubble

formation was a minor issue. The 3M™ sealing tape was hydrophobic and could also be the reason for the nucleation points. In future work, hydrophilic sealing tape should be examined.

The geometry of the fabricated microchips showed specific areas, which typically generated bubbles. For the laser ablated chips, gas bubbles were created in all transitions between channel and reaction chambers during detection. WYKO measurements revealed that the transition area of these microchips had trenches with depth differences in the order of 100 μm between the reaction chamber and the channel. Unevenness along the walls of the channels and the chambers can have the same effect as the trenches. Such critical structural features of the chips will most likely trap air during filling and cause nucleation points for bubble formation Figure 9c. To avoid problems with bubbles, it is therefore of importance to have smooth surfaces at least if elevated temperatures are involved.

Enzyme stability at high temperatures

In order to develop a simple microchip employing NASBA and instrument, reducing the number of components in the instrument and the number of actuation steps on the chip would be preferable. The NASBA reaction itself is isothermal, but it is often necessary to initiate the reaction with a temperature boost at 65°C to break the secondary structures of a complex sample material before the isothermal amplification starts at 41°C, at which point the enzymes are added. Previously, the custom-made instrument was set up to contain two separate Peltier elements to handle this task. As two Peltier elements require much space on the chip and in the instrument as well as complex control systems and additional electronic components, the use of only one Peltier element would be desirable.

Experiments were performed by incubating several lyophilized enzyme spheres at 65°C for 15, 30, 60, 90 and 120 minutes prior to dissolving the enzyme spheres in enzyme diluent, followed by a conventional 20 μl NASBA reaction detected by the Lambda FL600. All the different incubation times of the enzyme spheres gave positive amplification reactions for both CaSki cells and HPV 16 oligonucleotides. Figure 10 shows the results obtained with 0.1 μM HPV 16 oligonucleotides. The sample which was not exposed to 65°C gave the highest fluorescent ratios. However, even after incubation at 65°C for 120 minutes the enzymes were still active with acceptable amplification for the three targets tested, *i.e.* CaSki (1:100), 10^{-3} μM HPV 16

oligonucleotide and 0.1 μM HPV 16 oligonucleotide. The standard procedure operates with an incubation step at 65˚C for 3 minutes for the mastermix and sample. These results confirm that only one Peltier element is sufficient in a future instrument.
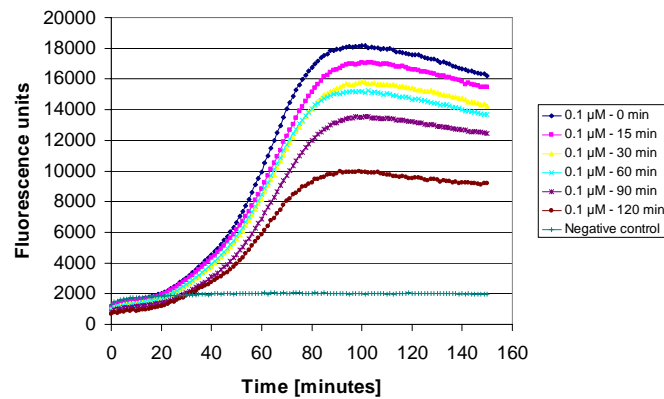
Figure 10 Amplification curves for incubation of the lyophilized enzyme spheres at 65˚C from 0 to 120 minutes. In this case, the activated enzyme solutions were tested on 0.1 μM HPV 16 oligonucleotide. (NC – negative control)

Having only few actuation steps on the chips are of advantage, with regard to the "robustness" and reliability of the instrument operations. Figure 11 shows the results where all reagents in the NASBA reaction, including the enzymes, were mixed prior to the 65˚C preheating step. However, the enzymes were completely inactivated during this treatment. We conclude that at high temperatures, dried enzymes are more robust than enzymes in solution.
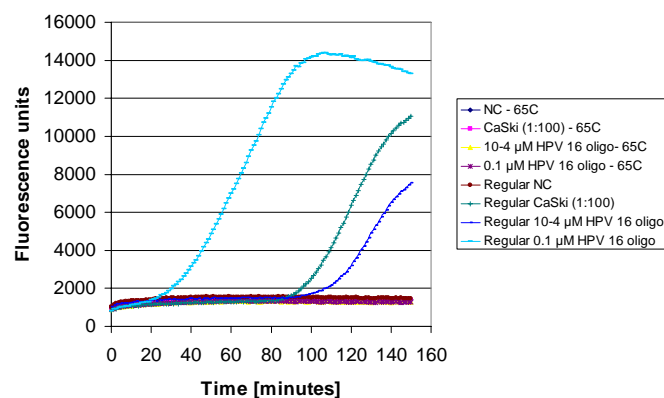
Figure 11 Amplification curves for incubation of enzyme in solution at 65˚C for 3 minutes. Enzyme solutions which have not been incubated were performed for comparison. The incubation at 65˚C inactivated the enzymes completely. (NC – negative control)

30

Inhibition of the NASBA reaction

Two experiments related to the ratio between the mastermix and the enzyme solutions were performed on macroscale. The first experiment explored the performance of the NASBA reaction with decreasing the amount of enzyme added to the reaction mixture. As expected, the best performance was shown for 5 µl enzyme solution, see Figure 12. However, it was surprising that 1 µl enzyme solution resulted in the same enzyme kinetics as the standard 5 µl. Amplification was even possible to detect for only 0.5 µl enzyme solution. However, in this case the reaction kinetics was different than for the other amplifications.
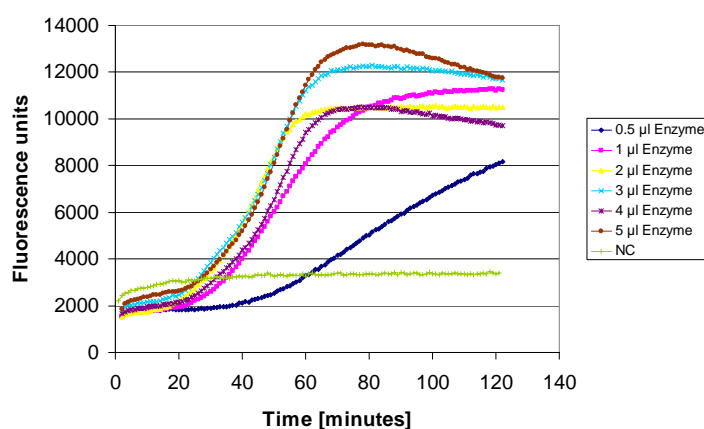
Figure 12 Amplification curves for decreasing the amount of enzyme in the NASBA reaction. The standard volume added in the reaction is 5 µl. Sample is 0.1 µM HPV 16 oligonucleotide. (NC – negative control)

In order to evaluate the robustness of the amplification reaction, the ratios of the mastermix solution and enzyme solution were altered. Table 8 shows that decreasing the amount of mastermix (0.5×) reduces both the level of fluorescence and the ratio. It was, however, still possible to achieve amplification. This was not surprising as the total amount of reagents in the reaction mixture, including the fluorescent molecular beacon, was reduced. However, increasing the enzyme concentration in combination with this mastermix solution resulted in stepwise steeper slopes of the amplification curve indicating increasing amplification efficiency.

When the enzyme concentration relative to a standard mastermix solution (1×) is doubled (2×) or quadrupled (4×), a slight increase in amplification efficiency can be seen as compared to the standard reaction. When the enzyme concentration was reduced to the half (0.5×), an earlier onset of amplification (TTP) was obtained then in

the standard reaction. However, this was not the same result as shown in Figure 12, where the onset of amplification was the same as for the standard reaction. The reason for this deviation in the results is not clear. Increasing the mastermix concentration, on the other hand, inhibited the amplification reaction completely (Table 8).

Table 8 Changing the ratios of the mastermix and enzyme solutions. Sample is 0.1 μM HPV 16 oligonucleotide.

	Enzymes	**0.5×**	**1×**	**1.5×**	**2×**	**4×**
Mastermix						
0.5×		+	+	+		
1×		+ +	+ +		+ +	+ +
1.5×			-			
2×			-		-	

Protectants

Reagents on a chip can be stored either in solution or in dried state. When storing the reagents on a chip, it is crucial that the reagents maintain their activity over a long period of time. For fragile reagents, such as enzymes which are only active if they possess the correct three-dimensional structures, it is usually preferred to dry them, because of prolonged stability.[12, 13] However, when exposed to conditions such as drying and freezing these fragile molecules can easily be destroyed. To minimize inactivation during these processes, protectants can be added.

According to others,[33, 34, 35] the protectants trehalose, PEG, PVP and BSA are judged to be efficient protectants for drying and freezing processes. A preliminary NASBA experiment was performed to test the various concentrations of these protectants to determine whether they inhibit the reaction. Table 2 shows the range of concentrations tested.

The protectants were first tested using HPV 16 oligonucleotide. The results displayed (data not shown) that the reaction was only slightly inhibited. Specifically, the fluorescent ratio was lower for 5%, 7.5% and 10% of PEG, while the TTP was prolonged in the case of 75 mM and 100 mM of trehalose. Subsequently, the CaSki samples were only tested for one concentration of each protectant: 10 mM trehalose, 1% PEG, 1% PVP and 50 μg/ml BSA (Table 2). The CaSki samples obtained positive amplifications for all the protectants. For the CaSki samples, as well as for the HPV 16 oligonucleotides, the TTP for the standard reaction mixture was higher than for the

reaction mixtures containing protectants. In these experiments, the standard NASBA mixture had DMSO and sorbitol in the mastermix and enzyme solution, while in the NASBA mixtures containing protectants, the DMSO and sorbitol were mixed with the sample. The sequence in which the reagents were mixed appeared to alter the kinetics of the reaction. Previous experiments have shown the same phenomenon (data not shown), when DMSO and sorbitol were added to the sample instead of the mastermix and enzyme solution. The same results were obtained when no sorbitol was added in the reaction mixture at all (data not shown). It was possible to amplify the HPV 16 oligonucleotides without DMSO and sorbitol. However, this was not feasible for the CaSki samples. High concentrations of sorbitol increase the viscosity of the reagents and appear to slow down certain steps of the reaction (*e.g.* primer annealing and polymerase binding to the primer-template duplex).[21] Since sorbitol is a mild DNA denaturant, it is believed that sorbitol will increase the specific product yield and assay sensitivity. Although the amplification reaction starts earlier for the mixtures with DMSO and sorbitol in the sample, the final levels of fluorescence for both CaSki and HPV 16 oligonucleotides vary, and are mostly lower than the standard reaction mixture. Obviously, the protectants do affect the amplification when introduced in this manner.

Drying of the NASBA reagents with protectants

The standard NASBA reaction mixture consists of three main solutions; the first solution is the mastermix containing nucleotides, primers, fluorescent molecular beacon probes, ions, reaction buffer and antioxidant. Secondly, there is the enzyme solution, and finally the sample containing the RNA or ssDNA target to be amplified. Preliminary testing of the drying of the NASBA reagents was done on macroscale with conventional volumes. Two schemes were followed concerning drying of the NASBA reagents: (1) The mastermix and enzyme solution were mixed before drying. (2) The mastermix and enzyme solution were dried separately.

Mixing the mastermix and enzyme solution together before drying resulted in no amplification for neither the HPV 16 oligonucleotides nor the CaSki samples. However, according to the data in Figure 11 amplification was not to be expected, due to the fact that the enzymes would be inactivated at 65˚C. It is therefore established that the mastermix and the enzyme solution should be dried separately on the chips, in order to obtain an amplification of the dried reagents. However, Weigl *et al.*[7] were able

to dry and rehydrate PCR mixes in 96-well plates containing mastermix, enzymes and varying concentration of trehalose, followed by successful amplification of *Salmonella* on a Mylar-based microfluidic card. In these experiments, the absence of trehalose resulted in loss of enzyme activity within 24 hours.

Table 9 shows the results of drying the mastermix and the enzyme solutions separately on a PEG coated COC surface.

Table 9 Drying the NASBA reagents with protectants. [CaSki (1:100): "++" TTP < 90 minutes, Ratio > 6, "+" TTP <150 minutes, Ratio > 1.4 and < 6, "-" no amplification] [0.1 μM HPV 16 oligo: "++" TTP < 40 minutes, Ratio > 6, "+" TTP <150 minutes, Ratio > 1.4 and <6, "-" no amplification] "/" separation of two experiments

Protectants Concentration		Sample	Conventional NASBA Before drying	Conventional NASBA After drying
Trehalose				
	5 mM	0.1 μM HPV 16	++*	++*
		CaSki 1:100	++*	+*
	10 mM	0.1 μM HPV 16	++* / ++*	++* / ++*
		CaSki 1:100	+* / ++*	+ / +*
	25 mM	0.1 μM HPV 16	++*	++*
		CaSki 1:100	++*	+*
	50 mM	0.1 μM HPV 16	++*	++*
		CaSki 1:100	++*	+
PEG				
	0.50%	0.1 μM HPV 16	++*	++*
		CaSki 1:100	++*	++*
	0.75%	0.1 μM HPV 16	++*	++*
		CaSki 1:100	+	+*
	1.00%	0.1 μM HPV 16	++* / ++*	++* / ++*
		CaSki 1:100	+* / -	+ / +
	2.50%	0.1 μM HPV 16	++*	++
		CaSki 1:100	-	-
Trehalose + PEG				
	10 mM + 1%	0.1 μM HPV 16	++*	++*
		CaSki 1:100	-	-
PVP				
	1%	0.1 μM HPV 16	++*	-
		CaSki 1:100	+*	-
BSA				
	50 μg/ml	0.1 μM HPV 16	++*	++*
		CaSki 1:100	-	-
PVP + BSA				
	1% + 50 μg/ml	0.1 μM HPV 16	++*	+*
		CaSki 1:100	+*	-
No protectant		0.1 μM HPV 16	++	++° / ++
		CaSki 1:100	++	- / -
No protectant – DMSO/sorbitol in sample		0.1 μM HPV 16	++*	++*
		CaSki 1:100	+	-

* The TTP was earlier than for the standard newly made reaction

° The TTP was later than for the standard newly made reaction

Dried reagents without protectants did not result in amplification of the CaSki extract. The only protectants resulting in positive amplification of the CaSki extract after drying were trehalose and PEG (Table 9). In this case, all CaSki samples were amplified, except in the presence of 2.5% PEG. The best amplification reactions for the CaSki samples after drying were obtained with 0.5% PEG, followed by 10 mM trehalose, 0.75% PEG and 25 mM trehalose. For the HPV 16 oligonucleotides, all the added protectants resulted in amplification after drying. Even when using dried reagents without protectants, amplification was successful.

The reagent spheres and the enzyme spheres in the original kit are already lyophilized. It is most likely that protectants have been added to these spheres during production. However, it was clear that the quality of the enzymes was reduced in the second drying, since it was difficult to amplify the CaSki samples, and addition of extra protectants contributed to preserve the activity of the enzymes. HPV 16 oligonucleotides were easier to amplify than the CaSki sample, probably due to higher concentration of target. In addition, the oligonucleotides were designed to avoid or minimalize intramolecular secondary structures.

One main source of error in these macroscale drying experiments was the degree of reagent dissolution and transfer when rehydrating the mastermix and enzymes with water.

### Drying of the NASBA reagents with protectants on chip

Of the newly fabricated chips, the hot embossed COC chips were fabricated with the lowest surfaces roughness and smoothest walls, and were therefore chosen for the drying experiments. A couple of milled single chamber chips were used for preliminary testing and spotted together with the hot embossed chips. In order to deposit a droplet of reagents on the surface, it was necessary for the droplet to be in contact with the surface. However, it was important that the droplet did not touch the surface of the sidewalls as this would make the droplet creep into the channel system, leaving no liquid in the chamber for drying. Hence, the large size of the reaction chamber was essential. The water within the spotted droplets evaporated within minutes. It was crucial that the droplets were almost dried out before the next droplet was dispensed due to the positioning of the reagents. Otherwise, the droplets would easily come in contact with the sidewalls. When performing the spotting it was observed that the milled chips spread out the droplet more than the hot embossed chips. As the only difference between these chips was the surface roughness, we conclude that the topography of the surface clearly affected the wetting. Preliminary

spotting of the enzymes in the reaction chambers of the milled chips showed that the dried enzymes built up ~30 – 50 μm in the spotted area. The height of the cake will obviously depend on the surface area on which the droplet spread out.

In Table 10 the amplification results of the spotted, dried and rehydrated mastermix and enzymes are shown. Only one hot embossed chip with dried enzymes has so far given successful amplification results. All 6 reaction chambers on this chip showed positive amplification, Figure 13.

Table 10 Amplification results on the COC chips tested with spotted, dried and rehydrated mastermix and enzymes.

Fabrication method	Milling	Hot embossing	Hot embossing
Dried reagents	Enzymes	Enzymes	Mastermix
Number of chips	2	3	3
Positive results	0	6	0
Negative results	12	12	18
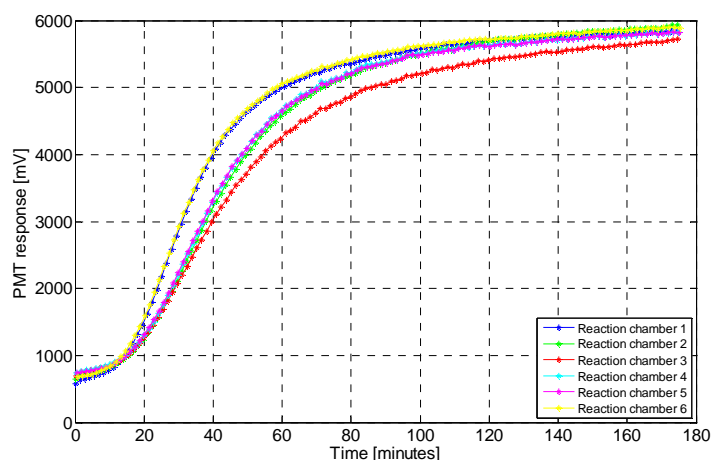
Figure 13 Simultaneous amplification curves of 0.1 μM HPV 16 oligonucleotide with spotted, dried and rehydrated enzymes in a hot embossed chip with detection volumes of 500 nl.

There is no obvious explanation to why only one of the chips with dried reagents showed successful amplification. Results from macroscale (Table 9) illustrated that it was possible to dry both mastermix and enzymes, although separately, followed by rehydration and successful amplification. Contamination of the chips or reagents

during the production and assembly of the chips could be one possible cause, in addition to contamination of the sample.

Table 8 indicates that the ratio of concentration between the mastermix and enzyme reagents was of importance for the NASBA reaction. The Nanoject II is able to dispense volumes in the range of 2.3 – 69 nl. However, the accuracy of the actual volume spotted depends on the properties of the liquid and the surface of the chip. The contact angle for the enzyme solution on a PEG coated surface is less than 10˚, while the mastermix shows a contact angle of approximately 33˚. Hence, the spotted volume can deviate to a large extent from the volume stated on the Nanoject II. Additionally, the liquid to be dispensed evaporates fast at the dispensing tip. Consequently, the reagents concentrate over time if the spotting is delayed. Accuracy of the sample volume applied to the chips will depend on the accuracy of the pipettes used and the shape of the cut membrane at the inlet hole.

The order in which the reagents were applied in the macroscale experiments compared to the single chamber chips deviated slightly. On macroscale, the mastermix and enzymes were rehydrated separately and then mixed together before the sample was added. On chip, the rehydration of the mastermix was accomplished by applying a mixture of the enzymes, DMSO/sorbitol and oligonucleotide sample. The dried and highly concentrated mastermix deposited in the chip could influence the activity of the enzymes in the mixture entering the chip. To investigate the importance of the order in which the reagents are applied, chips with two chambers in series should be tested. Within these chips, the sample would first rehydrate the mastermix, then the enzymes. The chips with chambers in series were spotted with mastermix in the first chamber and enzymes in the second chamber. The first microfluidic tests demonstrated that when the sample solution containing DMSO/sorbitol was added to the chip, the liquid was pulled in by capillary forces past the first chamber. We observed that the mastermix reagents dissolved into the sample, as the round shaped cake of reagents disappeared when visualizing it in a video camera (Panasonic NV-GS75E). At the same time, in these experiments, the volume of the plug within the reaction chambers diminished. Upon close inspection, we found that the sample was wetting the edges of the channels in the chip, pulling the liquid from the sample plug further into the channel system along the corners. In this case, the sample plug applied to the chip did not obtain static equilibrium of the meniscus, due to the high wetting properties of the sample plug on this PEG coated surface. This instability will drive the liquid along the corners up to

the very end of the channel system, as long as enough liquid is provided in the system.[31] This effect was not observed in the single chamber chips, as the reagents applied to these chips were mixed with additional reagents, which altered the wetting properties of the liquid mixture. In order to handle the problem with creeping liquid plugs, hydrophobic valves were spotted in the channels of the chips, Figure 14. The hydrophobic valves stopped the creeping and a pressure difference of ~1000 Pa was needed to overcome the strength of the valve in order to move the sample to the second chamber.
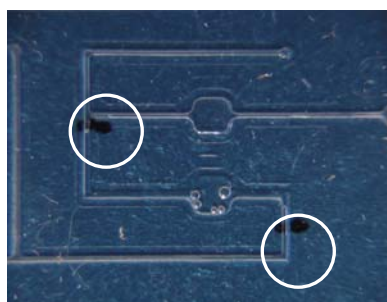
Figure 14 COC microchip with two chambers in series. The two white circles indicate the area where the hydrophobic valves were spotted on the chip. The first chamber was emptied as the sample plug was moved to the second chamber. The black lines indicate the initial position of the meniscus of the sample plug before incubation. The picture is taken after 3 hours incubation at 41˚C.

The picture in Figure 14 was taken 3 hours after incubation of the chip at 41˚C without sealing the inlet or the outlet. The sample plug was restrained between the hydrophobic valves during the measurement, but the picture demonstrates that generation of bubbles within the reaction chamber was still a problem for these chips. Preliminary results showed that the evaporation of the NASBA mixture was in the order of ~7% per hour and ~3% per hour with regard to open and sealed ends, respectively. In this case, it was difficult to determine the loss of sample due to the bubbles generated within the chamber during incubation. The bubbles displaced the liquid meniscus at each end of the channels closer to the initial position (black lines). However, these preliminary evaporation tests were performed in milled chips with different channel dimensions and several more restrictions than the hot embossed chips. As the evaporation depends on the cross section area of the end meniscus, the diffusion length and the gradient of the vapour pressure within the gas volume of the system, the actual evaporation rate in the hot embossed chips could deviate from the milled chips.

38

In order to find the evaporation rate, new experiments should be performed with the correct chips.

From Table 10 it can be seen that it was possible to achieve successful amplification of premixed NASBA within the chip with chambers in series. However, no amplification was observed in a chip that had been stored at room temperature with dried mastermix and enzymes for 3 weeks. Neither the mastermix nor the enzymes were dissolved, even though the sample plug was placed over the mastermix for 10 minutes at room temperature and the enzyme cake for 2.5 hours at 41˚C. As rehydration had not previously been experienced as a problem, it is likely that the reagent stability during storage at room temperature was poor. Thus, spotted chips should be stored at -20°C.

Conclusions

Several aspects of the development of a self-contained microchip for isothermal amplification of nucleic acids by NASBA were tested. The work presented here provides useful guidelines towards the development of a complete automatic chip employing NASBA with regard to design, fabrication, surface modification and performance of the amplification reaction. However, a number of issues still remain to be settled before satisfactory results may be obtained.

The reaction volumes were increased compared to previous chip designs, as the focus changed from cost of reagents on chip to robustness and reliability of the diagnostic application. When increasing the detection volume to 500 nl, it might be possible to obtain consistent amplification at lower concentrations than within 80 nl detection volumes as more molecules enter the reaction chambers. This should be verified with dilution series of both oligonucleotides and cell lines.

Rough surfaces in the microchips were proven to have an impact on the generation of bubbles. Rough surfaces increase the risk of areas not being completely covered by coating. The hydrophobic areas not covered constitute potential nucleation points for bubble formation as air may become trapped in these areas during filling, due to insufficient wetting. Adsorption of enzymes can be a problem if the surface is not completely covered by a biocompatible PEG coating, as enzymes tend to adsorb on hydrophobic surfaces.

Hydrophobic valves should be included to define the borders of the chambers, and to prevent creeping of the sample throughout the enzymatic process. Enzyme adsorption did not seem to be a problem with regard to the hydrophobic valves, as it is only the meniscus of the sample which will be in contact with this area over time.

The experiments showed that 2 chambers were sufficient for reagent storage and detection. Mastermix was dried in the first chamber, while enzymes were dried in the second chamber. It was essential to dry the solutions separately; otherwise no amplification could be detected. Additionally, either PEG or trehalose was required to restore enzyme activity after drying. The successful amplification of the dried enzymes on chip revealed that no external mixing was required, as the reagents were mixed sufficiently by diffusion alone. Experiments related to successful drying, rehydration and amplification of mastermix on chip need to be pursued further to systematically explore their limits. This is essential for the chip to work as intended in a point-of-care setting. To solve the remaining problems, it also seems essential to investigate the sequence in which the reagents are applied on chip, the concentration ratios and the contamination issue. Furthermore, the dried reagents on chip need to be evaluated with regards to cell line samples and sensitivity.

Acknowledgement

Notes and References

‡   *In memoriam* – Dr. Henrik Rogne (1969 - 2006)

1. Lagally, E. T., Simpson, P. C., and Mathies, R. A., (2000) Monolithic integrated microfluidic DNA amplification and capillary electrophoresis analysis system, *Sens Actuators B*, **63**, 3, 138 - 146

2. Khandurina, J., McKnight, T. E., Jacobson, S. C., Waters, L. C., Foote, R. S., and Ramsey, J. M., (2000) Integrated system for rapid PCR-based DNA analysis in microfluidic devices, *Anal Chem*, **72**, 13, 2995 - 3000

3. Wang, J., Chen, Z. Y., Corstjens, P. L. A. M., Mauk, M. G., and Bau, H. H., (2006) A disposable microfluidic cassette for DNA amplification and detection, *Lab Chip*, **6**, 1, 46 - 53

4. Liu, R. H., Yang, J. N., Lenigk, R., Bonanno, J., and Grodzinski, P., (2004) Self-contained, fully integrated biochip for sample preparation, polymerase chain reaction amplification, and DNA microarray detection, *Anal Chem*, **76**, 7, 1824 - 1831

5. Panaro, N. J., Lou, X. J., Fortina, P., Kricka, L. J., and Wilding, P., (2004) Surface effects on PCR reactions in multichip microfluidic platforms, *Biomed Microdevices*, **6**, 1, 75 - 80

6. Garcia, E., Kirkham, J. R., Hatch, A. V., Hawkins, K. R., and Yager, P., (2004) Controlled microfluidic reconstitution of functional protein from an anhydrous storage depot, *Lab Chip*, **4**, 1, 78 - 82

7. Weigl, B. H., Gerdes, J., Tarr, P., Yager, P., Dillman, L., Peck, R., Ramachandran, S., Lemba, M., Kokoris, M., Nabavi, M., Battrell, F., Hoekstra, D., Klein, E. J., and Denno, D. M. (2006) Fully integrated multiplexed lab-on-a-card assay for enteric pathogens, *Proc. of SPIE*, **6112**, 1 - 11

8. Seetharam, R., Wada, Y., Ramachandran, S., Hess, H., and Satir, P., (2006) Long-term storage of bionanodevices by freezing and lyophilization, *Lab Chip*, **6**, 9, 1239 - 1242

9. Puckett, L. G., Dikici, E., Lai, S., Madou, M., Bachas, L. G., and Daunert, S., (2004) Investigation into the applicability of the centrifugal microfluidics development of protein-platform for the ligand binding assays incorporating enhanced green fluorescent protein as a fluorescent reporter, *Anal. Chem.*, **76**, 24, 7263 - 7268

10. Chen, D. L. and Ismagilov, R. F., (2006) Microfluidic cartridges preloaded with nanoliter plugs of reagents: an alternative to 96-well plates for screening, *Curr Opin Chem Biol.*, **10**, 3, 226 - 231

11. Linder, V., Sia, S. K., and Whitesides, G. M., (2005) Reagent-loaded cartridges for valveless and automated fluid delivery in microfluidic devices, *Anal Chem*, **77**, 1, 64 - 71

12. Kobayashi, S., Beppu, K., Shimizu, H., Ogawa, S., and Kotani, R., (1984) *Stable enzyme composition*, US 4451569

13. Roser, B. J., (1990) *Protection of proteins and the like*, US 4891319

14. Compton, J., (1991) Nucleic acid sequence-based amplification, *Nature*, **350**, 6313, 91 - 92

15. Gulliksen, A., Solli, L. A., Drese, K. S., Sörensen, O., Karlsen, F., Rogne, H., Hovig, E., and Sirevåg, R., (2005) Parallel nanoliter detection of cancer markers using polymer microchips, *Lab Chip*, **5**, 4, 416 - 420

16. Niesters, Hubert G. M., (2001) Quantitation of Viral Load Using Real-Time Amplification Techniques, *Methods*, **25**, 4, 419 - 429

17. deBaar, M. P., vanDooren, M. W., deRooij, E., Bakker, M., vanGemen, B., Goudsmit, J., and deRonde, A., (2001) Single rapid real-time monitored isothermal RNA amplification assay for quantification of human immunodeficiency virus type 1 isolates from groups M, N, and O, *J Clin Microbiol*, **39**, 4, 1378 - 1384

18. Hawkins, K. R. and Yager, P., (2003) Nonlinear decrease of background fluorescence in polymer thin-films - a survey of materials and how they can complicate fluorescence detection in mu TAS, *Lab Chip*, **3**, 4, 248 - 252

19. Piruska, A., Nikcevic, I., Lee, S. H., Ahn, C., Heineman, W. R., Limbach, P. A., and Seliskar, C. J., (2005) The autofluorescence of plastic materials and chips measured under laser irradiation, *Lab Chip*, **5**, 12, 1348 - 1354

20. Malek, L. T., Davey, C., Henderson, G., and Sooknanan, R., (1992) *Enhanced nucleic acid amplification process*, US 5130238

21. McLaughlin, I. J., Coticone, S. R, and Bloch, W., (2003) *Method of reducing non-specific amplification in PCR*, US 2003/0104395 A1

22. Goudsmit, J., Oudshoorn, P., Jurriaans, S., and Lukashov, V. V., (2002) *Nucleic acid sequences that can be used as primers and probes in the amplification and detection of all subtypes of HIV-1*, EP 1002138 B1

23. de Rosier, T. A., de la Cruz, N. B., and Wilkosz, R. K., (2001) *Method and formulation for stabilization of enzymes*, US 6294365 B1

24. Jeon, S. I. and Andrade, J. D., (1991) Protein Surface Interactions in the Presence of Polyethylene Oxide.2. Effect of Protein Size, *J Colloid Interface Sci*, **142**, 1, 159 - 166

25. Beissinger, R. L. and Leonard, E. F., (1981) Plasma protein adsorption and desorption rates on quartz: approach to multi-component systems, *Trans Am Soc Artif Intern Organs*, **27**, 225 - 230

26. Lionello, A., Josserand, J., Jensen, H., and Girault, H. H., (2005) Protein adsorption in static microsystems: effect of the surface to volume ratio, *Lab Chip*, **5**, 3, 254 - 260

27. Lionello, A., Josserand, J., Jensen, H., and Girault, H. H., (2005) Dynamic protein adsorption in microchannels by "stop-flow" and continuous flow, *Lab Chip*, **5**, 10, 1096 - 1103

28. Krishnan, M., Burke, D. T., and Burns, M. A., (2004) Polymerase chain reaction in high surface-to-volume ratio SiO_2 microstructures, *Anal Chem*, **76**, 22, 6588 - 6593

29. Jeon, S. I., Lee, J. H., Andrade, J. D., and Degennes, P. G., (1991) Protein Surface Interactions in the Presence of Polyethylene Oxide.1. Simplified Theory, *J Colloid Interface Sci*, **142**, 1, 149 - 158

30. Shoffner, M. A., Cheng, J., Hvichia, G. E., Kricka, L. J., and Wilding, P., (1996) Chip PCR .1. Surface passivation of microfabricated silicon-glass chips for PCR, *Nucleic Acids Res*, **24**, 2, 375 - 379

31. Goldschmidtboeing, F., Rabold, M., and Woias, P., (2006) Strategies for void-free liquid filling of micro cavities, *J Micromech Microeng*, **16**, 7, 1321 - 1330

32. Gulliksen, A., Solli, L., Karlsen, F., Rogne, H., Hovig, E., Nordstrøm, T., and Sirevåg, R., (2004) Real-time nucleic acid sequence-based amplification in nanoliter volumes, *Anal Chem*, **76**, 1, 9 - 14

33. Carpenter, J. F., Prestrelski, S. J., and Arakawa, T., (1993) Separation of Freezing- and Drying-Induced Denaturation of Lyophilized Proteins Using Stress-Specific Stabilization: I. Enzyme Activity and Calorimetric Studies, *Arch Biochem Biophys*, **303**, 2, 456 - 464

34. Prestrelski, S. J., Arakawa, T., and Carpenter, J. F., (1993) Separation of Freezing- and Drying-Induced Denaturation of Lyophilized Proteins Using Stress-Specific Stabilization: II. Structural Studies Using Infrared Spectroscopy, *Arch Biochem Biophys*, **303**, 2, 465 - 473

35. Anchordoquy, T. J. and Carpenter, J. F., (1996) Polymers protect lactate dehydrogenase during freeze-drying by inhibiting dissociation in the frozen state, *Arch Biochem Biophys*, **332**, 2, 231 - 238

,